

UNIVERSIDADE DE BRASÍLIA – FACULDADE DE CEILÂDIA PROGRAMA DE PÓS-GRADUAÇÃO STRICTU-SENSU EM CIÊNCIAS E TECNOLOGIAS EM SAÚDE

Elaboração de nanopartículas de maguemita recobertas com ouro e funcionalizadas com ftalocianina de alumínio para aplicações multitarefa em imageamento e terapias médicas

BRENO CUNHA P. COELHO

ORIENTADOR: Prof. Dr. MARCELO HENRIQUE SOUSA

BRASÍLIA, 09 DE DEZEMBRO DE 2016

UNIVERSIDADE DE BRASÍLIA – FACULDADE DE CEILÂNDIA PROGRAMA DE PÓS-GRADUAÇÃO *STRICTU-SENSU* EM CIÊNCIAS E TECNOLOGIAS EM SAÚDE

Elaboração de nanopartículas de maguemita recobertas com ouro e funcionalizadas com ftalocianina de alumínio para aplicações multitarefa em imageamento e terapias médicas

BRENO CUNHA P. COELHO

Tese apresentada à Faculdade da Ceilândia da Universidade de Brasília como requisito parcial para obtenção do título de Doutor em Ciências e Tecnologias em Saúde

ORIENTADOR: Prof. Dr. MARCELO HENRIQUE SOUSA

BRASÍLIA, 09 SW DEZEMBRO DE 2016

UNIVERSIDADE DE BRASÍLIA
FACULDADE DE CEILÂNDIA
PROGRAMA DE PÓS-GRADUAÇÃO EM CIÊNCIAS E TECNOLOGIAS EM SAÚDE
BRENO CUNHA P. COELHO

Área de concentração: Mecanismos Básicos e Processos Biológicos em Saúde

Linha de pesquisa: Nanobiotecnologia Aplicada à Saúde.

Tese de doutorado submetida ao programa de Pós-Graduação em Ciências e Tecnologias da Saúde da Universidade de Brasília como parte dos requisitos necessários para a obtenção do grau de doutor.

APROVADA POR:

Dr. MARCELO HENRIQUE SOUSA (UnB) - Orientador

Dr. VICTOR MARCELO DEFLON (USP) – Examinador externo 1

Dra. MARIA MARCIA MURTA (UnB) – Examinador externo 2

Dr. ALEX FABIANO CORTEZ CAMPOS (UnB) – Examinador externo 3

Dr. JULIANO ALEXANDRE CHAKER (UnB) - Examinador interno

Dr. JOÃO PAULO FIGUEIRÓ LONGO (UnB) – Examinador (Suplente)

BRASÍLIA/DF: 09 DE DEZEMBRO DE 2016

AGRADECIMENTOS

O processo de evolução intelectual é construído dias após dia, pensamento após pensamento, sempre desfrutando de fracassos, angústias, imperfeições e reconhecimento que durante este caminho, a determinação, inspiração, coragem, força e desejo de se alcançar algo melhor devem estar constantemente presentes. A maturidade alcançada nos faz perceber que os professores, antes questionados e algumas vezes criticados, se tornam dignos de admiração, merecedores de grande respeito e notoriedade, pois a obtenção de um título de doutor e a coragem de mergulhar em meio ao desconhecido, desbravando e produzindo novos conhecimentos é algo que exige um valor elevado a ser pago, seu custo é de uma parte de nossa identidade, personalidade, reflexões e essência, algo capaz de conduzir o indivíduo a um patamar nem sempre perceptível aos olhos de todos. Manter-se neste patamar, conseguindo blindar-se de sentimentos egoístas, compartilhando esse saber, aprimorando-se para ser melhor é algo que realmente merece ser ovacionado.

Neste percurso, reconheço que me transformei como cientista, professor, pessoa, pai e ser humano. É válido agradecer fortemente várias pessoas, desde as professoras de ciências do ensino fundamental, amigos que inspiraram pensamentos críticos, professores do ensino médio, vários professores inspiradores da graduação, tais como Victor Deflon, Hugo Monteiro, Carlos Kleber, Márcia Murta, Roberto Ribeiro (Bob), Patrícia Lotens e em especial o professor Peter Bakuzis que muito me motivou, ensinou e direcionou os pensamentos nos mais diversos ramos das ciências e academia.

Uma consideração especial se faz aos membros de nosso laboratório, Marcelão, Mari, Ataílson, Josy, Kat, Abraham e com um nobre destaque ao professor Marcelinho, que tanta paciência teve, passando seus conhecimentos que a cada dia mais me surpreende, demonstrando uma enorme intuição química e grandeza de espírito, mantendo o característico bom humor, que é sua marca registrada, um sincero muito obrigado por todos os momentos de aprendizagem professor.

Algo que seria indispensável destacar é a parceria de minha família, que mesmo ainda não possuindo um histórico no mundo acadêmico, sofre com as minhas aflições, frustrações, erros e incompreensões a serem lidadas. Meus filhos que mesmo ainda sem terem a consciência deste fato são os despertadores do mais sincero amor que um dia poderei experimentar, arrancando o melhor de mim e me alimentando de sonhos e vontades de ser alguém melhor, na intenção de compartilhar

tudo que puder fazê-los ir à frente e avançarem como pessoas mais felizes, realizando seus mais sinceros sonhos...

"Nem todos são merecedores de nossas verdades."

SUMÁRIO

RESUMO.....	X
ABSTRACT.....	XI
INTRODUÇÃO GERAL.....	1
ARTIGO CIENTÍFICO.....	4
ANEXOS	
Anexo I – Normas de publicação para a revista Journal of Materials Chemistry B....	27
Anexo II – Confirmação Qualis da revista.....	34
Anexo III – Comprovante de envio (submissão) do artigo para a revista Journal of Material Chemistry B.	36
Anexo IV – Template.....	38.
Referências.....	37

LISTA DE ABREVIATURAS, NOMENCLATURAS E SÍMBOLOS

ACI – Contraste para Tomografia a base de Iodo

CT – Tomografia computadorizada

DLS – Espalhamento Dinâmico de Luz

D_H – Diâmetro Hidrodinâmico

DMEM - Dulbecco's Modified Eagle's Medium

DMSO - dimethylsulfoxide

FCC – Cubico de Face Centrada

FFT – Transformada Rápida de Fourier

HaCAT - Human Keratinocyte cells

HRTEM – Microscopia Eletrônica de Transmitância de Alta Eficiência

ICO-OES – Espectrometria de Emissão Óptica com Plasma

MNP – Amostra $\gamma\text{-Fe}_2\text{O}_3$ citratada

MNP@Au1 - Amostra $\gamma\text{-Fe}_2\text{O}_3$ citratada recoberta com menos ouro

MNP@Au2 - Amostra $\gamma\text{-Fe}_2\text{O}_3$ citratada recoberta com mais ouro

MRI - magnetic Resonance Image

MTT - 3(4,5-dimethylthiazol-2-yl)-2,5diphenyltetrazoliumbromide

NIH-3T3 - Murine fibroblast cells

NP – Nanoparticles

PANI – Polyaniline

PB – Polybutylene

PDT – Terapia Foto Dinâmica

PEI – Polyethylenimine

PTC – Ftalocianina de alumínio

PZS - poly(cyclotriphosphazene-co-4,40-sulfonyldiphenol)

SEM - Standart error mean

SPION - Super Paramagnetic Iron Oxide Nanoparticle

TEM - Trasmition Electron Microscopy

XDR – Difração de raio X

ZS- Zeta Sizer

SEM – Erro Padrão

RESUMO

Neste estudo foi reportado a elaboração e caracterização de nanopartículas núcleo-camada (maguemita-ouro) com a camada modulada em diferentes espessuras abaixo de 2 nm. As nanopartículas recobertas com ouro possuem núcleo com tamanho médio de 9 nm, que foi elaborada com um protocolo em um único passo, envolvendo a redução do cátion Au^{3+} na presença de nanopartículas de maguemita recobertas com citrato. Adicionalmente, a pós-funcionalização das estruturas núcleo-camada com ftalocianina de alumínio foi realizada com sucesso, objetivando a produção de um material como plataforma para terapia fotodinâmica. As amostras produzidas foram estruturalmente, morfologicamente, magneticamente e opticamente caracterizadas e apresentaram uma estabilidade coloidal de longa duração no pH fisiológico. Impressionantemente, foi encontrado que as amostras sintetizadas apresentam uma boa propriedade de atenuação de raios X, tornando-os capazes de serem utilizados como nanosondas para tomografia computadorizada. Além disso, testes de nanotoxicidade *in vivo* confirmaram uma biocompatibilidade superior para as amostras produzidas, fazendo das mesmas uma plataforma bastante promissora para multifunções em aplicações *in vivo*.

Palavras chave: Core-shell, ouro, maguemita, ftalocianina, tomografia computadorizada.

ABSTRACT

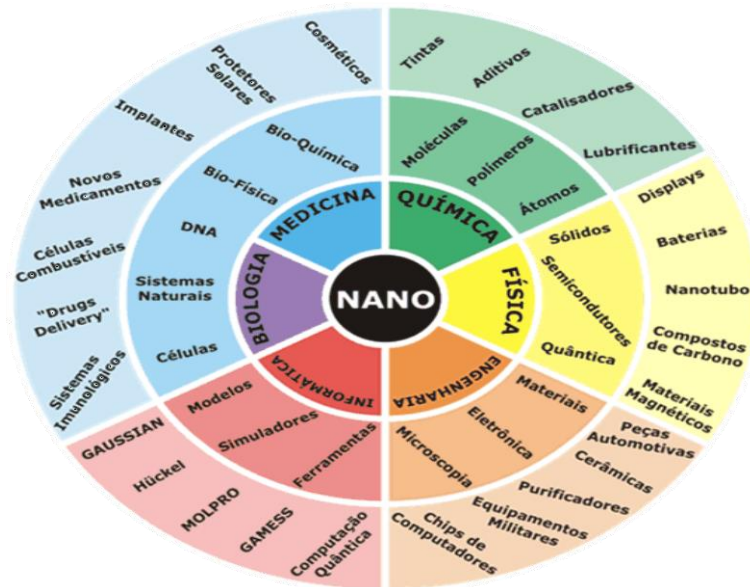
In this study we report on elaboration and characterization of core–shell maghemite-Gold nanoparticles (NPs) with shell modulated for different thicknesses below 2 nm nm. Gold-shelled maghemite NPs with average core size about 9 nm were elaborated by a single-step protocol involving reduction of Au³⁺ in the presence of citrated-coated maghemite NPs. Additionally, post-functionalization of the core-shell structures with aluminium phthalocyanine was successfully accomplished, aiming the production of a material platform for photodynamic therapy. The as-produced samples were structurally, morphologically, magnetically and optically characterized and presented long-term colloidal stability at physiological pH. Impressively, we found the as-produced samples showing good X-ray attenuation property, rendering them with ability to be used as a nanoprobe for targeted computed tomography. Moreover, *in vitro* nanocytotoxicity tests confirmed superior biocompatibility of the as-produced samples, making them a very promising multi-task platform for *in vivo* applications.

Key word: Core-shell, gold, maghemite, phthalocyanine and computed tomography.

1- INTRODUÇÃO GERAL

Nanotecnologia é um ramo multidisciplinar da ciência que engloba inúmeros campos da ciência e tecnologia, tais como o biomédico, farmacêutico, agricultura, meio ambiente, materiais avançados, química, física, eletrônica, tecnologia da informação, dentre outros mais (figura 1).

Figura 1: Relação entre as diversas áreas do conhecimento com a nanotecnologia



A síntese, propriedades e aplicação de materiais e dispositivos numa escala inferior a 100nm tem contribuído severamente em vários campos biomédicos como: agentes de imagem, veículos de entrega de fármacos, ferramentas de diagnósticos, dentre outras, mixando diferentes áreas do conhecimento¹. A engenharia biomédica possui a ponte que liga a biologia com a medicina convencional, pela aplicação de conhecimentos de engenharia em diagnósticos cirúrgicos, monitoramento e terapia.¹

No início do século XXI, o controle do câncer é considerado ser um dos principais problemas de saúde comunitária. Apenas dos intensivos esforços nas décadas passadas, o câncer persiste como uma das principais causas de morte no mundo^{2,3}. O câncer é conhecido por desenvolver, através de um processo em várias etapas e envolvendo numerosos sistemas fisiológicos, como sinalização celular e apoptose, tornando-se uma doença altamente complexa e de difícil compreensão. Diversos novos métodos e técnicas têm sido desenvolvidos na intenção de melhorar o diagnóstico e o tratamento do câncer, muitas vezes promissores no início, mas com resultados limitados durante o curso de sua aplicação^{4,5,6}.

Nanociência e nanotecnologia está na vanguarda do desenvolvimento de novos conceitos terapêuticos e diagnósticos em todas as áreas da medicina, especialmente câncer, emergindo assim um novo campo disciplinar denominado "nanomedicina"⁷. Nanomedicina pode ser definido como a

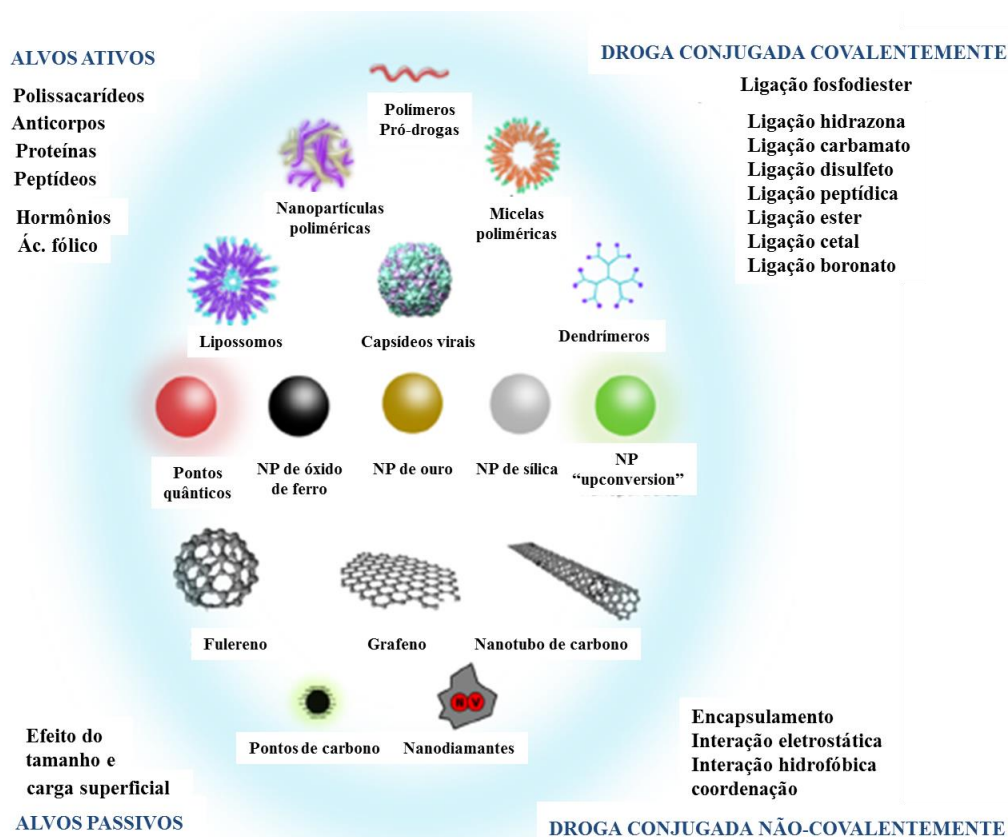
aplicação de nanotecnologia que envolve o uso de objetos nanométricos para aprimorar diagnóstico, tratamento e prevenção de doenças e lesões traumáticas.

O pequeno tamanho e alta superfície, para a razão volumétrica (Superfície/Volume) das nanopartículas são os recursos chave que as fazem úteis nos campos biomédicos, devido ao desenvolvimento de várias novas propriedades, facilidade na funcionalização, conjugação de biomoléculas, etc.⁸

A aplicação da nanotecnologia neste campo mostra ainda o avanço em várias áreas específicas tais como drogas mais direcionadas, bio-diagnóstico, bioimagem e manipulação genética. Nanopartículas inorgânicas podem ser produzidas em uma grande variedade de tamanhos e formas^{9,10,11} e possuem um vasto número de propriedades físicas que surgem a partir das características quânticas dos materiais que compõem seu núcleo^{12,13}.

Muitos tipos de carreadores de drogas têm sido desenvolvidos até o presente momento, incluindo carreadores poliméricos de alto peso molecular solúveis em água, nanopartículas poliméricas, micelas poliméricas, dendrímeros, lipossomos, nanopartículas virais, sistemas baseados em carbono (nanotubos de carbono e óxido de grafeno), nanopartículas magnéticas (óxidos de ferro por exemplo) e nanopartículas de sílica e ouro (figura 2).

Figura 2: Visão geral dos sistemas de entrega de drogas com várias possibilidades de alvos e seus ligantes.



Avanços recentes na química dos polímeros e o desenvolvimento de novas técnicas de polimerização têm permitido a síntese de polímeros com estruturas bem definidas, restringindo a distribuição do peso molecular e propriedades ajustáveis^{14,15,16}. Analogicamente, desenvolvimentos na química de nanomateriais têm produzido nanopartículas carreadoras com distribuição de tamanho limitado e propriedades físico-químicas controladas que podem ser controladas para vários propósitos, como monitoramento da eficiência de tratamentos ou o aumento de sua eficiência. Juntamente com os avanços da biologia celular e molecular, estes desenvolvimentos oferecem oportunidades de criar uma sofisticada seletividade dos alvos, baseados nos carreadores e carreadores conjugados com várias moléculas biologicamente ativas, como drogas, genes, enzimas e outras proteínas ou nucleotídeos. Como agentes poderiam, potencialmente, formar bases de alta especificidade, segurança e eficiência para o tratamento de câncer.

Outro importante benefício do uso de polímeros e nanopartículas como carreadores de drogas derivam de suas habilidades de aumentar a solubilidade de drogas hidrofóbicas, estendendo a circulação da droga na corrente sanguínea e suprimindo ou eliminando a rápida excreção renal.

Juntos, o uso de carreadores de drogas aumenta dramaticamente o acúmulo de drogas em órgão ou células,^{17,18} e torna possível a possibilidade de ativação controlada (liberação) de drogas em que o efeito terapêutico é necessário, como por exemplo, em tumores. A ativação seletiva neste sentido poderia prevenir a intoxicação medicamentosa ocorrida por interação em tecidos em células saudáveis, mitigando ou eliminando qualquer efeito colateral que seria possível haver.

A diversidade de ambos, estrutura e propriedades, permitem novas estratégias para o desenvolvimento de terapias e agentes de imagem^{19,20}, com exemplos de sistemas baseados em nanopartículas a partir da entrada dos tratamentos clínicos.

Novas questões que surgem a partir da interação desses materiais com biosistemas, no entanto, colocam em cheque algumas possibilidades de atuação de alguns nanomateriais¹⁰. Algumas dessas questões se mostram insuperáveis, algumas exigem mais pesquisas para serem vencidas e algumas proporcionam novas direções que não eram esperadas com poderosos potenciais a serem explorados e utilizados.²¹

Nanopartículas magnéticas

Particularmente, nanopartículas magnéticas vêm exibindo suas vantagens pelas inovadoras propriedades. As nanopartículas magnéticas podem ser controladas separadamente em sistemas aglomerados, por meio de um campo magnético externo. Esta propriedade permite ao pesquisador imobilizar enzimas sobre a superfície do substrato²² e então construir sistemas bioeletroquímicos por meio de controle magnético^{23,24,25}.

O advento das nanopartículas tem aberto novos caminhos em muitos diferentes

campos de estudo, juntamente com outros nanomateriais²⁶. O ramo da engenharia biomédica tem sido igualmente influenciado. A elevada razão superfície/volume das nanopartículas as proporciona uma maior energia de superfície, atividades óticas únicas²⁷, eletrônicas e excelentes propriedades magnéticas²⁸, dentre outras mais.

A elevada área de superfície também permite a nanopartícula ser modificada adequadamente no sentido de promover suas propriedades farmacocinéticas, aumentar o tempo de vida na circulação vascular, juntamente com a melhoria da biodisponibilidade, especialmente para aplicações biomédicas. O aprimoramento das propriedades foi revolucionário no campo da entrega de drogas no organismo, o aumento no tempo de vida de circulação aumenta a eficácia do medicamento, o aumento da biodisponibilidade de drogas significa poder efetivamente usar muito menor dosagem em vez de medicamentos volumosos.²⁹ Como mencionado anteriormente, a mais importante característica que tem atraído à atenção de pesquisadores ao redor do mundo é a habilidade de ter melhores modificações superficiais, fato que não ajuda somente na elaboração de drogas específicas, mas pode resolver o duplo propósito tanto de monitoramento quanto a liberação de drogas. Em geral, as propriedades dependentes do tamanho das nanopartículas (principalmente as óticas, eletrônicas e magnéticas) têm sido observadas em serem muito mais úteis em aplicações biomédicas³⁰.

Muitos tipos de nanopartículas magnéticas (NPM) têm sido sintetizadas ao longo dos anos, sendo principalmente desenvolvidas para aplicações biomédicas, como separação de biomoléculas³¹, ressonância magnética de imagem³², agente de contraste³³, carreador de drogas³⁴ e biodetecção³⁵.

Qualquer sistema de entrega de droga, seja ele baseado em polímeros ou nanopartículas magnéticas, devem satisfazer um número de critérios em comum³⁶:

- (i) evitar interações não-específicas com o corpo ou a indução de reações adversas e evitar captura por células do sistema reticuloendotelial,
- (ii) proteger o transporte das moléculas biologicamente ativas para os locais de ação (tecido, órgão, célula ou organela) para o local de administração em um alto rendimento, enquanto mantém a molécula biologicamente ativa em um estado livre (inativa) durante o transporte,
- (iii) proteger as moléculas biologicamente ativas de efeitos prejudiciais durante o transporte (por exemplo degradação enzimática ou hidrólise) no corpo,
- (iv) liberar quantidades de moléculas biologicamente ativas no local, ou em torno deste, idealmente de forma controlada, de tal forma que seja conseguida uma concentração tecido/célula desejada,
- (v) permitir eliminação de todos os componentes do sistema de entrega de drogas do componente após a sua função como transportador ter sido cumprida.

Existem várias maneiras para que estes requerimentos sejam alcançados, e cada sistema de entrega de drogas oferece seu próprio conjunto de soluções específicas. Algumas dessas são comuns a muitos (ou quase todos) sistemas, mas outros são únicos e dependem de detalhes da estrutura do carreador e sua arquitetura^{37,38,39}.

Falando de forma mais genérica, estas abordagens são aplicáveis para diversos tipos de sistemas de entrega de drogas para tratamento de câncer, incluindo nanopartículas magnéticas e nanoclusters, assim como conjugados droga-polímero, micelas poliméricas e nanopartículas poliméricas. Outros sistemas de entrega de drogas baseados em polímeros como lipossomos nanomodificados e polímero-modificados (um dos poucos sistemas de entrega de drogas que têm sido extensivamente testados clinicamente e aprovados para uso clínico⁴⁰).

NANOPARTÍCULAS MAGNÉTICAS DE ÓXIDO DE FERRO COMO SISTEMAS DE ENTREGA DE DROGAS

Uma das classes mais exploradas de nanosistemas adequadas para a liberação de drogas são nanopartículas inorgânicas. Assim como as nanopartículas poliméricas, nanopartículas inorgânicas variam em uma escala de 1 a 1000nm. Contudo, para propósitos de entrega de drogas elas não devem ser maiores que 200nm, para evitar opsonização e consequente eliminação pelo sistema reticuloendotelial.

Comparado aos sistemas de entrega de drogas baseados em polímeros, as vantagens em se usar nanopartículas inorgânicas para entrega de drogas são que podem aumentar a eficiência e também facilitar o monitoramento por imagens e monitoramento da eficácia do tratamento. Uma classe das nanopartículas inorgânicas que é amplamente utilizada como sistema de entrega de drogas são as nanopartículas de óxido de ferro superparamagnéticas (SPIONs). Elas podem ser preparadas em vários tamanhos (que podem ser definidos em termos do tamanho hidrodinâmico ou tamanho do núcleo), são biocompatíveis e possuem um amplo faixa de propriedades mais interessantes e complexas, que são úteis para a entrega de fármacos, que as nanopartículas inorgânicas baseadas em carbono ou sílica. A maior vantagem das SPIONs como sistemas de entrega de fármacos deriva de seu comportamento magnético.

Isto as permite agir como agentes de contraste em ressonância magnética de imagem (RMI), o que é atualmente uma das mais populares e amplas técnicas médicas de imagem disponível. Isto também as permite serem guiadas e mantidas em uma localidade desejada, por meio de um campo magnético e induzir um aquecimento local, em uma região tumoral, utilizando hipertermia fluida magnética.

Isto pode ser usado como gatilho para liberação para uma droga carregada ou para causar a morte celular por apoptose induzida por temperatura, Estas propriedades dá as SPIONs uma ampla faixa de potenciais aplicações como agentes teranósticos avançados (medicamentos que são úteis para ambos, terapia e diagnóstico) e nanocarreadores para entrega de drogas. Por exemplo, elas podem potencialmente serem entregues em uma região do tecido tumoral via condução magnética, local onde seria liberada a droga carregada/aderida enquanto todo o processo estaria sendo acompanhado por

RMI. Contudo, as propriedades magnéticas das SPIONs também apresentam algumas desvantagens e desafios; notavelmente, elas aumentam a tendência das partículas em se agregarem. Portanto, SPIONs são comumente combinadas com poliméricos biológicos ou sintéticos, para formarem nanoestruturas como os nanoclusters magnéticos ou aprisionados em matrizes sensíveis a estímulos orgânicos ou micelas magnéticas, dentre outros.

AVANÇOS NO USO DE SPIONs PARA ENTREGA DE DROGAS

Estratégias que explorem as propriedades magnéticas intrínsecas dos carreadores de drogas baseados em SPIONs se baseiam em sua forte resposta a um pequeno campo magnético aplicado. Além disso, uma vez que o tamanho das SPIONs diminui abaixo de um limiar característico elas se tornam paramagnéticas (25nm para Fe_3O_4 e 30 nm para a $\gamma\text{-Fe}_2\text{O}_3$)⁴¹. Isto facilita grandemente sua visualização por aumentar seu contraste em imagem, assim como sua habilidade em ser manipulada no espaço por um campo magnético e sua capacidade de induzir calor localmente. Conseqüentemente, as partículas superparamagnéticas não apresentam magnetização remanescente e podem apresentar uma melhor estabilidade coloidal.

Superparamagnetismo é um efeito de tamanho finito, que surge quando o tamanho da nanopartícula cai abaixo de um valor limiar, entrando em um estado de domínio único, por exemplo, um estado em que todos os momentos magnéticos atômicos dentro da nanopartícula apontam em um mesmo eixo de direção de magnetização, estabelecida e mantida pela anisotropia magnética das partículas. Assim, em esta do domínio único, pode-se definir o momento magnético de uma nanopartícula, geralmente denominado superspin, como um simples produto da magnitude de todos os momentos magnéticos atômicos dentro da nanopartícula e apontando ao longo do eixo de fácil magnetização. Desta forma, todos os momentos magnéticos estão alinhados devido a troca de interações magnéticas. Uma vez em estado de superparamagnetismo, o superspin flutua entre as direções favorecidas pela anisotropia magnética da partícula, se a energia térmica fornecida ao sistema é suficiente para superar as barreiras impostas pela anisotropia magnética da nanopartícula, em um nível atômico, todos os momentos magnéticos dos átomos flutuarão, mas de uma forma cooperativa, devido troca de interações existentes, mantendo o alinhamento magnético mútuo dos átomos dentro das nanopartículas.

O campo magnético externo irá segurar a nanopartícula no local tumoral se as forças magnéticas excederem as forças de arraste hidrodinâmicas exercidas pela corrente sanguínea. Uma vez que os carreadores de drogas estiverem concentrados no local do tumor, com o auxílio de um campo magnético externo, a droga é liberada pela atividade enzimática ou pelas alterações das condições fisiológicas (alguma combinação do pH, temperatura ou osmolaridade).

Nanopartículas baseadas em $\gamma\text{-Fe}_2\text{O}_3$ e Fe_3O_4 têm se provado serem particularmente promissoras devido a suas propriedades magnéticas; elas são ambas ferrimagnéticas e suas nanopartículas apresentam comportamento superparamagnético. Além disso, SPIONs possuem baixa toxicidade, são biodegradáveis, considerável biocompatibilidade e eficientemente eliminadas pelo corpo humano, através do metabolismo do $\text{Fe}^{42,43}$. Nanopartículas alternativas são baseadas em nanometais (ferro, cobalto ou níquel), nanoalojamentos ou granadas contendo ferro. Contudo, elas são mais tóxicas que óxidos de ferro e devem, desta maneira ser funcionalizadas com outros compostos para reduzir esta toxicidade.

Até o presente momento, tem sido demonstrado que a eficiência do direcionamento magnético depende de vários parâmetros. Além das propriedades magnéticas intrínsecas do veículo e das características do campo magnético aplicado (força e gradiente), é importante considerar os parâmetros hidrodinâmicos e fisiológicos, como a rota de infusão, tempo de meia vida na corrente sanguínea, a reversibilidade/força da ligação da droga/carreador e o volume do tumor.

Como já citado, o magnetismo das nanopartículas de óxido de ferro as rende fácil aquecimento por um campo magnético externo, para agirem como sondas em tratamentos de câncer por magnetohipertermia⁴⁴, onde o aquecimento é acompanhado através da frequência (aplicando um campo magnético variável).

MAGNETOHIPERTERMINA (MHT)

Basicamente, hipertermia significa uma elevação anormal da temperatura corporal. Isto pode ser causado como parte de um tratamento, por uma infecção ou por uma exposição ao calor. E a terapia por hipertermia é um tipo de tratamento no qual o tecido corporal é exposto a altas temperaturas, para danificar e matar células cancerígenas ou para fazer estas células mais sensíveis ao efeito de radiações e certas drogas anticâncer⁴⁵.

O tratamento por hipertermia pode ser dividido basicamente em duas partes, hipertermia interna e hipertermia externa. Na hipertermia externa o calor é aplicado de uma fonte externa ao corpo, usando-se vários meios, como micro-ondas, radiofrequência, ultrassom, etc. Enquanto na hipertermia interna certas substâncias exógenas, como nanopartículas magnéticas, são inseridas dentro do corpo para agir como fontes de calor⁴⁶.

MEDIADORES MAGNÉTICOS PARA MAGNETOHIPERTERMINA

Devido a excelente dissipação de calor em campo magnético de corrente alternada, vários tipos mediadores magnéticos tem sido desenvolvidos. Os mediadores magnéticos principalmente trabalham na liberação do calor por perdas magnéticas, por exemplo, a quantidade de energia do

campo magnético convertida em calor durante inversão da magnetização. São causados por processos que ocorrem no sistema de partículas:

- i) histerese,
- ii) relaxação Braowniana ou de Neel,
- iii) corrente parasita,
- iv) perdas friccionais em suspensões⁴⁷.

A perda de histereses é devido ao processo de magnetização irreversível em um campo magnético de corrente alternada, originado principalmente em partículas com multidomínio. Com a diminuição do tamanho da partícula existe a ocorrência da rotação homogênea de magnetização, através do estado de pseudo domínio único, em que são observadas as perdas de relaxamento Neel. A transição de multidomínio da partícula para domínio único depende principalmente do tamanho da partícula, o que depende completamente das propriedades intrínsecas do material.

Tipicamente, esses materiais que possuem grande geração de energia de aquecimento por unidade de massa de partícula são aplicados principalmente em hipertermia. Portanto vários tipos de nanopartículas magnéticas são desenvolvidas e usadas como mediadores magnéticos. O tipo mais bem sucedido e que tem sido amplamente investigado consiste em nanopartículas superparamagnéticas de óxido de ferro (SPION)⁴⁸. Juntamente a essas vários tipos de nanopartículas baseadas em óxido de ferro, tais como MFe_2O_4 ($M = Co, Ni, Mn, Zn, Cu, Mg$ etc) e LSMO têm sido desenvolvidos e investigados para hipertermia. Até agora, nanopartículas magnéticas baseadas em óxido de ferro são usadas predominantemente como mediadores em hipertermia. Hoje em dia os mediadores magnéticos são comercializados pela Chemicell, Micromod e Bayer-Schering⁴⁹.

EFEITOS ESPECIAIS DOS MEDIADORES MAGNÉTICOS BASEADOS EM ÓXIDO DE FERRO

Vários métodos estão sendo desenvolvidos para sintetizar nanopartículas magnéticas, o sucesso de sua aplicação como nanopartícula magnética é altamente dependente da estabilidade da partícula em diferentes condições. Mas o melhor desempenho da partícula ocorre quando a mesma está abaixo de um tamanho crítico, por exemplo, na faixa de 10-20nm, faixa na qual promove seu uso em várias aplicações.

Abaixo do tamanho crítico, as nanopartículas magnéticas se comportam como partículas em domínio único, apresentando comportamento superparamagnético quando a temperatura é superior a chamada temperatura de bloqueio. Essas nanopartículas individuais se comportam como gigantes átomos paramagnéticos com um grande momento magnético constante, coercividade zero e reminiscência insignificante⁵⁰. Esses recursos tornam as nanopartículas magnéticas muito atraentes para uma ampla gama de aplicações biomédicas. No entanto, duas questões importantes, efeito do tamanho finito e controle dos efeitos magnéticos de superfície das nanopartículas magnéticas oferecem condições especiais para este tipo de material.

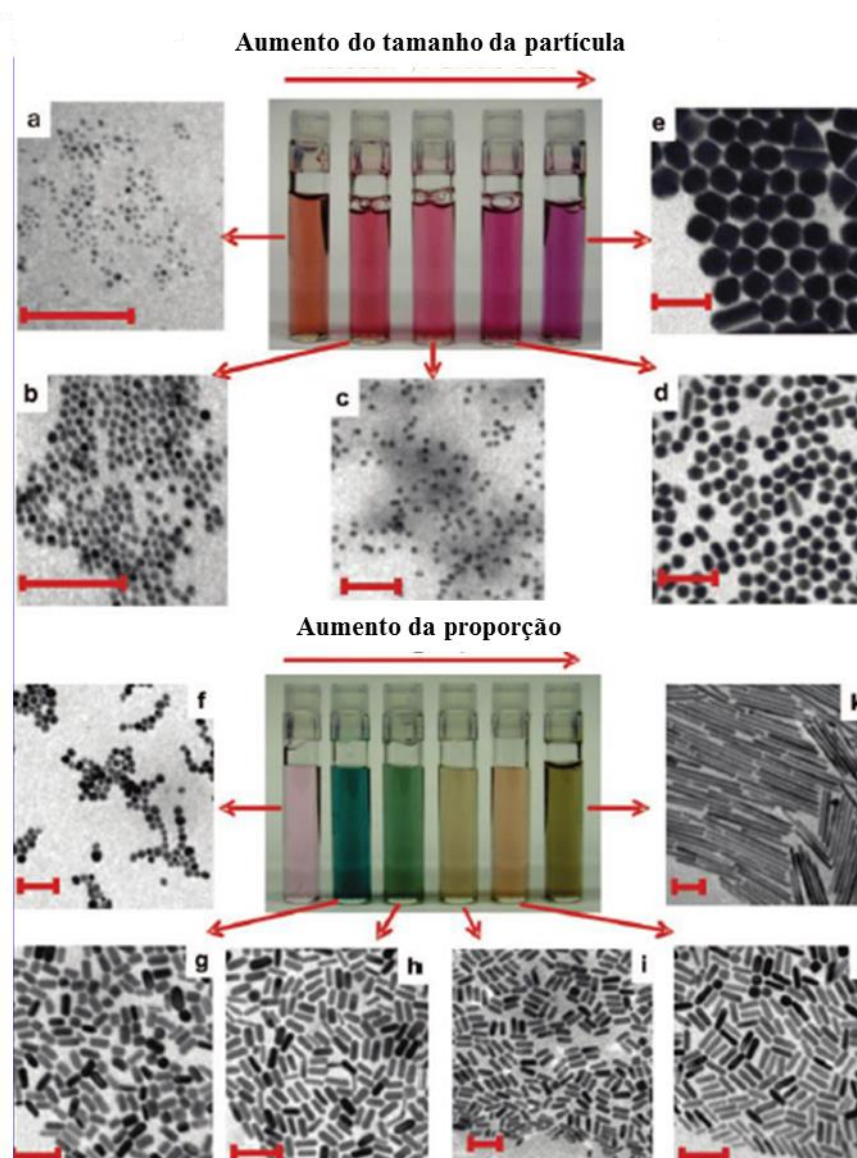
NANOPARTÍCULAS DE OURO

O ouro tem sido o objeto de fascínio por longa data, tanto por seu valor medicinal como por seu valor ornamental^{51,52,53}. O ouro vermelho para vitral era conhecido pelos artesãos medievais como “ouro finamente dividido”, disperso em vidro liso⁵⁰⁻⁵⁴. As amostras de ouro coloidal de Michael Faraday, as quais foram feitas em solução, ainda estão em exibição no Museu de Faraday, em Londres⁵³. Nos dias atuais é sabido que nanopartículas de ouro (~100nm ou menos) são responsáveis por cores brilhantes. O que faz o ouro nanoparticulado aparecer na cor vermelha ou roxa, ou outras cores diferentes do dourado presente em sua forma mais aglomerada? A resposta quantitativa é de certa forma surpreendentemente complicada⁵⁵, mas qualitativamente a imagem é razoavelmente clara. Na faixa de 5-200 nm de diâmetro, as nanopartículas de ouro são grandes o bastante para suportar uma banda de condução, são comparáveis ao percurso livre médio do elétrons no metal à temperatura ambiente (~100 nm), mas são bastante pequenos em comparação com os comprimentos de onda da luz visível (~400 – 750 nm). Irradiação com luz em certas frequências resultam em oscilações coletivas dos elétrons na superfície das partículas, conhecidas como “oscilações plásmicas” ou “Plasmônicas”⁵⁶ ou “ressonância plasmônica localizada na superfície”, RPLS. As propriedades ópticas de pequenas nanopartículas metálicas são dominadas por tais oscilações coletivas que estão em ressonância com a radiação eletromagnética incidente. Para o ouro, isto acontece na mesma frequência de ressonância que sua oscilação, governada pela sua constante dielétrica aglomerada, que se encontra na região visível do espectro eletromagnético⁵⁶. Devido ao fato das nanopartículas possuírem uma elevada área superficial, a frequência plasmônica é primorosamente sensível á natureza dielétrica (índice de refração) de sua interface com o meio em que se encontra. Qualquer mudança nas redondezas dessas partículas (modificações superficiais, agregação, índice de refração do meio, etc.) conduz a mudanças colorimétricas de dispersão^{57,58,59}. Agregação particular conduz ao acoplamento plasmônico, com uma mudança concomitante de frequência plasmônica, resultando em uma sensibilidade superficial que tem sido amplamente usada em detecção química, assumindo que a agregação química é controlada pela química de superfície^{57,58}. Não somente a luz é fortemente absorvida pelos plasmons, mas também a dispersão de Rayleigh (elasticamente), e com o aumento da partícula, maior é a saída de luz dispersa em relação é luz absorvida⁵⁵. Devido à luz espalhada pelas nanopartículas de ouro na porção visível do espectro eletromagnético de acordo com suas bandas plasmônicas, é possível opticamente traçar a posição individual de cada nanopartícula, pavimentando o caminho para aplicações de imagens.

Na década passada, numerosos avanços químicos na síntese de nanopartícula de ouro, que não sejam esféricas, especialmente formatos anisotrópicos, como os nanobastões têm aberto ainda mais possibilidades para aplicações em sensores e imagens, por várias diferentes razões. Primeiro, nanobastões de ouro tipicamente exibem duas bandas plasmônicas (uma no visível e outra tanto no

visível quanto no infravermelho próximo) que são tunáveis dependendo da dimensão do nanobastão; estas duas bandas correspondem aos modos plasmônicos de eixo curto (transversal) e ao de eixo longo (longitudinal)^{60,61,62}. Assim, se alguém desejar que nanopartículas de ouro absorvam em certo comprimento de onda ou frequência de luz no visível ou infravermelho próximo, pode-se produzir partículas com formato apropriado para tal fim. Segundo, nanopartículas anisotrópicas podem ter diferentes reatividades químicas para diferentes faces cristalinas⁶⁰⁻⁶². Esta propriedade pode conduzir para novas estratégias de montagem ou estratégias de detecção química, por exemplo, a banda plasmônica longitudinal e não a transversal, ocorrendo assim um deslocamento para o vermelho, devido à agregação ponta a ponta dos nanobastões de ouro⁶³.

Figura 3: Fotografia de soluções aquosas de nanoesferas de ouro (imagens superiores) e nanobastões (imagens inferiores) em função do incremento em sua dimensão.



APLICAÇÃO DE NANOPARTÍCULAS DE OURO COMO AGENTES DE CONTRASTE EM RAIOS X – APLICAÇÕES EM MICROCT

Ao longo da última década, nanopartículas de ouro (AuNPs) tem ganhado atenção como um agente de contraste para raio x, seguindo relatórios iniciais propostos por Hainfeld *et al.* Em 2004 e 2006^{64,65}. Subsequente interesse acadêmico e clínico, Como medido pelo número anual de publicações sobre AuNPs como agente de contraste de raios X têm crescido de forma constante devido a uma série de propriedades favoráveis das AuNPs. O ouro exibe um coeficiente de atenuação de raios X relativamente alto em comparação com sulfato de bário e iodo, especialmente nos níveis de energia utilizados para CT clínica⁶⁶. Além disso, AuNPs exibem um maior tempo de retenção vascular se comparado com moléculas iodadas, devido ao seu mais elevado peso molecular, o que potencialmente aumenta a janela de viabilidade para imagens⁶⁵. AuNPs são prontamente funcionalizadas para melhorar a estabilidade coloidal e/ou atuar como entregador de fármacos. De fato, um aumento incisivo no número de publicações sobre as AuNPs como agentes de contrastes para raios X ocorreu em 2010, quando vários grupos demonstraram alvos ativos *in vivo* com AuNPs funcionalizadas em sua superfície, fato que capacitava a geração molecular de imagens com CT^{67,68,69,70}. Investigações das AuNPs como agentes de contraste para raios X podem ser categorizadas por três potenciais aplicações em imagem de diagnóstico⁷¹: conjunto sanguíneo, alvo ativo e alvo passivo. Agentes de contraste “piscina de sangue” são designados para permanecer na corrente sanguínea por um tempo prolongado, limitando a difusão através do endotélio vascular⁷² a fim de permitir uma maior janela de imagem⁷³. Alvo passivo consiste em uma acúmulo não específico de AuNPs dentro de um sítio de interesse aumentando a permeabilidade e o efeito da retenção, fazendo com que moléculas de tamanho apropriado ou nanopartículas acumulem mais prontamente nos tecidos tumorais, em comparação com os tecidos circundantes saudáveis^{74,75}. A vascularização tumoral é descrita como permeável devido a uma distorção da camada endotelial dos vasos sanguíneos, permitindo as AuNPs “escaparem” dos vasos e entrarem no meio tumoral. Alvo ativo é a habilidade de entregar e reter um agente de contraste a um lugar específico de interesse através da funcionalização de superfície com moléculas, como peptídeo ou anticorpos, que exibam uma afinidade específica com o referido alvo^{74,75}.

TOXICIDADE

AuNPs menores que 2 nm são mais propensas a induzirem toxicidade que as AuNPs maiores (≥ 3 nm)^{76,77,78,79,80}, devido a habilidade das nanopartículas menores que 2 nm de se ligar de forma irreversível a biomoléculas, incluindo ao DNA⁸⁰. AuNPs maiores que 3 nm são consideradas não tóxicas *in vitro* e *in vivo*^{75,77}; contudo, toxicidade a longo prazo é dependente da acumulação das AuNPs em órgãos específicos. É importante lembrar que AuNPs de 10-20 nm exibem a mais ampla biodistribuição, resultando em mais órgãos sendo expostos às AuNPs. Por outro lado, AuNPs maiores permitem a entrega de uma maior concentração de massa, mas com menor número de nanopartículas. Sendo assim, evoluções sistemáticas da toxicidade a longo prazo das AuNPs de vários tamanhos são necessária tanto para nível celular quanto dos tecidos. Além disso, uma ênfase deve ser colocada da

potencial toxicidade hepática, devido ao fígado apresentar um maior acúmulo de AuNPs, independentemente do tamanho das mesmas.

EFEITO DOS LIGANTES NA TOXICIDADE

O efeito da funcionalização na toxicidade é relacionada a alteração da biodistribuição das AuNPs funcionalizadas superficialmente em comparação com as AuNPs nuas. Contudo, como já mencionado, a maioria das AuNPs administradas *in vivo* se acumulam no fígado. Um objetivo dos alvos ativos é reduzir o acúmulo das AuNPs em órgão saudáveis. Infelizmente, este objetivo não tem sido alcançado para administração intravascular das AuNPs. Por exemplo, AuNPs orientadas apresentam um aumento de seu acúmulo nos tumores, em comparação às não orientadas, mas a massa acumulada de AuNP, direcionada para o tamanho de interesse ainda é inferior a encontrada no fígado ou no baço⁸¹. A administração localizada (intratumoral e intramamária) melhorou de forma notável o acúmulo das AuNPs na área de interesse, em relação à outros órgãos^{82,83,84,85} e pode oferecer assim, um meio alternativo de fornecer a concentração de massa necessária ao local de interesse, minimizando a concentração das mesmas no fígado.

SÍNTESE QUÍMICA DE NANOPARTÍCULAS DE OURO COM DIFERENTES TAMANHOS E FORMAS

Simple redução do sal metálico por agentes redutores de forma controlada produz nanopartículas esféricas, por que as esferas são a forma de menor energia. Alguns dos métodos mais conhecidas e usados para sintetizar nanopartículas esféricas de ouro incluem (a) o método Turkevich (1951) envolvendo a redução do cloreto de ouro pelo citrato produzir nanopartículas de 15 nm em águas fervente, (b) o relacionado método de Frens (1973), (c) e o método de Brust (1994) para nanopartículas de ouro menores (~2 nm), no qual uma solução de aquosa contendo íons de ouro é transferida para uma fase orgânica, mediada por agente de transferência de fase, seguido pela redução com borohidreto de sódio, (d) o método da microemulsão em que os sais de ouro são reduzidos no núcleo aquoso das micelas invertidas, e (e) o método de sementeamento em que sementes de partículas de ouro (preparadas por um dos outros métodos) são usadas para crescerem mais ouro na presença de um fraco agente redutor⁸⁶.

Estudos sobre a cinética do crescimento e propostas do crescimento anisotrópico para nanobastões de metais têm sido documentados por alguns grupos^{87,88}. Têm-se notado que nanoesferas de sílica com uma capa nanométrica de ouro (“nanocamadas”) também apresentam absorção tunável no visível e no infravermelho próximo, e estes materiais são objetos de alguns estudos⁸⁹.

TERAPIA FOTOTÉRMICA (TFT) BASEADA EM NANOSFERAS DE OURO

Terapia fototérmica, uma estratégia terapêutica minimamente invasiva, na qual a energia dos fótons é convertida em calor suficiente para destruir células cancerígenas, tem sido usada para tratar câncer em algum grau nas últimas décadas⁹⁰. Fontes de calor, incluindo infravermelho próximo ou luz visível, ondas de radiofrequência, microondas e ondas de ultrassom têm sido usados para induzir o aumento moderado da temperatura em uma determinada região para destruir células cancerígenas, clinicamente denominadas como hipertermia. Devido ao pequeno coeficiente de absorção dos absorventes dos tecidos naturais, corantes orgânicos sintéticos, como a indocianina verde, naftalocianinas e porfirinas coordenadas com metais de transição são administradas externamente dentro dos tecidos tumorais para aumentar os efeitos fototérmicos. Como as moléculas corantes fobloqueiam rapidamente a TFT não tem sido usada amplamente em situações clínicas.

Recentemente a TFT tem atraído novos interesses na batalha contra o câncer devido a geração de uma nova classe de agentes fototérmicos sintéticos, ouro manométrico. O ouro manométrico apresenta uma eficiência na absorção da luz bem acima dos corantes moleculares convencionais. Por irradiação com radiação eletromagnética um forte campo eletromagnético é induzido, devido a excitação dos elétrons do ouro manométrico. A relaxação rápida desses elétrons excitados produz um forte calor localizado capaz de destruir células cancerígenas próximas por hipertermia ou outro efeito térmico. Esta terapia fototérmica induzida pelas nanopartículas plasmônicas de ouro é chamada de terapia fototérmica plasmônica (TFTP)⁹¹.

TFTP envolvendo agentes de contrastes baseados em nanopartículas de ouro foi reportado pela primeira vez por Lin e colaboradores em 2003, usando nanosferas de ouro em combinação com laser visível nanosegundo pulsado⁹². Nanopartículas anti-CD8 de imunoouro ligadas especificamente a células de linfócitos T e submetidas subsequentemente a irradiação com pulsos de laser levaram a destruição de mais de 90% das células. TFTP visível em células cancerígenas usando nanopartículas de ouro com pulsos de laser tem sido extensivamente estudado por posteriormente a esta evidência por Zharov et al⁹³. Foi achado que a morte das células poderia ser induzida por um único nanosegundo de pulso a uma energia de 2-3 J/cm² com 10-15 nanopartículas por célula. TFTP visível para células cancerígenas foi mais tarde estudada pelo grupo de El-Sayed, usando um laser contínuo de íons de argônio⁹⁴. Utilizando um modelo numérico, o grupo encontrou que por volta de 75°C foi alcançada morte celular com aquecimento por laser e nanopartícula nas células⁹⁵. TFTP visível pode ser usada para estudos fundamentais em células, mas sua aplicação prática em estudo *in vivo* é limitada, pois a luz visível não penetra bem nos tecidos. Para terapia *in vivo* e clínica de tumores subcutâneos e em estados mais profundos dentro do tecido, é necessário utilizar luz no infravermelho próximo, pois este apresenta uma melhor penetrabilidade, devido à mínima absorção da hemoglobina e das moléculas de

água nos tecidos em regiões específicas. Sendo assim, Absorção nanopartículas plasmônicas com infravermelho próximo são favorecidas na TFTP em câncer.

NANOPARTÍCULAS DO TIPO NÚCLEO-CAMADA (CORE-SHELL)

Nanopartículas de óxido de ferro, principalmente magnetita (Fe_3O_4) e maguemita ($\gamma\text{-Fe}_2\text{O}_3$), possuem várias aplicações no campo biológico⁹⁶ devido ao seu tamanho reduzido, propriedades físicas (como as ópticas e magnéticas) e capacidade química para modificação de superfície, o que não somente auxilia no aumento da biocompatibilidade/especificidade, mas pode resolver o duplo propósito que são as aplicações em terapia e o diagnóstico – o teranóstico – destes nanomateriais⁹⁷. Desta forma, conciliar óxido de ferro magnético com ouro metálico, para formar um heteromaterial núcleo-camada, tem atraído um vasto interesse para aplicações como materiais multifuncionais⁹⁸.

Nanocompósitos núcleo camada é definido como uma nanopartícula com um único núcleo e completamente coberta por uma camada. Em contraste com a estrutura núcleo-satélite, a superfície do núcleo é completamente ocultada embaixo da camada, diminuindo as propriedades do material nuclear. A superfície uniforme do nanocompósito core-shell pode ser melhor funcionalizada com novos ligantes para gerar estruturas bem definidas.

Estruturas de compósitos core-shell FexOy@Au uniformes tem sido extensivamente usados em algumas diferentes aplicações. Geralmente, existem duas estratégias diferentes para sintetizar estruturas de compósitos core-shell FexOy@Au . Estruturas core-shell FexOy@Au podem ser alcançadas tanto pelo recobrimento uniforme com uma camada de Au de uma estrutura núcleo-satélite FexOy@Au ou recobrimento diretamente um núcleo de FexOy . A cobertura com uma camada de ouro requer a redução do HAuCl_4 . Quando compostos núcleo-satélite FexOy@Au são isolados ou preparados *in situ*, a nanopartícula satélite de ouro no núcleo FexOy irá servir como um local de nucleação para a cobertura com Au a partir da reação do Au^{3+} e o agente redutor. Esta estratégia é capaz de produzir uma ampla variedade de tamanho de camadas para núcleos de FexOy , variando de até 634 nm a 100 nm^{99,100}, com diferentes morfologias especiais como arroz¹⁰⁰ e cubos⁹⁹. Na intenção de se reduzir o HAuCl_4 a ouro metálico, vários agentes redutores foram reportados na intenção de facilitar este processo. Como por exemplo, formaldeído com cabonato de potássio^{99,100,101,102} e hidroxilamina (NH_2OH)^{103,104} são capazes de executar a redução do Au^{3+} . Em comparação, a redução com NH_2OH requer um controle mais cuidadoso da temperatura e sonicação¹⁰⁴, ou agregados e superfícies ásperas serão formadas¹⁰³. Enquanto que o formaldeído reduz o HAuCl_4 de uma forma mais facilmente controlável, desta forma, camadas mais regulares e controlavelmente mais grossas espessas de Au podem ser feitas sobre o núcleo de Fe_xO_y . Ajustando a razão de sementes de nanopartículas de Au para uma solução de HAuCl_4 , a espessura da camada de ouro pode ser controlada entre 11 a 45 nm⁹⁹. Além do uso de pequenas nanopartículas de Au como agentes

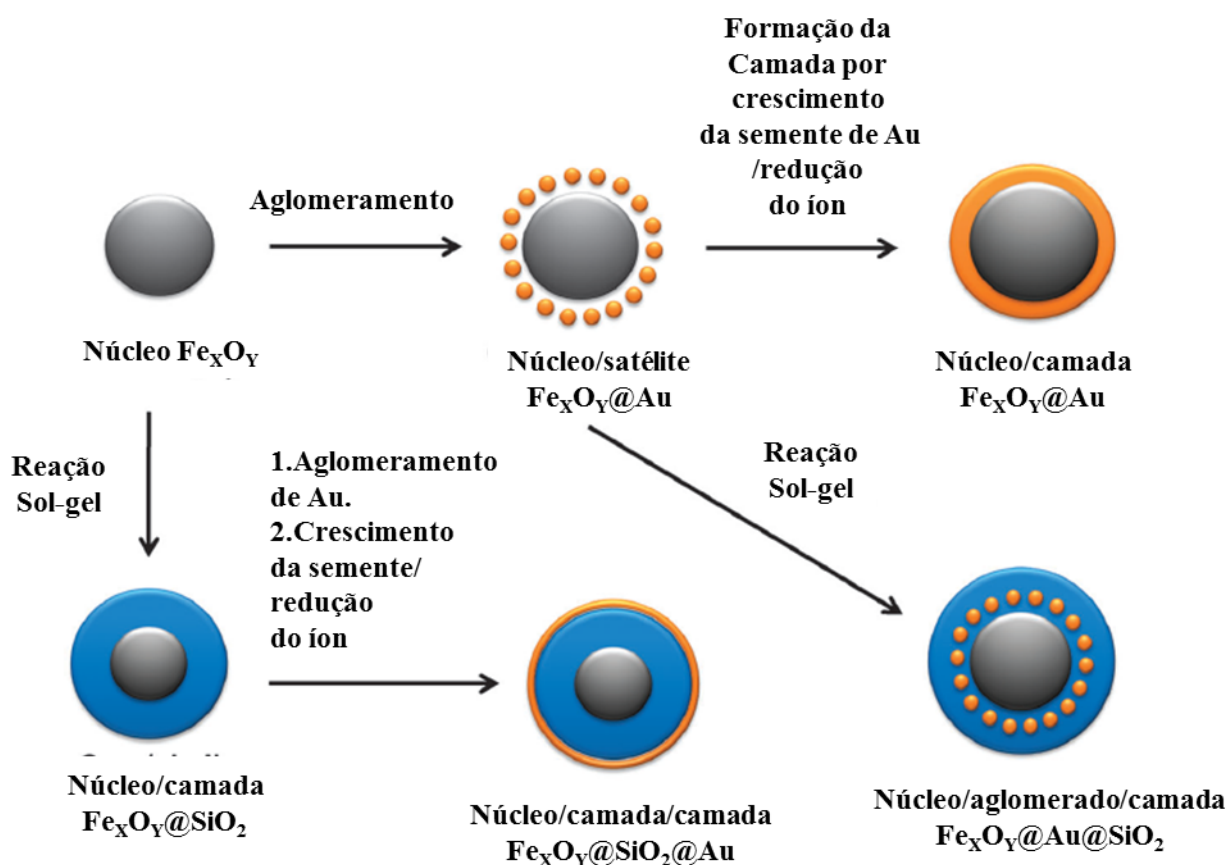
nucleadores para recobrirem com uma camada de ouro sobre o núcleo de Fe_xO_y , a cobertura de Au pode ser formada diretamente sobre a superfície da Fe_3O_4 ^{105,106}. Basicamente, a superfície do núcleo de Fe_3O_4 deve ser modificada com grupos funcionais que sirvam como modelos para a nucleação do ouro.

Estruturas Fe_xO_y -Au são basicamente materiais bicomponentes. Muitos cientistas estão interessados em estender o escopo dos nanocompostos do tipo Fe_xO_y -Au pela introdução de mais camadas de materiais sobre elas na abordagem de sínteses “All in one”. Recobrimentos com camadas de sílica são comuns logo após a síntese do núcleo de Fe_xO_y , devido a sua habilidade de estabilizar o núcleo de Fe_xO_y , evitando agregação. A camada de cobertura sobre a nanopartícula de Fe_xO_y , tetraetilortosilicato (TEOS) é o composto geralmente utilizado para as reações sol-gel. Durante a síntese dos nanocompostos de Fe_xO_y -Au, a camada de sílica é introduzida na intenção de aumentar o tamanho e a estabilidade do Fe_xO_y . Por exemplo, Huang *et al.* Reportou que as nanopartículas de Fe_xO_y primeiramente recobertas com a camada de sílica antes da construção da estrutura do núcleo-satélite e do núcleo-camada¹⁰⁷. Uma dupla camada de Au pode ser construída pelo revestimento da camada de sílica sobre a camada de Au interna, seguido por outro revestimento de camada de Au sobre a camada de sílica¹⁰⁸. Estruturas núcleo-satélite construídas em esferas funcionalizadas por aminas são instáveis, como falado anteriormente. A Figura 2 ilustra a formação de compostos multicamadas do tipo $\text{Fe}_x\text{O}_y@Au$ ¹⁰⁹.

Além da baixa toxicidade, a camada de ouro amplia a estabilidade coloidal e apresenta uma plataforma mais versátil para bioconjugação¹¹⁰. Desta maneira, uma das mais importantes características do ouro, em uma escala nanométrica, é a superfície plasmônica, que resulta em uma absorção óptica significativa na região do visível e do infravermelho próximo (IVP), com uma janela biológica de tecidos humanos, por exemplo, em uma região espectral onde os tecidos são parcialmente transparentes¹¹¹. Estas características fazem das Nanopartículas magnéticas de ouro do tipo núcleo-camada para terapia fototérmica, onde o aquecimento é realizado através da irradiação de luz¹¹². Além disso, devido a essas características ópticas, na área de diagnóstico, nanoestruturas de ouro podem atuar como sondas fluorescentes para imagens *in vivo*, por meio de tomografia computadorizada (TC)¹¹³.

Atualmente, tomografia computadorizada (CT) é uma das técnicas mais utilizadas para a geração de imagens no campo biomédico. CT proporciona uma visualização superior de estruturas ósseas devido ao contraste inerente entre a alta densidade eletrônica dos ossos e os tecidos moles circundantes, mais permeáveis. No entanto, a CT é limitada em distinguir entre diferentes tecidos moles, que possuem uma densidade semelhante¹¹⁴.

Figura 4. Representação esquemática da conversão de compósitos para multicamadas $\text{Fe}_x\text{O}_y@Au$.



O número atômico do ouro (79) é muito superior que o do contraste atualmente utilizado para CT – iodo (53), e desta forma o ouro pode induzir uma forte atenuação de raios X¹¹⁵. Além de que, o pequeno tamanho das moléculas contendo iodo permitem apenas pequenos tempos de imagem, devido a rápida excreção das mesmas pelos rins. Em contraste, as nanopartículas de ouro (GNP) podem ser de forma a superar estas barreiras biológicas e permanecer confinadas no espaço intravascular por períodos prolongados^{116,117,118}.

Utilizando técnicas simples de laboratório, nanopartículas de ouro tem sido fabricadas em diversas formas e tamanhos, sendo utilizadas como núcleos ou camadas para nanopartículas híbridas de sistemas núcleo camada do tipo metal-metal^{119,120}.

Além disso, para aperfeiçoar o desempenho óptico das nanopartículas de ouro, fluoróforos podem ser carregados em sua superfície. Particularmente, ftalocianinas, que são fotosensibilizadores capazes de converter uma energia luminosa específica em potencial químico, são poderosos candidatos para terapia fotodinâmica (TFD)¹²¹. Contudo, devido a sua elevada hidrofobicidade e tendência de auto-agregação em meio aquoso, o uso de ftalocianinas é limitado no meio biológico. Desta forma, ftalocianinas têm sido incorporadas em sistemas nanoestruturais, como nanoemulsões¹²², ou ligadas à superfície de nanopartículas magnéticas¹²³ e de ouro¹²⁴

resultando no melhoramento da atividade na TFD. Ainda na área de diagnóstico, como o ouro possui alta densidade eletrônica, ele induz uma forte atenuação de raios-X podendo ser utilizado como agente de contraste em imagem de tomografia computadorizada (TC)¹²⁵. Os contrastes convencionais baseados em iodo usualmente possuem desvantagens como um pequeno tempo de imagem e baixa especificidade. Este trabalho descreve a elaboração de nanoestruturas que são formadas por um núcleo magnético (maguemita) com uma camada de ouro, coberta com ftalocianina de alumínio, como nanoplataformas candidatas para combinação de técnicas de multiterapias e multi-imagens.

Nanopartículas recobertas com ouro, com diferentes espessuras de camadas, são sintetizadas pela redução do Au^{3+} mediada pelo borohidreto de sódio na presença de nanopartículas de maguemita recobertas com citrato, obtido pelo melhoramento da co-precipitação. Sendo assim, as estruturas núcleo-camada foram funcionalizadas, com base em nosso conhecimento, pela primeira vez, com ftalocianina de alumínio, resultando sols com longa estabilidade coloidal.

O potencial dos materiais sintetizados como agentes de contrastes em tomografia computadorizada foi desenvolvido *in vitro*, utilizando um microtomógrafo. O efeito do capeamento com ouro e adsorção da ftalocianina na atividade citotóxica das nanoestruturas foi investigado *in vitro* antes do material ser aplicado como apresentado.

Objetivo geral:

Elaborar e caracterizar nanopartículas núcleo-camada ($\gamma\text{-Fe}_2\text{O}_3\text{@Au}$), funcionalizadas com ftalocianina de alumínio visando aplicações em terapias (magnetohipertermia, terapia fototérmica e terapia fotodinâmica) e como contrastantes em técnicas de diagnóstico por imagem *in-vivo* (microtomografia e fluorescência).

Objetivo específico:

- Realizar a síntese das nanopartículas de maguemita pelo método de co-precipitação e posterior recobrimento das mesmas com citrato.
- Recobrir núcleo magnético (maguemita) com ouro metálico pela redução do íon Au^{3+} com boroidreto.
- Realizar a adsorção de ftalocianinas de alumínio na superfície desses materiais cobertos e descobertos com ouro, por meio de uma estratégia simples e eficiente.
- Caracterizar opticamente, estruturalmente, morfológicamente e magneticamente os nanomateriais sintetizados.

- Realizar teste de toxicidade destes materiais em células de queratinócitos – HaCAT e fibroblastos NIH3T3.
- Realizar testes de microtomografia computadorizada para verificar potencial capacidade de atenuação dos raios X, quantificados em Unidades de Houston (HU)

Este trabalho foi realizado no programa de Pós-Graduação em Ciências e Tecnologias da Saúde da Universidade de Brasília, que possibilita a defesa da tese de doutorado na forma de artigo. Nessa formatação exigem-se os tópicos: elementos pré-textuais, introdução geral com objetivos e justificativa, artigo submetido, discussão geral e anexos contendo critérios necessários para publicação na revista em questão, comprovação de submissão e classificação qualis na área interdisciplinar. A revista escolhida foi a Journal of Materials Chemistry B, da Royal Society

2- ARTIGO CIENTÍFICO

Maghemite-Gold core-shell nanostructures ($\gamma\text{-Fe}_2\text{O}_3\text{@Au}$) surface-functionalized with aluminium phthalocyanine for multi-task imaging and therapy

B. C. P. Coelho,^a E. R. Siqueira,^b A. S. Ombredane,^b G. A. Joanitti,^b S. B. Chaves,^b J. A. Chaker,^c J. P. F. Longo,^b R. B. Azevedo,^b P. C. Morais,^{d,e} M. H. Sousa^{*c}

In this study we report on elaboration and characterization of core-shell maghemite-Gold nanoparticles with shell modulated for different thicknesses below 2 nm. Gold-shelled maghemite nanoparticles with average core size about 9 nm were elaborated by a single-step protocol involving reduction of Au^{3+} in the presence of citrated-coated maghemite nanoparticles. Additionally, post-functionalization of the core-shell structures with aluminium phthalocyanine was successfully accomplished, aiming the production of a material platform for photodynamic therapy. The as-produced samples were structurally, morphologically, magnetically and optically characterized and presented long-term colloidal stability at physiological pH. Impressively, we found the as-produced samples showing good X-ray attenuation property, rendering them with ability to be used as a nanoprobe for targeted computed tomography. Moreover, *in vitro* nanocytotoxicity tests confirmed superior biocompatibility of the as-produced samples, making them a very promising multi-task platform for *in vivo* applications.

^a Instituto Federal de Educação Ciências e Tecnologia de Brasília, Gama, DF 72429-005, Brazil.

^b Department of Genetics and Morphology, Institute of Biological Sciences, Brasília University, Brasília, 70919-900, Brazil.

^c Green Nanotechnology Group, Faculdade de Ceilândia, Universidade de Brasília, Ceilândia, DF 72220-900, Brazil. E-mail: mhsousa@unb.br

^d Universidade de Brasília, Instituto de Física, Brasília DF 70910-900, Brazil.

^e Anhui University, School of Chemistry and Chemical Engineering, Hefei 230601, China.

See DOI: 10.1039/x0xx00000x

Introduction

Iron oxide nanoparticles, mainly magnetite (Fe_3O_4) and maghemite ($\gamma\text{-Fe}_2\text{O}_3$), found numerous applications in the biomedical field, credited to their size-dependent physical (e.g. magnetic and optical) and chemical (e.g. surface reactivity) properties, which can be used not only to improve biocompatibility and specificity, but also offer the way to achieve the dual goal of theranostics (diagnostics plus therapy)¹²⁶. Along this line, co-assembled nanosized magnetic iron oxide and metallic Gold in a core-shell heteromaterial has attracted broad interest, aiming its application as a multifunctional material nanoplatform¹²⁷. Magnetism associate with the core iron oxide renders for noninvasive manipulation (using gradient of magnetic field) and heating (using AC magnetic field), which are key features for site targeting and magnetohyperthermia¹²⁸, respectively. Additionally, while lowering nanotoxicity the Gold-shell increases long-term colloidal stability and presents a versatile platform for bioconjugation¹²⁹. Furthermore, at the nanoscale surface plasmon in Gold is enhanced, which results in

significant and tunable optical absorption and emission in the visible (VIS) and near-infrared (NIR) regions, covering the biological window of human tissues while allowing partial transparency to light¹³⁰. Therefore, in addition to magnetohyperthermia, Gold-shelled magnetic nanoparticles are useful in photothermal therapy, where localized heating is accomplished via light irradiation¹³¹. Besides, due to their unique optical properties Gold-based nanostructures can act as fluorescent probes for *in vivo* imaging¹³². Moreover, fluorophores can easily functionalize Gold-terminated surfaces, thus enhancing the optical performance of Gold-shelled magnetic iron oxide nanoparticles. Particularly interesting for surface-functionalization are phthalocyanines, which are photosensitizers capable of converting specific light energy into chemical potential and widely used in photodynamic therapy (PDT)¹³³. However, due to the high hydrophobicity and tendency to self-aggregate in aqueous medium the use of phthalocyanines is quite limited in the bioenvironment. To circumvent this drawback phthalocyanines have been incorporated into nanostructured systems, such as nanoemulsions¹³⁴ or linked to magnetic¹³⁵ and Gold¹³⁶ nanoparticle surfaces, resulting in improvement in PDT efficacy. Still in the diagnostics area, while presenting high electron density and strong X-ray attenuation Gold-based nanostructures can be used as contrast agents for computed tomography (CT) imaging¹³⁷. Worth mentioning that the conventional Iodine-based contrast agents usually present severe limitations, such as short imaging time and low specificity.

This study reports on the elaboration and investigation (structural, morphological, magnetic, optical, and biological) of nanostructures comprising a magnetic core (maghemite) surface-shelled with Gold, which is further surface-functionalized with aluminium phthalocyanine to act as a nanoplatform for multi-therapy and multi-imaging combined techniques. Gold-shelled maghemite nanoparticles, with Au-shell modulated for different thicknesses, were elaborated by borohydride-mediated reduction of Au³⁺ in the presence of citrate-capped maghemite nanoparticles, the latter obtained by co-precipitation in aqueous medium. Maghemite-Gold core-shell nanostructures surface-functionalized with aluminium phthalocyanine is a novelty in the literature, yielding sols with long-term colloidal stability and biocompatibility. The promising application of the as-elaborated materials as contrast agents in computed tomography imaging was herein evaluated using a commercial microtomograph (SkyScan1076, Bruker). In order to support the bioimaging application of the as-elaborated nanoplatform *in vitro* assays were performed to assess the nanocytotoxicity.

Experimental

All chemicals listed in the present report were of analytical degree and used as received without any further purification. Water used to perform the experiments was purified by a Milli-Q water system (Millipore, USA).

Samples

Citrate-capped maghemite nanoparticles (MNP)

As schematically shown in Fig. 1 citrate-capped maghemite (γ -Fe₂O₃) nanoparticles were synthesized using a slightly modified procedure already described in the literature¹³⁸. Briefly, 50 mL of aqueous solution containing 50 mmol of Fe²⁺, 25 mmol of Fe³⁺ and 20 mmol of HCl were quickly poured into 250 mL of NH₄OH aqueous solution (1 mol/L), under vigorous stirring (1000 rpm) at room temperature. The as-formed black precipitate of magnetite (Fe₃O₄) was magnetically separated and washed with water several times until the solution reached neutral pH. Then, the precipitate was acidified with HNO₃ aqueous solution (0.5 mol/L) and magnetically separated from the supernatant. Next, the slurry containing magnetite was oxidized to maghemite by boiling the precipitate with 0.5 mol/L Fe(NO₃)₃ for 30 min. The as-treated precipitate was removed out from the solution by magnetic decantation. Citrate-capped maghemite nanoparticle was prepared from the as-produced bare maghemite using trisodium citrate solution (1.0 mol/L) at 80 °C for 30 min (molar ratio of citrate to iron = 0.1). The obtained precipitate was magnetically collected, washed twice with acetone (excess of acetone evaporated), re-suspended in water, adjusted pH to 7.0 and labeled as sample MNP.

Gold-coated nanoparticles (MNP@Au1 and MNP@Au2)

Gold-shelled maghemite was formed by reduction of Au³⁺ (from HAuCl₄) onto citrate-capped maghemite nanoparticles using sodium borohydride (NaBH₄) as reducing agent (see scheme Fig. 1). Typical Au-coating protocol is as follows: 80 μ L of 400 mg/mL of the as-produced MNP sample was dispersed in 80 mL of water. Next, under sonication, 180 μ L of HAuCl₄ (1 ww%) was added. After 10 min, 150 μ L of NaBH₄ (0.3 mol/L, in ethanol) was added to the reaction medium and the system was sonicated for 10 min more. This HAuCl₄/NaBH₄ cycle was repeated four times and the final sample was

labeled MNP@Au1. Similarly, sample MNP@Au2 was produced, but the amount of H₂AuCl₄ and NaBH₄ was twice of that used to produce sample MNP@Au1.

Aluminium phthalocyanine-functionalized nanoparticles (MNP/PTC and MNP@Au/PTC)

In order to attach aluminium phthalocyanine (PTC) to the as-produced nanoparticles 100 μ L of aluminum phthalocyanine chloride (0.4 mmol/L in DMSO) was added to 7.5 mL (100 μ g/mL) of sample MNP (or MNP@Au2) to form the phthalocyanine-modified nanoparticles labeled as MNP/PTC (or MNP@Au/PTC). All PTC-functionalized samples were sonicated for 10 min, centrifuged to eliminate supernatant and re-dispersed in water. All the steps performed while preparing the final MNP/PTC, MNP@Au/PTC samples are schematically shown in Fig. 1.

Characterization

X-ray diffraction (XRD) powder analyses of the samples were carried out in a Miniflex 600 diffractometer (Rigaku) over 2θ range of $20^\circ - 70^\circ$, using Cu-K α radiation ($\lambda = 1.541 \text{ \AA}$) and operating at 40 kV and 30 mA. Size and morphology of the as-produced materials were examined by high-resolution transmission electron microscopy (HRTEM) using a JEOL 1100 apparatus. Room temperature magnetization curves were obtained using a vibrating sample magnetometer (VSM) ADE model EV7. Hysteresis loops were recorded in the ± 18 kOe range. Chemical analyses of the as-produced samples¹³⁹ were determined using an inductively coupled plasma optical emission spectrometer (ICP-OES) Perkin Elmer model Optima 8000, with radiofrequency power of 1400 W, 1.5 mL/min sample flux, 10 L/min argon plasma flux, nebulizer flux 0.7 L/min and flux of auxiliary gas (argon) of 0.2 L/min. Hydrodynamic average diameter (D_H), polydispersity indexes (PDI) and zeta potential (ξ -potential) of the as-produced nanoparticles were assessed from aqueous dispersions using a dynamic light scattering (DLS) Zetasizer nano ZS system (Malvern Instrument). Ultraviolet visible (UV-vis) spectra of aqueous dispersions were recorded on a spectrophotometer Shimadzu UV 2600. The X-ray density of samples was evaluated in plastic microtubes using a microtomograph device (SkyScan1076, Bruker) with the following parameters: 50kv, 180 μ A, 0.5nm Al filter, 100 ms of exposition and pixels size of 35 μ m. NRecon[®] and CTAn[®] softwares were employed respectively for reconstruction and image analysis. Slices were analyzed with Dataviewer[®] software. The Hounsfield scale (HU units) was used to quantify the X-ray density and a 3D image of the samples was prepared for qualitative evaluation.

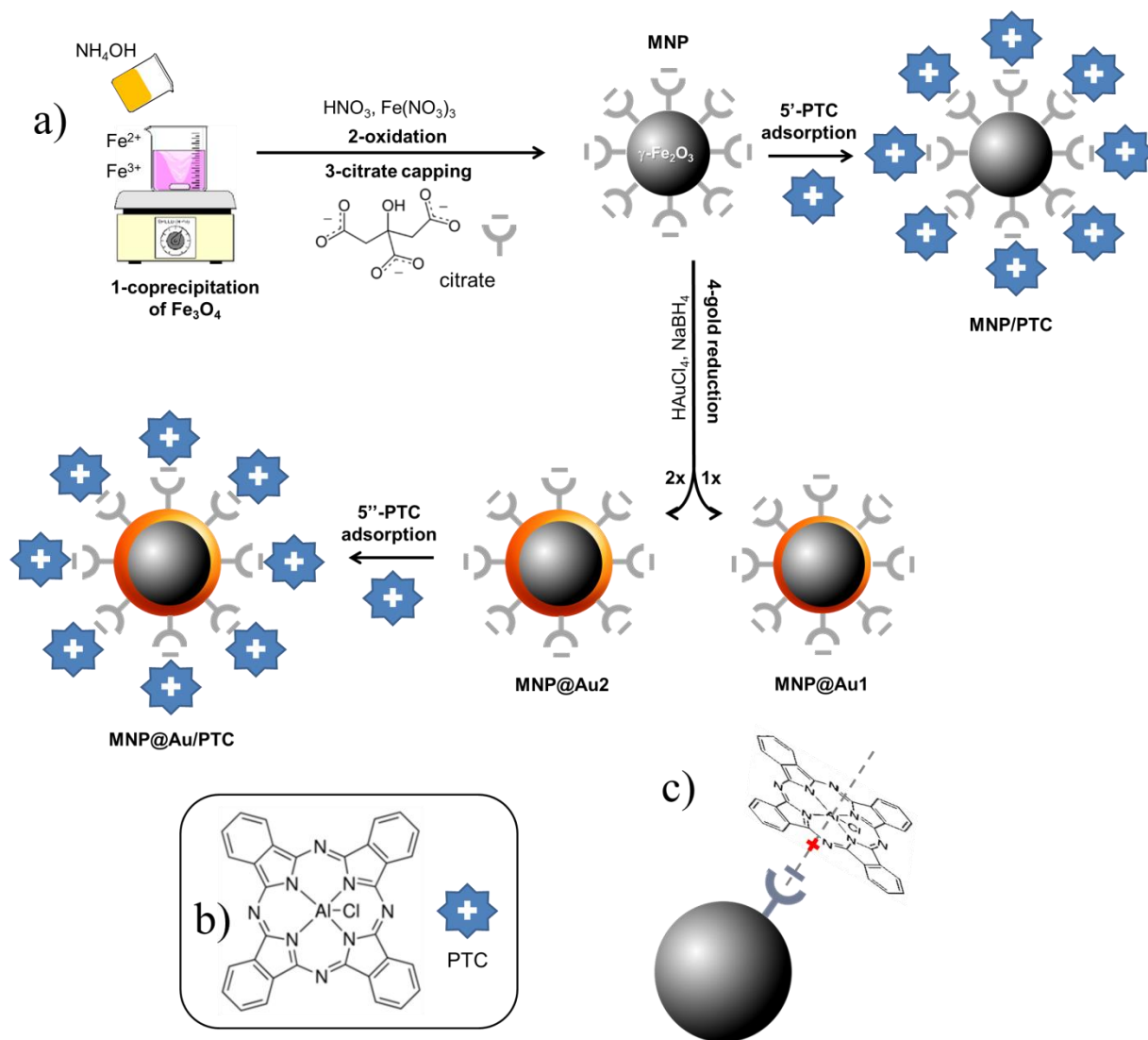


Figure 1. Scheme used in the preparation of samples MNP, MNP/PTC, MNP@Au1, MNP@Au2 and MNP@Au/PTC.

Cell culture

Murine fibroblast cells (NIH-3T3) and human keratinocyte cells (HaCAT) were acquired from cell bank of Rio de Janeiro (Brazil). *Dulbecco's Modified Eagle's Medium* (DMEM) (Life, EUA) completed with 10 % of fetal bovine serum and 1 % of antibiotic solution (100 IU/mL Penicillin – 100 $\mu\text{g}/\text{mL}$ Streptomycin, Life, EUA) was used to grow the cells at 37 $^\circ\text{C}$ and 5% CO_2 in humid atmosphere.

Cell treatment

The cells were grown into polystyrene culture flask of 75 cm². The cells were counted using a Neubauer chamber and the number of the cells per mL was determined by the equation:

Number of cells/mL = (number of counted cells/4)*dilution factor*104. For each experiment, the cells were seeded into a 96-well culture plates at the density of 3.103 cells per well in DMEM. The plates were incubated at 37 °C and 5% CO₂ in humid atmosphere overnight.

Table 1. Quantitative data of pool content

Groups	MNP and MNP@Au (µg/mL)	MNP and MNP@Au (µL)	H ₂ O (µL)	culture medium (µL)
Control	-	-	50	150
1	100	50	-	150
2	50	25	25	150
3	25	12,5	37.5	150
4	12.5	6.25	43.75	150
5	6.25	3.12	46.88	150

Cell-viability assay

Cell-viability assay was realized using MTT (3-[4, 5-dimethylthiazol-2-yl]-2,5-diphenyltetrazolium bromide) dry reduction method. After 24 and 72 hours of incubation, 150 µL of the MTT solution (0.5 mg/mL in DMEM) was added in each well and the plates were incubated for 2 hours at 37 °C and 5% CO₂ in humid atmosphere. The medium culture was discarded and 100 µL of dimethyl sulfoxide (DMSO) were added in each well. The absorbance was monitored using a spectrophotometer with a microplate reader at 595 nm (Molecular Devices, EUA).

Statistical analysis

The results were expressed as mean \pm standard error of the mean (SEM). Evaluation of possible significant differences among the groups was determined by analysis of variance (ANOVA) and Bonferroni post-hoc test using the program Prism 5 (EUA). The significance level was set at $P < 0.05$.

Results and discussion

Samples

Fig. 2 shows XRD spectra of samples MNP and MNP@Au2. For the employed synthesis route all diffraction peaks observed sample MNP are consistent with the standard data of maghemite (JCPDS card no. 39-1346). The average crystallite size of the magnetic core, calculated from the 311 XRD line broadening of sample MNP using the Scherrer's formula, is about 9.3 nm. Additionally, for the MNP@Au2 sample, the XRD peaks appearing at 38.4° and 44.6° can be respectively assigned to (111) and (200) crystalline plane diffraction peaks of Gold, in good agreement with standard data of Gold (JCPDS file no. 040784).

Moreover, one can notice a reduction of the maghemite XRD peak intensities after Au-capping, which is more likely due to the heavy atom effect of Gold as a result of the formation of Au-coated γ -Fe₂O₃ nanoparticles¹⁴⁰. Similar results were found in the XRD data of sample MNP@Au1 (XRD data not shown here). Chemical analyses using ICP-OES revealed samples MNP@Au1 and MNP@Au2 with increasing Gold content (Au/Fe₂O₃ ratio) of 7.3% and 12.1% (w/w), in agreement with the preparation protocol. Cross-linking ICP-OES data with XRD analyses strongly supports core-shell (γ -Fe₂O₃-Au) formation in samples MNP@Au1 and MNP@Au2, which is corroborated by the TEM data. As shown in Fig. 3a, maghemite nanoparticles (MNP) are polydisperse in size, but showing nearly spherical morphology. Moreover, the cubic structure of the maghemite phase is confirmed by fast Fourier transform (FFT) image shown in the inset of Fig. 3b (lower right hand-side), revealing planes (440), (311), (220) and (111) of the spinel phase. Figure 3c shows a typical TEM image of sample MNP@Au2, with darker γ -Fe₂O₃ nanoparticle spots (darker than in the MNP sample) due to the Au-shell. Sparse-filled (MNP) and dense-filled (MNP@Au2) histogram patterned bars, assessed from the TEM micrographs, are shown in Fig. 3d,

where black solid lines are the best fit using the lognormal size distribution. From this analysis, the average diameters (polydispersity index) of maghemite (MNP) and gold-coated nanoparticles (MNP@Au2) are respectively 12.9 nm ($\sigma = 0.34$) and 12.1 nm ($\sigma = 0.30$), suggesting there is no significant difference in average size and polydispersity index of uncoated and Gold-coated nanoparticles. However, HRTEM of Gold-coated nanoparticles shown in Fig. 3e clearly reveal core-shell formation with Au-shell thickness in the range of 1-2 nm, in good agreement with previous works¹⁴¹. Furthermore, Fig. 3f shows HRTEM of an isolated core-shell (Au- γ -Fe₂O₃) nanoparticle where the interfringe spacings of the face centered cubic (FCC) Gold (111) and (311) reflections are clearly seen in the FFT image (upper left hand-side inset), indicating that the maghemite nanoparticles are coated with a layer of crystalline Gold.

Magnetization measurements were performed for evaluating the Au-coating in the magnetic properties of the as-produced nanoparticles. Figure 4 shows typical room temperature magnetization as a function of applied magnetic field recorded for samples MNP (red data) and MNP@Au2 (black data). We found the saturation magnetization decreasing from 47.9 emu/g (sample MNP) to 44.6 emu/g (sample MNP@Au1) and 42.4 emu/g (sample MNP@Au2), supporting the claim that a magnetic core (maghemite) is coated with a non-magnetic shell (Gold).

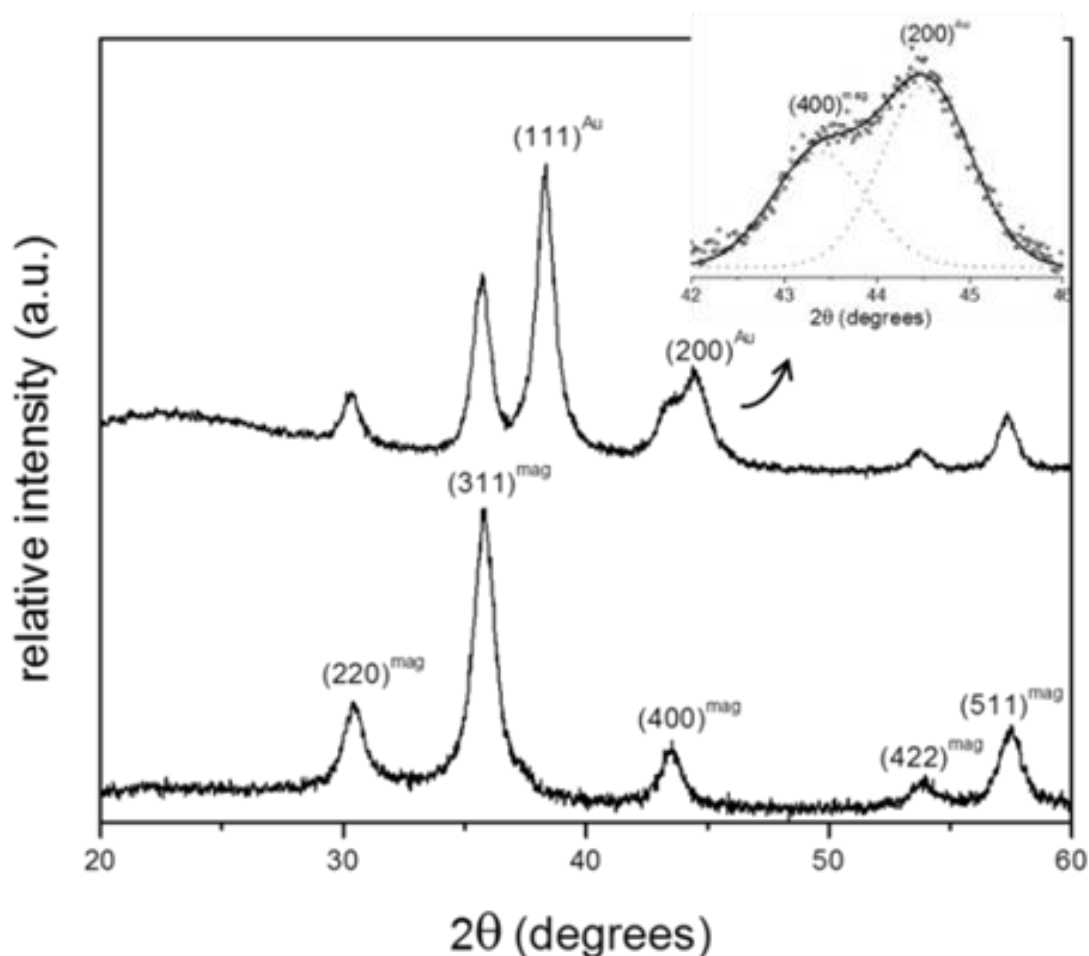


Figure 2 – Diffractograms of samples MNP (lower panel) and MNP@Au2 (upper panel). The inset shows a detail of the XRD spectrum of sample MNP@Au2 in the 2θ range of about 42° to 46° , emphasizing the deconvolution of the 44.6° XRD feature into two components.

Thus, considering there is no phase change of the magnetic core after Au-coating a Au/Fe₂O₃ ratio of 6.6% and 11.3% (w/w) can be estimated from the magnetization data respectively for samples MNP@Au1 and MNP@Au2, in good agreement with the chemical analysis (ICP-OES). Moreover, at room temperature the as-prepared uncoated and Gold-coated nanoparticles shows superparamagnetic behavior, with negligible remanence and coercivity as shown in Fig. 4 (see lower right hand-side inset). Besides, saturation magnetization of the as-prepared core maghemite is lower than typical bulk values (60–80 emu/g), credited to the nanometer size¹⁴² and surface functionalization¹⁴³. Likewise, the as-prepared samples functionalized with phthalocyanine also presented similar magnetic behavior, with no alteration of saturation magnetization. Moreover, as can be observed in the inset of Fig. 4 (upper left hand-side), separation of the magnetic nanoparticles out from the transparent solvent can be observed while adding acetone to the water-based suspension and

keeping a permanent magnet attached to the sample holder for several hours. This finding strongly indicates attachment of Gold and phthalocyanine onto maghemite nanoparticles.

The nature of maghemite surface-coating (Gold, citrate, and/or aluminum phthalocyanine) changes the interface nanoparticle surface/solution and thus colloidal stability, which indeed affects optical properties. Therefore, DLS and UV-vis spectroscopy were used to assess surface modification information of bare maghemite nanoparticles. Table 2 lists DLS data for the as-prepared samples. All measurements were performed at pH~7 and 25 °C. The ξ -potential of citrate-coated maghemite nanoparticles (sample MNP) is highly negative (about -38 mV) and is likely due to the ionization of attached citrate molecules onto the oxide surface^{144,145}. The ξ -potential of Gold-coated nanoparticles (samples MNP@Au1 and MNP@Au2) are also highly negative, not differing significantly from the value found for citrate-coated nanoparticles in sample MNP (see Table 2). Actually, it is well known that reduction of Gold in the presence of sodium citrate yields Gold-coated inorganic core nanoparticles with citrate molecules attached onto the surface, providing a negatively charged surface for the Au-coated nanoparticle¹⁴⁶. In the case of our samples, at neutral pH the free carboxyl groups of citrate are fully deprotonated, providing extra colloidal stability to the as-suspended nanoparticles via electrostatic repulsion. Magnetic separation of the as-produced sols (see inset of Fig. 4) is only achieved by adding a non-aqueous solvent, such as acetone.

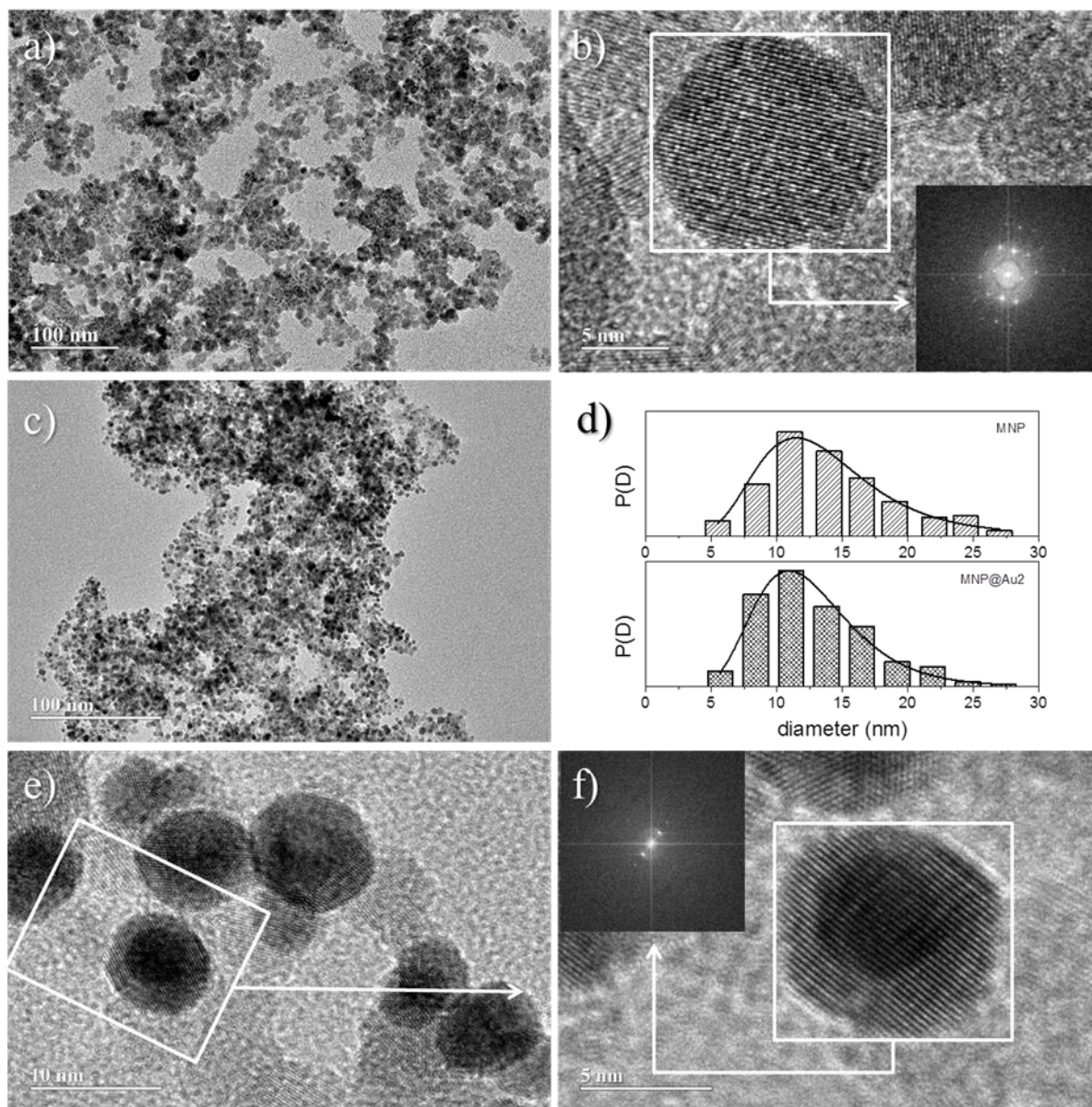


Figure 3 –TEM images of MNP (a) and MNP@Au2 (c) nanoparticles; HRTEM image of selected region in sample MNP (b); histograms of particle diameters for MNP and MNP@Au2 samples (d); HRTEM image of selected region in sample MNP@Au2 (e); magnified TEM image of the boxed region in the left image (f). The insets show the FFT calculated from the areas marked with white squares.

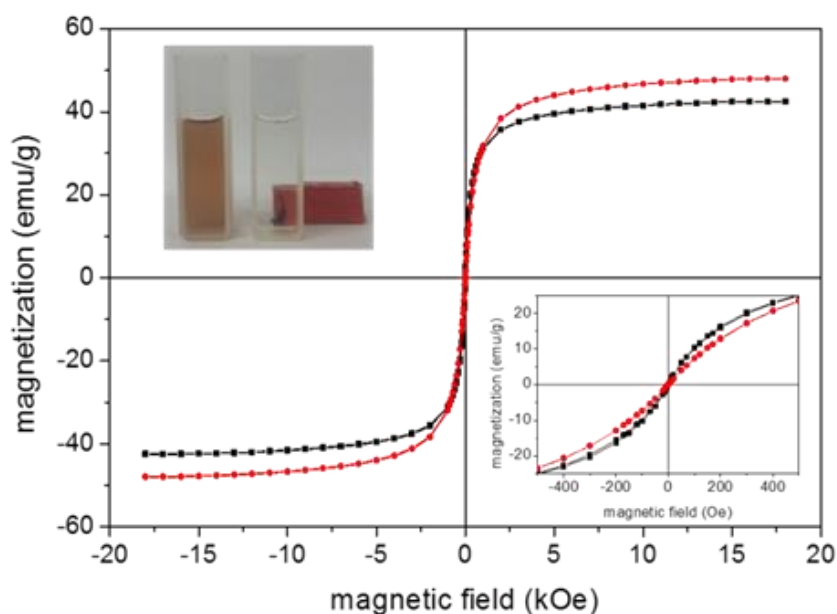


Figure 4. Magnetization hysteresis loops at room temperature for samples MNP (red) and MNP@Au2 (black); picture of the sample MNP@Au2 under action of a permanent magnet (upper left hand-side inset); magnetization at low field range (lower right hand-side inset).

Moreover, the hydrodynamic sizes of citrate-coated maghemite nanoparticles (sample MNP) increased from 68.1 nm to 114.3 nm and 156.6 nm for samples MNP@Au1 and MNP@Au2, respectively. This finding is credited to the increasing thickness of the deposited Gold-shell onto the maghemite core. However, possible nanoparticle agglomeration must be considered in this analysis. On the other hand, data listed in Table 2 show that adsorption of aluminium phthalocyanine significantly reduces the ξ -potentials of samples MNP/PTC (-12.6 mV) and MNP@Au/PTC (-25.5 mV). The colloidal stability reduces while the ξ -potential decreases, reflecting on increasing hydrodynamic diameters after PTC coating (see Table 2). These results indicate that electrostatic interaction between negatively charged citrate-coated nanoparticles and positively charged aluminium phthalocyaninate occurs, as schematically shown in Fig. 1c. Previous work⁸ showed similar results where zinc tetrasulfonated phthalocyanine (a tetra-anion) was strongly adsorbed onto positively charged surface of maghemite nanoparticles. Furthermore, once PTC presents small charge-to-area ratio formation of a PTC layer onto the nanoparticle surface is not enough to neutralize all negative nanoparticle surface sites and therefore a net negative surface charge still remains, but smaller than before PTC coating.

Table 2. Hydrodynamic average diameter, PDI and ξ -potentials of samples

Sample	D_H (nm)	PDI	ξ -potential (mV)
MNP	68.1	0.23	-38.6
MNP@Au1	114.3	0.19	-34.3
MNP@Au2	156.6	0.18	-39.6
MNP/PTC	235.9	0.21	-12.6
MNP@Au/PTC	211.1	0.25	-25.5

Typical UV-vis spectra of surface-coated (citrate, Gold, and PTC) maghemite nanoparticles in suspension are shown in Fig. 5a. Citrated-coated maghemite nanoparticles present a wide silent feature in the visible region. On the other hand, Gold-coated maghemite nanoparticles exhibit an absorption band centered around 555 nm, which is due to the surface plasmon absorption¹⁴⁷. In fact, it is reported that the position of this band depends on the core size as well as on the Au-shell thickness¹⁴⁸. In our case, as the ratio Au/Fe₂O₃ increases a blue shift of the surface plasmon peak is observed (see the inset of Fig. 5a), in good agreement with previous works¹⁴⁹. A reddish-pink color was observed in the brown tinged γ -Fe₂O₃ sol after Au-coating, indicating the formation of Gold shell onto maghemite nanoparticles (see Fig. 5b). Moreover, after magnetic separation of nanoparticles from suspension of sample MNP@Au2 the supernatant remains colorless (see inset of Fig. 4), supporting this claim. Figure 5a also shows the UV-vis spectrum of PTC solution, showing a major band at 680 nm, which is characteristic of phthalocyanine monomeric state. Besides, two others bands labeled at 606 nm and 640 nm are present and assigned to vibrational transition¹⁵⁰. As shown in Fig. 5b after functionalizing maghemite (sample MNP) and Gold-coated maghemite (sample MNP@Au2) nanoparticles with PTC to prepare samples MNP/PTC and MNP@Au/PTC the color of formed sols drastically changes to green and violet, respectively. Magnetic separation of suspensions of samples MNP/PTC and MNP@Au/PTC led to colorless supernatants, meaning that adsorption of PTC onto magnetic nanoparticles were effective. A surface plasmon absorption at 530 nm was still observed in sample MNP@Au/PTC, due to the Au-shell contribution.

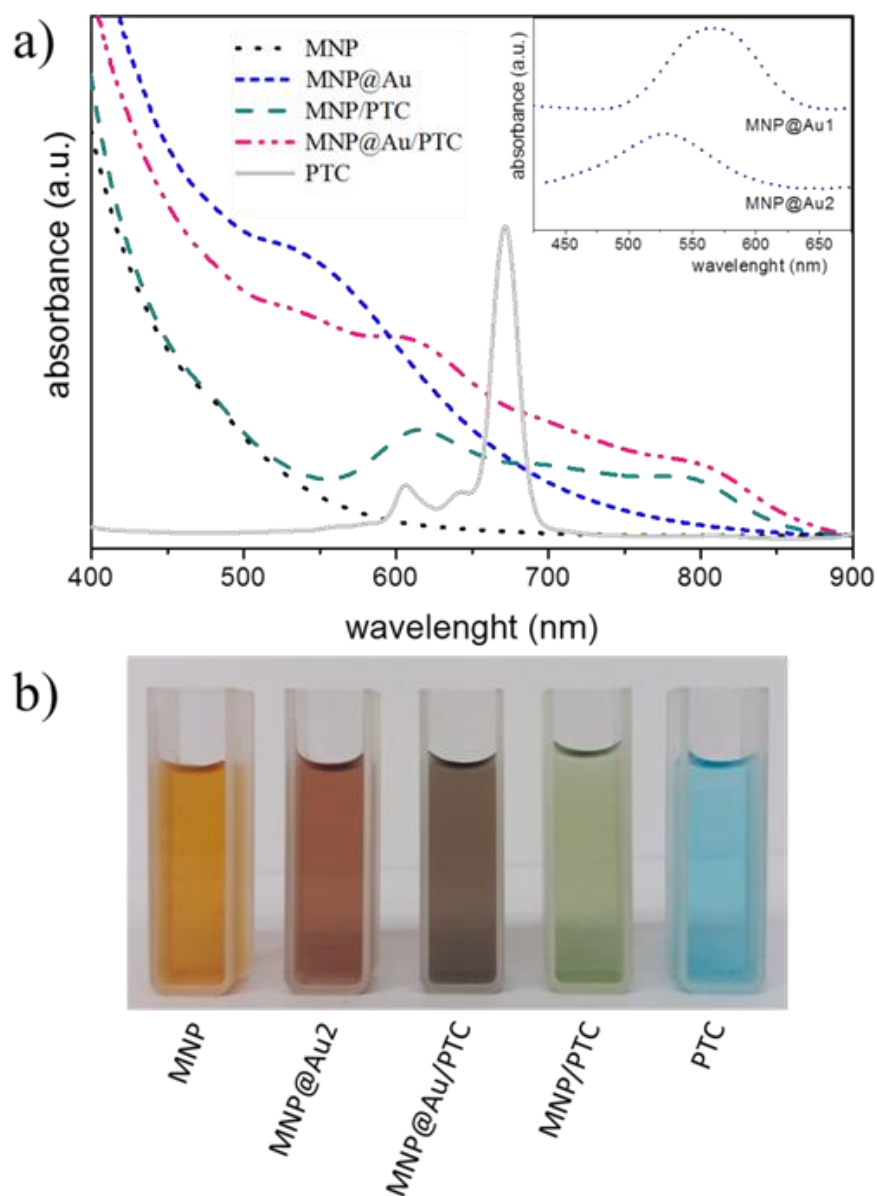


Figure 5. (a) UV-vis spectra of samples MNP (black/dot), MNP@Au2 (blue/short-dash), PTC (gray/solid), MNP/PTC (green/dash) and MNP@Au/PTC (pink/dash-dot). The inset shows a detail of spectra of samples MNP@Au1 and MNP@Au2 in the wavelength range of about 420 to 680 nm; b) Pictures of diluted sol of synthesized samples

Nevertheless, for PTC-functionalized samples (MNP/PTC and MNP@Au/PTC) the intense absorption band at 684 nm, typical of pure PTC, was practically suppressed. However, in the 606 nm and 640 nm regions, a broad band with a hypsochromic shift appears in PTC-functionalized nanoparticles (samples MNP/PTC and MNP@Au/PTC). This finding indicates interaction of PTC with magnetic nanoparticles¹⁵¹.

Nanocytotoxicity

The cytotoxicity of the nanoparticles on keratinocyte cells after 24 hours of exposure is illustrated in the Fig. 6. The sample MNP and MNP@Au1 presented significant decrease of cell viability in all concentrations (6.25 to 100 $\mu\text{g/mL}$). However, only MNP at higher concentration showed a significant biological decrease of 30% of cell viability. At others concentrations, the decrease was about 5 to 10%, which is not considered biologically significant.

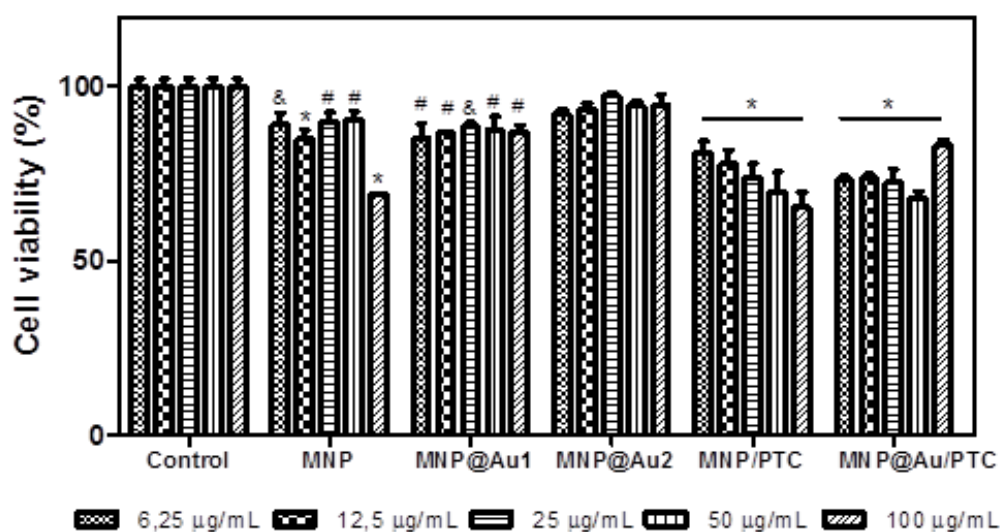


Figure 6. Percent cells viability of keratinocytes - HaCAT in presence of nanostructures: maghemite (MNP), maghemite coated with gold (MNP@Au1) and maghemite coated with 2x gold (MNP@Au2), MNP conjugated with phthalocyanine of aluminum (MNP/PTC) and MNP@Au conjugated with phthalocyanine of aluminum (MNP@Au/PTC) after 24 hours of incubation. Ultrapure water was used as negative control. Viability assay by MTT. Significantly different from the control: * $P < 0,001$ - # $P < 0,01$ - & $P < 0,05$.

The nanoparticle MNP@Au2 did not demonstrate cytotoxic activity in any concentration tested, probably due to the presence of gold that turned the nanostructure more biocompatible. In parallel, the nanoparticles associated to phthalocyanine were more cytotoxic. In fact, the MNP/PTC showed a dose-dependent activity and reduced the cell viability of 20 to 35%. The MNP@Au/PTC also demonstrated cytotoxic activity of 17 to 32%, but independent of the concentration.

The effect of the samples on the HaCAT cell viability after 72h of incubation is shown in Fig. 7. The MNP is not represented in the graph because the sample precipitate during the experiment making unfeasible the analysis of the cell viability. It is possible to observe that MNP@Au1 and MNP@Au2 did not show cytotoxic activity. The nanoparticles coated with phthalocyanine showed a dose-dependent activity. The

MNP/PTC decreased the cell viability about 30% at higher concentration, similar to the activity observed after 24 hours of exposure. In parallel, the MNP@Au/PTC decreased the cell viability about 45% at 100 $\mu\text{g/mL}$, more than the decrease observed after 24 hours of exposure. Therefore, the MNP@Au/PTC was more efficient after 72 hours of exposure than the MNP/PTC.

The activity of the nanoparticles on the fibroblast cell viability was also investigated after 24 and 72 hours of exposure. Fig. 8 shows the result after 24 hours. In this analysis, it is possible to observe that all samples demonstrated significant decrease of cell viability. The MNP and MNP@Au1 presented a decrease of cell viability about 30 to 40% and 20 to 30%, respectively, with the increase of concentrations.

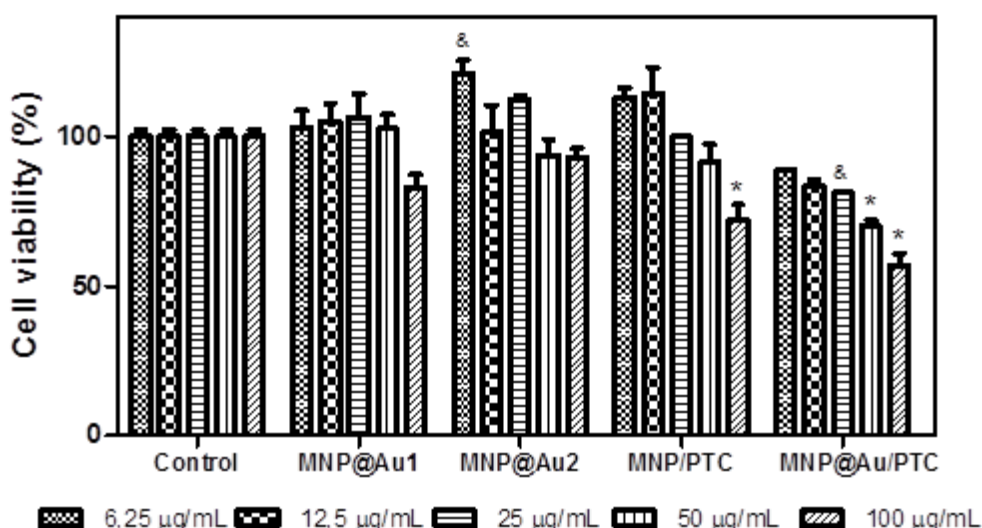


Figure 7. Percent cells viability of keratinocytes - HaCAT in presence of nanostructures: MNP@Au1, MNP@Au2, MNP/PTC and MNP@Au/PTC after 72 hours of incubation. Ultrapure water was used as negative control. Viability assay by MTT. Significantly different from the control: * $P < 0,001$ - &: $P < 0,05$.

The MNP@Au2 demonstrated less activity with reduction of cell viability of only 20%. This reduction of toxicity can be explained by the presence and increment on the gold shell which allowed improving the biocompatibility, in good agreement with previous work¹⁵². The sample with phthalocyanine reduced the cell viability in about 30%. Only the higher concentration of the MNP@Au/PTC did not demonstrated cytotoxic activity.

After 72 hours of exposure, MNP in all concentrations and MNP/PTC at 12.5 to 100 $\mu\text{g/mL}$ precipitate during the experiment making unfeasible the analysis of the cell viability.

The MNP@Au1 induced reduction of cell viability in about 20%. In parallel, the MNP@Au2 only showed decrease of the cell viability of 10% at 25 $\mu\text{g/mL}$, which is not considered biologically significant. The MNP@Au2 showed biocompatible property in fibroblast cells line NIH3T3. The MNP/PTC did not present cytotoxic activity at 6.25 $\mu\text{g/mL}$ after 72 hours of exposure. However, MNP@Au/PTC demonstrated a decrease of cell viability with the increase of concentration from 20 to 30%, which is more than after 24 hours of exposure (Fig. 9). An important remark is that toxicity studies of PTC-conjugated nanoparticles were carried out under light. As a result, radiation excites the light-sensitive PTC, generating cytotoxic species¹⁵³, essential tool for PDT application and result that could explain the deflated biocompatibility of these nanostructures.

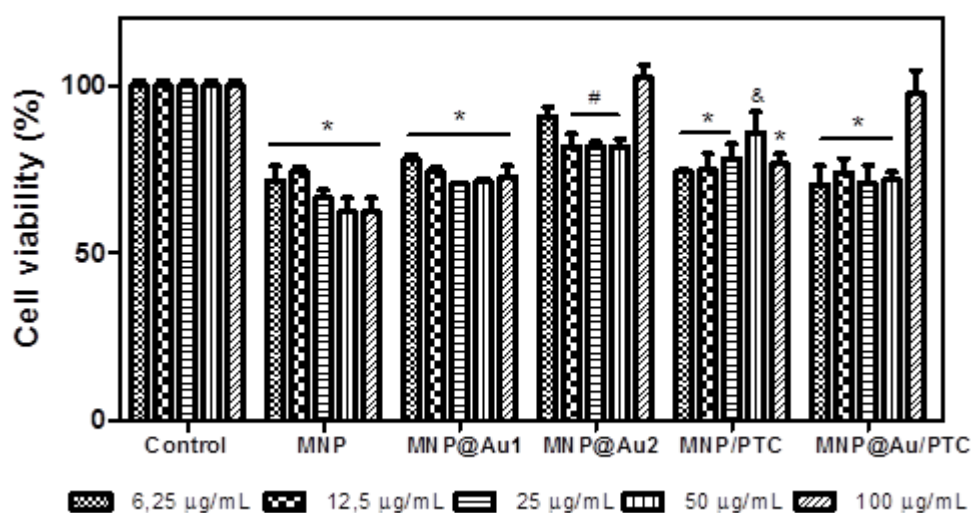


Figure 8. Percent cells viability of fibroblasts – NIH3T3 in presence of nanostructures: MNP, MNP@Au1, MNP@Au2, MNP/PTC and MNP@Au/PTC after 24 hours of incubation. Ultrapure water was used as negative control. Viability assay by MTT. Significantly different from the control: * $P < 0,001$ - #: $P < 0,01$ - &: $P < 0,05$.

An important remark is that toxicity studies of PTC-conjugated nanoparticles were carried out under light. As a result, radiation excites the light-sensitive PTC, generating cytotoxic species¹⁵⁴, essential tool for PDT application and result that could explain the deflated biocompatibility of these nanostructures.

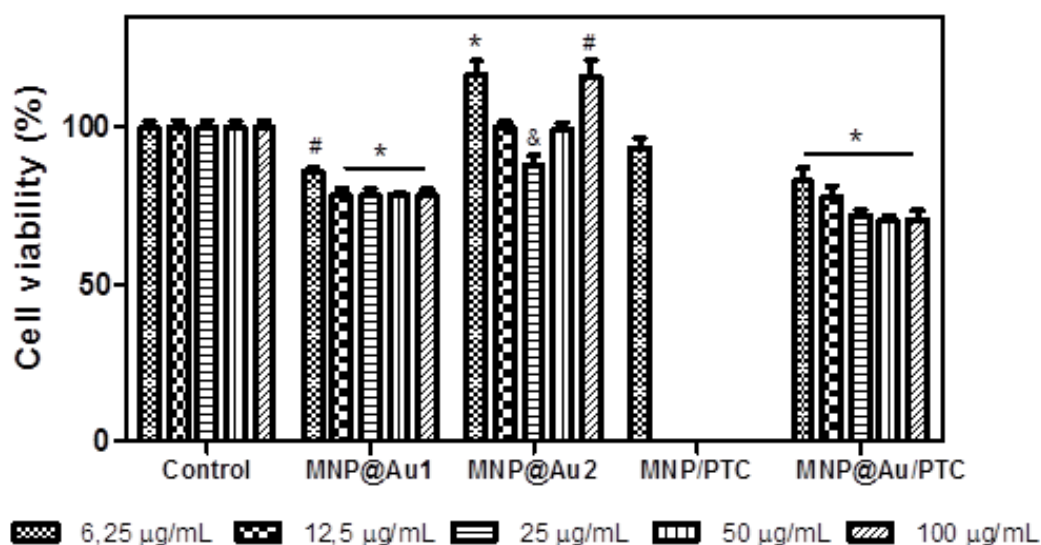


Figure 9. Percent cells viability of fibroblasts – NIH3T3 in presence of nanostructures: MNP@Au1, MNP@Au2, MNP/PTC and MNP@Au/PTC after 72 hours of incubation. Ultrapure water was used as negative control. Viability assay by MTT. Significantly different from the control: * P<0,001 - #: P<0,01 - &: P<0,05.

Computed tomography

Fig. 10a shows the CT signal intensity, in HU, for bare maghemite (MNP) and Gold-shelled MNP@Au1 and MNP@Au2 sols, compared to water (a negative control) and a positive control, an iodine-based contrast agent (ACI). The inset shows a detail of the CT signal for samples MNP, MNP@Au1 and MNP@Au2, compared to water. Moreover, qualitative images that represent the X-ray cell density of these samples are shown in Fig. 10b. These results indicate that X-ray attenuation increases as maghemite is coated with Gold and as the thickness of Au-shell increases, at the same $\gamma\text{-Fe}_2\text{O}_3$ concentration (0.4 mg/mL in maghemite). In spite of the higher X-ray attenuation, when compared to water, the CT signal for ACI is several times more intense.

Nevertheless sols analyzed here were highly diluted, being however more efficient than similar Gold-capped magnetic materials reported elsewhere¹⁵⁵. In that work, a signal of ~200 HU was observed for samples containing ~5 mg/mL of Au. Here, for a ~0.06 mg/mL of Au sample MN@Au2, the CT signal is about 430 HU. This enables the Gold-coated samples synthesized here as contrast agents for possible applications in CT imaging. Moreover, despite the high X-ray attenuation, the contrast agents commercially available – which present low molecular weight – are rapidly

eliminated by the kidneys, disabling their use in pre-clinical trials. In contrast, the kind of nanoparticles used here present long residence time in the blood stream, overcoming the challenge of pre-clinical tests.

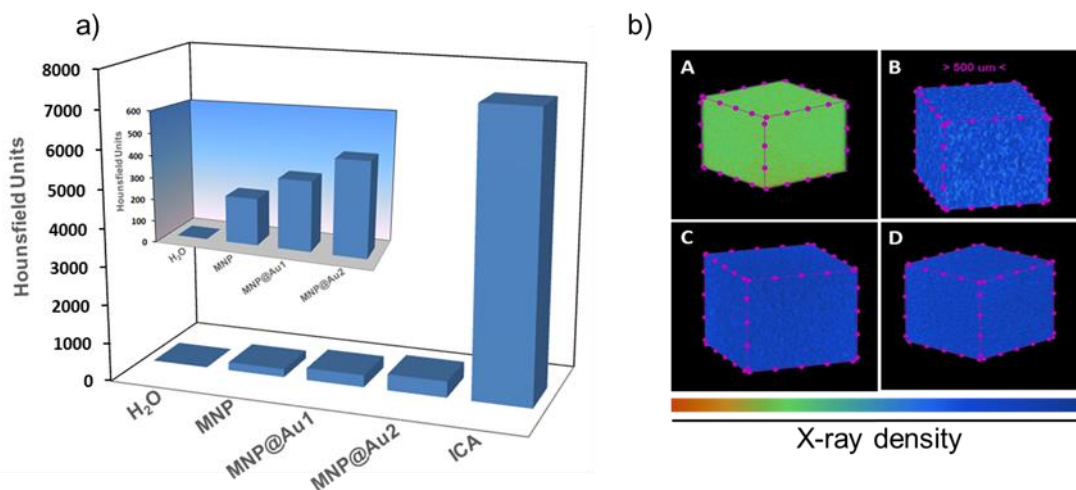


Figure 10. a) X-ray attenuation ability of MNP, MNP@Au1, MNP@Au2, water (negative control) and iodine-based contrast agent (positive control). The inset – highlight for samples MNP, MNP@Au1, MNP@Au2 and water; b) 3D qualitative images obtained for water (A), MNP (B), MNP@Au1 (C) and MNP@Au2 (D) samples, produced in an artificial colored scale presented at the bottom of the figure.

Conclusions

In conclusion, citrate-coated maghemite nanoparticles were elaborated via aqueous co-precipitation, following oxidation and citrate functionalization via an improved chemical route herein described. Gold shells were successfully deposited onto magnetic cores by reducing Au^{3+} ions in the presence of $\gamma\text{-Fe}_2\text{O}_3$ nanoparticles during 2 cycles of borohydride seeding. Moreover, we succeed in modulating the Gold shell thickness while increasing the Au- $\gamma\text{-Fe}_2\text{O}_3$ ratio during seeding. Successful Gold-shelling was confirmed by different characterization techniques. Particularly interesting were the optical absorption measurements, showing a blueshift depending on the shell thickness. All samples presented a long-term colloidal stability in physiological pH, even after functionalization with aluminium phthalocyanine (PTC), as confirmed by DLS measurements.

Moreover, according to *in vitro* nanocytotoxicity assays the Gold-shelling enhanced the biocompatibility of the $\gamma\text{-Fe}_2\text{O}_3$ nanoparticles. Differently from previous works, in which functionalization with PTC requires several steps to complete, extra-cappings and/or cross-linking molecules to be covalently attached to nanoparticles, our

data indicated strong electrostatic coupling between PTC and the nanoparticle surface, yet accomplished by a single-step process. Impressively, the Gold-shelled nanoparticles revealed efficient response as a contrast agent in computed tomography, dependent upon the Au/ γ -Fe₂O₃ ratio. Possible application of the as-elaborated core-shell nanoparticles will derive from the combination of magnetic properties of the core (maghemite) and the optical properties of the shell (Gold). From the therapeutic point of view, the as-elaborated samples represent a promising multi-task platform to perform magnetic hyperthermia (core) combined or not with photothermal therapy (shell) and/or photodynamic therapy (PTC functionalization). Taking into account the diagnosis approach, the nanomaterials herein reported can also be used as optical probes and contrast agents in *in vivo* medical imaging techniques.

Acknowledgements

The authors gratefully acknowledge financial support from Conselho Nacional de Desenvolvimento Científico e Tecnológico (CNPq), Fundação de Apoio à Pesquisa do Distrito Federal (FAPDF), and Fundação de Empreendimentos Científicos e Tecnológicos (FINATEC).

References

- [1] Chatterjee, K *et al.* *Advances in Colloid and Interface Science* 2014, **209**, 8-39.
- [2] Wang, X.; Yang, L.; Chen, Z.; Shin, D.M. Application of Nanotechnology in Cancer Therapy and Imaging. *A Cancer J Clin* 2008, **58**, 97–110.
- [3] Barreto, J.A.; O'Malley, W.; Kubeil, M.; Graham, B.; Stephan, H.; Spiccia, L. Nanomaterials: Applications in Cancer Imaging and Therapy. *Adv Mater* 2011, **23**, 18–40.
- [4] Mornet, S.; Vasseur, S.; Grasset, F.; Duguet, E. Magnetic nanoparticle design for medical diagnosis and therapy. *J Mater Chem* 2004, **14**, 2161-2175.
- [5] Pantic, I. Magnetic nanoparticles in cancer diagnosis and treatment: novel approaches. *Rev Adv Mater Sci* 2010, **26**, 67-73.
- [6] Roca, A.G.; Costo, R.; Rebolledo, A.F.; Veintemillas-Verdaguer, S.; Tartaj, P.; Gonzalez-Carreno, T.; Morales, M.P.; Serna, C.J. Progress in the preparation of magnetic nanoparticles for applications in biomedicine. *J Phys D: Appl Phys* 2009, **42**, 224002.
- [7] Robert, A. F. Current Status of Nanomedicine and Medical Nanorobotics. *J Comp. Theor. Nanosci* 2005, **2**, 1–25.
- [8] M. Auffan, J. Rose, J. Y. Bottero, G. V. Lowry, J. P. Jolivet, M. R. Wiesner, Towards a definition of inorganic nanoparticles from an environmental, health and safety perspective. *Nat Nanotechnol*, 2009, **4**, 634–41.

- [9] Jiang W, Kim BYS, Rutka JT, ChanWCW. Nanoparticle-mediated cellular response is size-dependent. *Nat Nanotechnol*, 2008, **3**, 145–50.
- [10] Rejman J, Oberle V, Zuhorn IS, Hoekstra D. Size-dependent internalization of particles via the pathways of clathrin and caveolae-mediated endocytosis. *Biochem J* 2004, **377**, 159–69.
- [11] Cho EC, Zhang Q, Xia YN. The effect of sedimentation and diffusion on cellular uptake of gold nanoparticles. *Nat Nanotechnol* 2011, **6**, 385–91.
- [12] Dreaden EC, Neretina S, Qian W, El-Sayed MA, Hughes RA, Preston JS, et al. Plasmonic enhancement of nonradiative charge carrier relaxation and proposed effects from enhanced radiative electronic processes in semiconductor-gold core-shell nanorod arrays. *J Phys Chem C*, 2011, **115**, 5578–83.
- [13] Yen CW, Hayden SC, Dreaden EC, Szymanski P, El-Sayed MA. Tailoring plasmonic and electrostatic field effects to maximize solar energy conversion by bacteriorhodopsin, the other natural photosynthetic system. *Nano Lett*, 2011, **11**, 3821–6.
- [14] Carraher, Ch. E., Jr. Carraher's Polymer Chemistry; *CRC Press*: Boca Raton, 2013.
- [15] Braunecker, W. A.; Matyjaszewski, K. Controlled/living radical polymerization: Features, developments, and perspectives. *Prog. Polym. Sci.*, 2007, **32**, 93–146.
- [16] Moad, G.; Rizzardo, E.; Thang, S. H. Radical addition-fragmentation chemistry in polymer synthesis. *Polymer* 2008, **49**, 1079–1131.
- [17] In Macromolecular anticancer therapeutics; Reddy, L. H., Couvreur, P., Eds.; *Springer: New York*, 2010.
- [18] In Drug delivery and targeting for pharmacists and pharmaceutical scientists; Hillery, A. M., Lloyd, A. W., Swarbrick, J., Eds.; *Taylor & Francis Inc.: London*, 2001.
- [19] Popovic Z, Liu WH, Chauhan VP, Lee J, Wong C, Greytak AB, et al. A nanoparticle size series for in vivo fluorescence imaging. *Angew Chem Int Ed* 2010, **49**, 8649–52.
- [20] Erogbogbo F, Yong KT, Hu R, Law WC, Ding H, Chang CW, et al. Biocompatible magnetofluorescent probes: luminescent silicon quantum dots coupled with superparamagnetic iron(III) oxide. *ACS Nano* 2010, **9**, 5131–8.
- [21] Verma A, Stellacci F. Effect of surface properties on nanoparticle–cell interactions. *Small* 2010, **6**, 12–21.
- [22] Dyal, A., Loos, K., Noto, M., Chang, S.W., Spagnoli, C., Shafi, K.V.P.M., Ulman, A., Cowman, M., Gross, R.A., *J. Am. Chem. Soc.* 2003, **125**, 1684–1685.
- [23] Willner, I., Katz, E., *Angew. Chem. Int. Ed.* 2003, **42**, 4576–4588.
- [24] Katz, E., Willner, I., *Angew. Chem. Int. Ed.* 2005, **44**, 4791–4794.
- [25] Hirsch, R., Katz, E., Willner, I., *J. Am. Chem. Soc.* 2000, **122**, 12053–12054.
- [26] Prasad G. Biomedical applications of nanoparticles. *Safety of Nanoparticles*. Springer; 2009 89–109.
- [27] Kelly KL, Coronado E, Zhao LL, Schatz GC. The optical properties of metal nanoparticles: the influence of size, shape, and dielectric environment. *J Phys Chem B* 2003, **107**, 668–77.
- [28] Predoi D, Kuncser V, Nogues M, Tronc E, Jolive J, Filoti G, et al. Magnetic properties of gamma-Fe₂O₃ nanoparticles. *J Optoelectron Adv Mater*, 2003, **5**, 211–6.
- [29] Murray CB, Kagan C, Bawendi M. Synthesis and characterization of monodisperse nanocrystals and close-packed nanocrystal assemblies. *Annu Rev Mater Sci* 2000, **30**, 545–610.

- [30] Cui H, Feng Y, Ren W, Zeng T, Lv H, Pan Y. Strategies of large scale synthesis of monodisperse nanoparticles. *Recent Pat Nanotechnol*, 2009, **3**, 32–41.
- [31] H. Gu, K. Xu, C. Xu, B. Xu, *Chem. Commun.*, 2006, **46**, 941–949.
- [32] L.E.W. Laconte, N. Nitin, O. Zurkiya, D. Caruntu, C.J.O. Connor, X. Hu, G. Bao, *J. Magn. Reson. Imaging*, 2007, **26**, 1634–1641.
- [33] B. Chertok, A.E. David, V.C. Yang, *Biomaterials*, 2010, **31** 6317–6324.
- [34] S. Bucak, D.A. Jones, P.E. Laibinis, T.A. Hatton, *Biotechnol. Progr.* 19 (2003) 477–484.
- [35] Y. Liang, J.L. Gong, Y. Huang, Y. Zheng, J.H. Jiang, G.L. Shen, R.Q. Yu, *Talanta* 72 (2007) 443–449.
- [36] In Targeted drug delivery: Concepts and design; Devajaran, P. V., Jain, S., *Eds.; Springer: Heidelberg*, 2015.
- [37] Elsabahy, M.; Wooley, K. L. Design of polymeric nanoparticles for biomedical delivery applications. *Chem. Soc. Rev.* 2012, **41**, 2545–2561.
- [38] Delplace, V.; Couvreur, P.; Nicolas, J. Recent trends in the design of anticancer polymer prodrug nanocarriers. *Polym. Chem.* 2014, **5**, 1529–1544.
- [39] Nicolas, J.; Mura, S.; Brambilla, D.; Mackiewicz, N.; Couvreur, P. Design, functionalization strategies and biomedical applications of targeted biodegradable/biocompatible polymer-based nanocarriers for drug delivery. *Chem. Soc. Rev.* 2013, **42**, 1147–1235.
- [40] Pillai, G. Nanomedicines for cancer therapy: an update of FDA approved and those under various stages of development. *SOJ. Pharm. Pharm. Sci.* 2014, **1**, 1–13.
- [41] Estelrich, J.; Escribano, E.; Queralt, J.; Busquets, M. Iron Oxide nanoparticles for magnetically-guided and magnetically-responsive drug delivery. *Int. J. Mol. Sci.* 2015, **16**, 8070–8101.
- [42] Lartigue, L.; Alloyeau, D.; Kolosnjaj-Tabi, J.; Javed, Y.; Guardia, P.; Riedinger, A.; Péchoux, C.; Pellegrino, T.; Wilhelm, C.; Gazeau, F. Biodegradation of Iron Oxide nanocubes: High-resolution in situ monitoring. *ACS Nano* 2013, **7**, 3939–3952.
- [43] Arami, H.; Khandhar, A.; Liggitt, D.; Krishnan, K. M. In Vivo Delivery, Pharmacokinetics, biodistribution and toxicity of Iron Oxide nanoparticles. *Chem. Soc. Rev.* 2015, **44**, 8576–8607.
- [44] A. B. Salunkhe, V. M. Khot, S. H. Pawar.; *Current Topics in Medicinal Chemistry*, 2014, **14**, 6.
- [45] Legendijk; J.J.W. Hyperthermia treatment planning. *Phys Med Biol* 2000, **45**, 61–76.
- [46] Mohite V. Self controlled magnetic hyperthermia. *Thesis of the florida state university college of engineering*, 2004.
- [47] Hergt, R.; Dutz, S. Magnetic particle hyperthermia-biophysical limitations of a visionary tumour therapy. *J Magn Magn Mater* 2007, **311**, 187–192.
- [48] Laurent, S.; Dutz, S.; Häfeli, U.O.; Mahmoudi, M.; Magnetic fluid hyperthermia: Focus on superparamagnetic iron oxide NPs. *Adv Colloid Interface Sci* 2011, **166**, 8-23.
- [49] Kallumadil, M.; Tada, M.; Nakagawa, T.; Abe, M.; Southern, P.; Pankhurst, Q.A. Suitability of commercial colloids for magnetic hyperthermia. *J Magn Magn Mater* 2009, **321**, 1509–1513.
- [50] Ho, D.; Sun, X.; Sun, S. Monodisperse magnetic nanoparticles for theranostic applications, *Accounts Chem. Res.* 2011, **44**, 875-882.

- [51] Higby, G. J. Gold in Medicine. *Gold Bull.* 1982, **15**, 130–140.
- [52] Wagner, F. E.; Haslbeck, S.; Stievano, L.; Calogero, S.; Pankhurst, Q. A.; Martinek, K.-P. Before Striking Gold in Gold-Ruby Glass. *Nature* 2000, **407**, 691–692.
- [53] Edwards, P. P.; Thomas, J. M. Gold in a Metallic Divided State-From Faraday to Present-Day Nanoscience. *Angew. Chem., Int. Ed.* 2007, **46**, 5480–5486.
- [54] Murphy, C. J. Nanocubes and Nanoboxes. *Science* 2002, **298**, 2139–2141.
- [55] Kelly, K. L.; Coronado, E.; Zhao, L. L.; Schatz, G. C. The Optical Properties of Metal Nanoparticles: The Influence of Size, Shape, and Dielectric Environment. *J. Phys. Chem. B* 2003, **107**, 668–677.
- [56] El-Sayed, M. A. Some Interesting Properties of Metals Confined in Time and Nanometer Space of Different Shapes. *Acc. Chem. Res.* 2001, **34**, 257–264.
- [57] Daniel, M.-C.; Astruc, D. Gold Nanoparticles: Assembly, Supramolecular Chemistry, Quantum-Size-Related Properties, and Applications toward Biology, Catalysis, and Nanotechnology. *Chem. Rev.* 2004, **104**, 293–346.
- [58] Rosi, N. L.; Mirkin, C. A. Nanostructures in Biodiagnostics. *Chem. Rev.* 2005, **105**, 1547–1562.
- [59] Burda, C.; Chen, X.; Narayanan, R.; El-Sayed, M. A. Chemistry and Properties of Nanocrystals of Different Shapes. *Chem. Rev.* 2005, **105**, 1025–1102.
- [60] Murphy, C. J.; Sau, T. K.; Gole, A. M.; Orendorff, C. J.; Gao, J.; Gou, L.; Hunyadi, S. E.; Li, T. Anisotropic Metal Nanoparticles: Synthesis, Assembly, and Optical Applications. *J. Phys. Chem. B* 2005, **109**, 13857–13870.
- [61] Murphy, C. J.; Gole, A. M.; Hunyadi, S. E.; Orendorff, C. J. One-Dimensional Colloidal Gold and Silver Nanostructures. *Inorg. Chem.* 2006, **45**, 7544–7554.
- [62] Murphy, C. J.; Gole, A. M.; Hunyadi, S. E.; Stone, J. W.; Sisco, P. N.; Alkilany, A.; Kinard, B. E.; Hankins, P. Chemical Sensing and Imaging with Metallic Nanorods. *Chem. Commun.* 2008, 544–557.
- [63] Thomas, K. G.; Barazzouk, S.; Ipe, B. I.; Joseph, S. T. S.; Kamat, P. V. Uniaxial Plasmon Coupling through Longitudinal Self-Assembly of Gold Nanorods. *J. Phys. Chem. B* 2004, **108**, 13066–13068.
- [64] Hainfeld JF, Slatkin DN, Smilowitz HM. The use of gold nanoparticles to enhance radiotherapy in mice. *Phys. Med. Biol.* 2004, **49**, 18, N309–N315.
- [65] Hainfeld JF, Slatkin DN, Focella TM, Smilowitz HM. Gold nanoparticles: a new x-ray contrast agent. *Br. J. Radiol.* 2006, **79**(939), 248–253.
- [66] Hubbell JH, Seltzer SM. Tables of x-ray mass attenuation coefficients and mass energy-absorption coefficients (version 1.4). National Institute of Standards and Technology, MD, USA 2004.
- [67] Sun I-C, Eun D-K, Na JH *et al.* Heparin-coated gold nanoparticles for liver-specific CT imaging. *Chem. Eur. J.* 2009 **15**(48), 13341–13347.
- [68] Chanda N, Kattumuri V, Shukla R *et al.* Bombesin functionalized gold nanoparticles show *in vitro* and *in vivo* cancer receptor specificity. *Proc. Natl Acad. Sci. USA*, 2009 **107**(19), 8760–8765.
- [69] Cormode DP, Roessl E, Thran A *et al.* Atherosclerotic plaque composition: analysis with multicolor CT and targeted gold nanoparticles. *Radiology* 2010, **256**(3), 774–782.
- [70] Eck W, Nicholson AI, Zentgraf H, Semmler W, Bartling S. Anti-CD4-targeted gold nanoparticles induce specific contrast enhancement of peripheral lymph nodes in x-ray computed tomography of live mice. *Nano Lett.* 2010, **10**(7), 2318–2322.

- [71] Shilo M, Reuveni T, Motiei M, Popovtzer R. Nanoparticles as computed tomography contrast agents. *Nanomedicine*, 2012, **7**(2), 257–269.
- [72] Jakhmola A, Anton N, Vandamme TF. Inorganic nanoparticles based contrast agents for x-ray computed tomography. *Adv. Healthc. Mater.* 2012, **1**(4), 413–431.
- [73] Hallouard F, Anton N, Choquet P, Constantinesco A, Vandamme T. Iodinated blood pool contrast media for preclinical x-ray imaging applications – a review. *Biomaterials*, 2010, **31**(24), 6249–6268.
- [74] Brannon-Peppas L, Blanchette JO. Nanoparticle and targeted systems for cancer therapy. *Adv. Drug Deliv. Rev.* 2004, **56**(11), 1649–1659.
- [74] Brigger I, Dubernet C, Couvreur P. Nanoparticles in cancer therapy and diagnosis. *Adv. Drug Deliv. Rev.* 2002, **54**(5), 631–651.
- [75] Khlebtsov N, Dykman L. Biodistribution and toxicity of engineered gold nanoparticles: a review of *in vitro* and *in vivo* studies. *Chem. Soc. Rev.* 2011, **40**(3), 1647–1671.
- [76] Alkilany AM, Murphy CJ. Toxicity and cellular uptake of gold nanoparticles: what we have learned so far? *J. Nanopart. Res.* 2010, **12**(7), 2313–2333.
- [76] Pan Y, Neuss S, Leifert A *et al.* Size-dependent cytotoxicity of gold nanoparticles. *Small* 2007**3**(11), 1941–1949.
- [77] Pan Y, Leifert A, Ruau D *et al.* Gold nanoparticles of diameter 1.4 nm trigger necrosis by oxidative stress and mitochondrial damage. *Small* 2009, **5**(18), 2067–2076.
- [78] Tsoli M, Kuhn H, Brandau W, Esche H, Schmid G. Cellular uptake and toxicity of Au₅₅ clusters. *Small*. 2005, **1**(8–9), 841–844.
- [79] Albanese A, Tang PS, Chan WCW. The effect of nanoparticle size, shape, and surface chemistry on biological systems. *Annu. Rev. Biomed. Eng.* 2012, **14**(1), 1–16.
- [80] Cole LE, Vargo-Gogola T, Roeder RK. Contrast-enhanced x-ray detection of breast microcalcifications in a murine model using targeted gold nanoparticles. *ACS Nano*. 2014, **8**(7), 7486–7496.
- [81] Wang H, Zheng L, Peng C, Shen M, Shi X, Zhang G. Folic acid-modified dendrimer-entrapped gold nanoparticles as nanoprobes for targeted CT imaging of human lung adenocarcinoma. *Biomaterials*. 2013 **34**(2), 470–480.
- [82] Yao L, Daniels J, Moshnikova A *et al.* pHLIP peptide targets nanogold particles to tumors. *Proc. Natl Acad. Sci. USA*. 2013 **110**(2), 465–470.
- [83] Chattopadhyay N, Fonge H, Cai Z *et al.* Role of antibody-mediated tumor targeting and route of administration in nanoparticle tumor accumulation *in vivo*. *Mol. Pharm.* 2012, **9**(8), 2168–2179.
- [84] Murphy, C. J.; Sau, T. K.; Gole, A. M.; Orendorff, C. J.; Gao, J.; Gou, L.; Hunyadi, S. E.; Li, T. Anisotropic Metal Nanoparticles: Synthesis, Assembly, and Optical Applications. *J. Phys. Chem. B*. 2005, **109**, 13857–13870.
- [85] El-Sayed, M. A. Some Interesting Properties of Metals Confined in Time and Nanometer Space of Different Shapes. *Acc. Chem. Res.* 2001, **34**, 257–264.
- [86] Jiang, X. C.; Pileni, M. P. Gold Nanorods: Influence of Various Parameters as Seeds, Solvent, Surfactant on Shape Control. *Colloids Surf. A*. 2007, **295**, 228–232.
- [87] Hirsch, L. R.; Gobin, A. M.; Lowery, A. R.; Tam, F.; Drezek, R. A.; Halas, N. J.; West, J. L. Metal Nanoshells. *Ann. Biomed. Eng.* 2006, **34**, 15–22.

- [88] Brunetaud JM, Mordon S, Maunoury V, Beacco C. *Lasers Med Sci* 1995, **10**, 3–8.
- [89] Huang X, Jain PK, El-Sayed IH, El-Sayed MA. *Lasers Med Sci* 2008, **23**, 217.
- [90] Pitsillides CM, Joe EK, Wei X, Anderson RR, Lin CP. *Biophys J* 2003, **84**, 4023.
- [91] Zharov VP, Kim JW, Curiel DT, Everts M. *Nanomed Nanotechnol Biol Med*. 2005, **1**, 326.
- [92] El-Sayed IH, Huang X, El-Sayed MA. *Cancer Lett.* 2006, **239**, 129.
- [93] Huang X, Jain PK, El-Sayed IH, El-Sayed MA. *Photochem Photobiol* 2006, **82**, 412.
- [94] G. S. Demirer, A. C. Okur, S. Kizilela, *Journal of Materials Chemistry B*, 2015, **3**, 7831-7849.
- [95] L. Wang, H.-Y. Park, S. I. I. Lim, M. J. Schadt, D. Mott, J. Luo, X. Wang and C.-J. Zhong, *Journal of Materials Chemistry*, 2008, **18**, 2629.
- [96] A. Ito, H. Honda and T. Kobayashi, *Cancer immunology, immunotherapy : CII*, 2006, **55**, 320-328.
- [97] C. S. Levin, C. Hofmann, T. A. Ali, A. T. Kelly, E. Morosan, P. Nordlander, K. H. Whitmire and N. J. Halas, *ACS Nano*, 2009, **3**, 1379–1388.
- [98] H. Wang, D. W. Brandl, F. Le, P. Nordlander and N. J. Halas, *Nano Lett.*, 2006, **6**, 827–832.
- [99] T. D. Giorgio, C. S. Bell and S. S. Yu, *Small*, 2011, **7**, 1158–1162.
- [100] S. I. Stoeva, F. W. Huo, J. S. Lee and C. A. Mirkin, *J. Am. Chem. Soc.*, 2005, **127**, 15362–15363.
- [101] R. Amal, I. Y. Goon, L. M. H. Lai, M. Lim, P. Munroe and J. J. Gooding, *Chem. Mater.*, 2009, **21**, 673–681.
- [102] L. Y. Wang, J. W. Bai, Y. J. Li and Y. Huang, *Angew. Chem., Int. Ed.*, 2008, **47**, 2439–2442.
- [103] H. Zeng and S. H. Sun, *Adv. Funct. Mater.*, 2008, **18**, 391–400.
- [104] V. C. Pierre, E. D. Smolensky, M. C. Neary, Y. Zhou and T. S. Berquo, *Chem. Commun.*, 2011, **47**, 2149–2151.
- [105] W.-C. Huang, P.-J. Tsai and Y.-C. Chen, *Small*, 2009, **5**, 51–56.
- [106] J. Lee, J. Yang, H. Ko, S. J. Oh, J. Kang, J.-H. Son, K. Lee, S.-W. Lee, H.-G. Yoon, J.-S. Suh, Y.-M. Huh and S. Haam, *Adv. Funct. Mater.*, 2008, **18**, 258–264.
- [107] S. H. Xuan, F. Wang, Y. X. J. Wang, J. C. Yu, X. L. Gong and K. C.-F. Leung, *Chem. Commun.*, 2011, **47**, 2514–2516.
- [108] N. S. Abadeer and C. J. Murphy, *The Journal of Physical Chemistry C*, 2016, **120**, 4691-4716.
- [109] J. Ren, S. Shen, Z. Pang, X. Lu, C. Deng and X. Jiang, *Chemical communications*, 2011, **47**, 11692-11694.
- [110] O. Chen, L. Riedemann, F. Etoc, H. Herrmann, M. Coppey, M. Barch, C. T. Farrar, J. Zhao, O. T. Bruns, H. Wei, P. Guo, J. Cui, R. Jensen, Y. Chen, D. K. Harris, J. M. Cordero, Z. Wang, A. Jasanoff, D. Fukumura, R. Reimer, M. Dahan, R. K. Jain and M. G. Bawendi, *Nature communications*, 2014, **5**, 5093.
- [111] J. C. O. Silva, M. H. Sousa, F. A. Tourinho and J. C. Rubim, *Langmuir*, 2002, **18**, 5511-5515.
- [112] Yu SB, Watson AD. Metal-based X-ray contrast media. *Chem Ver* 1999, **99**(9), 2353–2377.

- [113] Xu CJ, Tung GA, Sun SH. Size and concentration effect of gold nanoparticles on X-ray attenuation as measured on computed tomography. *Chem Mater*, 2008; **20**(13), 4167–4169.
- [114] Petros RA, DeSimone JM. Strategies in the design of nanoparticles for therapeutic applications. *Nat Rev Drug Discov* 2010, **9**(8), 615–627.
- [115] Hallouard F, Anton N, Choquet P, Constantinesco A, Vandamme T. Iodinated blood pool contrast media for preclinical X-ray imaging applications – a review. *Biomaterials* 2010, **31**(24), 6249–6268.
- [116] Allkemper T, Bremer C, Matuszewski L, Ebert W, Reimer P. Contrast-enhanced blood-pool MR angiography with optimized iron oxides: effect of size and dose on vascular contrast enhancement in rabbits. *Radiology* 2002, **223**(2), 432–438.
- [117] Han SY, Guo QH, Xu MM, et al. Tunable fabrication on iron oxide/Au/Ag nanostructures for surface enhanced Raman spectroscopy and magnetic enrichment. *J Colloid Interface Sci* 2012, **378**, 51–57.
- [118] Guo X, Zhang Q, Sun YH, Zhao Q, Yang J. Lateral etching of core-shell Au@metal nanorods to metal-tipped Au nanorods with improved catalytic activity. *ACS Nano* 2012, **6**(2), 1165–1175.
- [119] L. A. Muehlmann, M. C. Rodrigues, J. P. Longo, M. P. Garcia, K. R. Py-Daniel, A. B. Veloso, P. E. de Souza, S. W. da Silva and R. B. Azevedo, *Journal of nanobiotechnology*, 2015, **13**, 36.
- [120] O. Penon, M. J. Marin, D. B. Amabilino, D. A. Russell and L. Perez-Garcia, *Journal of colloid and interface science*, 2016, **462**, 154-165.
- [121] Y. Cheng, A. C. Samia, J. D. Meyers, I. Panagopoulos, B. Fei and C. Burda, *Journal of the American Chemical Society*, 2008, **130**, 10643–10647.
- [122] H. Cai, K. Li, M. Shen, S. Wen, Y. Luo, C. Peng, G. Zhang and X. Shi, *Journal of Materials Chemistry*, 2012, **22**, 15110.
- [123] S. Shrestha, P. Jiang, M. H. Sousa, P. C. Morais, Z. Mao and C. Gao, *J. Mater. Chem. B*, 2016, **4**, 245-256.
- [124] G. S. Demirer, A. C. Okur, S. Kizilela, *Journal of Materials Chemistry B*, 2015, **3**, 7831-7849.
- [125] L. Wang, H.-Y. Park, S. I. I. Lim, M. J. Schadt, D. Mott, J. Luo, X. Wang and C.-J. Zhong, *Journal of Materials Chemistry*, 2008, **18**, 2629.
- [126] A. Ito, H. Honda and T. Kobayashi, *Cancer immunology, immunotherapy : CII*, 2006, **55**, 320-328.
- [127] K. Saha, S. S. Agasti, C. Kim, X. Li and V. M. Rotello, *Chemical reviews*, 2012, **112**, 2739-2779.
- [128] N. S. Abadeer and C. J. Murphy, *The Journal of Physical Chemistry C*, 2016, **120**, 4691-4716.
- [129] J. Ren, S. Shen, Z. Pang, X. Lu, C. Deng and X. Jiang, *Chemical communications*, 2011, **47**, 11692-11694.
- [130] O. Chen, L. Riedemann, F. Etoc, H. Herrmann, M. Coppey, M. Barch, C. T. Farrar, J. Zhao, O. T. Bruns, H. Wei, P. Guo, J. Cui, R. Jensen, Y. Chen, D. K. Harris, J. M. Cordero, Z. Wang, A. Jasanoff, D. Fukumura, R. Reimer, M. Dahan, R. K. Jain and M. G. Bawendi, *Nature communications*, 2014, **5**, 5093.
- [131] J. C. O. Silva, M. H. Sousa, F. A. Tourinho and J. C. Rubim, *Langmuir*, 2002, **18**, 5511-5515.
- [132] L. A. Muehlmann, M. C. Rodrigues, J. P. Longo, M. P. Garcia, K. R. Py-Daniel, A. B. Veloso, P. E. de Souza, S. W. da Silva and R. B. Azevedo, *Journal of nanobiotechnology*, 2015, **13**, 36.
- [133] O. Penon, M. J. Marin, D. B. Amabilino, D. A. Russell and L. Perez-Garcia, *Journal of colloid and interface science*, 2016, **462**, 154-165.

- [134] Y. Cheng, A. C. Samia, J. D. Meyers, I. Panagopoulos, B. Fei and C. Burda, *Journal of the American Chemical Society*, 2008, **130**, 10643–10647.
- [135] H. Cai, K. Li, M. Shen, S. Wen, Y. Luo, C. Peng, G. Zhang and X. Shi, *Journal of Materials Chemistry*, 2012, **22**, 15110.
- [136] S. Shrestha, P. Jiang, M. H. Sousa, P. C. Morais, Z. Mao and C. Gao, *J. Mater. Chem. B*, 2016, **4**, 245-256.
- [137] M. H. Sousa, G. J. da Silva, J. Depeyrot, F. A. Tourinho and L. F. Zara, *Microchemical Journal*, 2011, **97**, 182-187.
- [138] M. Mandal, S. Kundu, S. K. Ghosh, S. Panigrahi, T. K. Sau, S. M. Yusuf and T. Pal, *Journal of colloid and interface science*, 2005, **286**, 187-194.
- [139] Z. Xu, Y. Hou and S. Sun, *Journal of the American Chemical Society*, 2007, **129**, 8698-8699.
- [140] C. R. Alves, R. Aquino, M. H. Sousa, H. R. Rechenberg, G. F. Goya, F.A. Tourinho and J. Depeyrot, *Journal of Metastable and Nanocrystalline Materials*, 2004, **20**, 694-699.
- [141] M. Mikhaylova, D. K. Kim, N. Bobrysheva, M. Osmolowsky, V. Semenov, T. Tsakalagos, and M. Muhammed, *Langmuir*, 2004, **20**, 2472-2477.
- [142] J-C. Bacri, R. Perzynski and D. Salin, *Journal of Magnetism and Magnetic Materials*, 1990, **85**, 27-32.
- [143] N. C. Feitoza, T. D. Goncalves, J. J. Mesquita, J. S. Menegucci, M. K. M. S. Santos, J. A. Chaker, R. B. Cunha, A. M. M. Medeiros, J. C. Rubim, M. H. Sousa, *Journal of Hazardous Materials*, 2014, **264**, 153–160.
- [144] Y. C. Yeh, B. Creran and V. M. Rotello, *Nanoscale*, 2012, **4**, 1871-1880.
- [145] K. C.-F. Leung, S. Xuan, X. Zhu, D. Wang, C.-P. Chak, S.-F. Lee, W. K. W. Ho and B. C. T. Chung, *Chemical Society Reviews*, 2012, **41**, 1911-1928.
- [146] L. Wang, J. Luo, Q. Fan, M. Suzuki, I. S. Suzuki, M. H. Engelhard, Y. Lin, N. Kim, J. Q. Wang and C-J. Zhong, *Journal of Physical Chemistry B*, 2005, **109**, 21593-21601.
- [147] J. L. Lyon, D. A. Fleming, M. B. Stone, P. Schiffer and M. E. Williams, *Nanoletters*, 2004, **4**, 719-723.
- [148] K. Liu, Y. Wang, J. Yao and Y. Luo, *Chemical Physics Letters*, 2007, **438**, 36-40.
- [149] M. Idowu and T. Nyokong, *Journal of Photochemistry and Photobiology A: Chemistry*, 2007, **188**, 200-206.
- [150] Y. Li, J. Liu, Y. Zhong, J. Zhang, Z. Wang, L. Wang, Y. An, M. Lin, Z. Gao and D. Zhang, *International journal of nanomedicine*, 2011, **6**, 2805-2819.
- [151] C. S. de Paula, A. C. Tedesco, F. L. Primo, J. M. Vilela, M. S. Andrade and V. C. Mosqueira, *European journal of pharmaceutical sciences : official journal of the European Federation for Pharmaceutical Sciences*, 2013, **49**, 371-381.
- [152] C. S. de Paula, A. C. Tedesco, F. L. Primo, J. M. Vilela, M. S. Andrade and V. C. Mosqueira, *European journal of pharmaceutical sciences : official journal of the European Federation for Pharmaceutical Sciences*, 2013, **49**, 371-381.

3- DISCUSSÃO GERAL

Nanopartículas de maguemita recobertas com citrato foram sintetizadas via co-precipitação aquosa – seguida pela oxidação e funcionalização com citrato. A camada de ouro foi depositada sobre o núcleo magnético pela redução dos íons Au^{3+} na presença de nanopartículas de $\gamma\text{-Fe}_2\text{O}_3$ durante dois ciclos de sementeamento com boroidreto. Aumentando a concentração de Au^{3+} durante em cada sementeamento, aumentando a razão $\text{Au}/\text{Fe}_2\text{O}_3$ (e logo a espessura da camada de ouro). O recobrimento com ouro pode ser confirmado por vários ensaios. Particularmente, medidas ópticas mostraram um deslocamento para o azul dependendo da espessura da camada de ouro. Todas as amostras apresentaram uma longa estabilidade coloidal em pH fisiológico, confirmado por medidas de DSL, mesmo depois da funcionalização com ftalocianina de alumínio. Além disso, este estudo mostrou que a camada de ouro fornece mais biocompatibilidade para as nanopartículas de $\gamma\text{-Fe}_2\text{O}_3$ de acordo com a evolução dos testes de citotoxicidade *in vitro*. Diferentemente de outros trabalhos, em que a ftalocianina precisa de vários passos recobrimentos extras e/ou moléculas cruzadas para serem covalentemente ligadas as nanopartículas, aqui os resultados indicam um forte acoplamento entre PTC e a superfície da nanopartícula, por interações eletrostáticas, em um processo de um único passo. Adicionalmente as nanopartículas recobertas mostraram respostas como agentes de contraste para CT dependendo da razão $\text{Au}/\text{Fe}_2\text{O}_3$. Possíveis aplicações destas nanopartículas núcleo-camada irão derivar da combinação das propriedades magnéticas do núcleo (maguemita) e das propriedades ópticas da camada (ouro). Do ponto de vista terapêutico, estas amostras podem oferecer uma plataforma para realizar hipertermia magnética (núcleo) combinada ou não com terapia fototérmica (camada) e/ou terapia fotodinâmica (+ftalocianina). Levando em consideração a abordagem para diagnóstico, os materiais aqui sintetizados podem ser utilizados concomitantemente como sondas e agentes de contraste em técnicas de imagens médicas *in vivo*.

Futuramente, algumas novas abordagens serão realizadas na tentativa de se aprimorar, testar e confirmar propriedades e aplicações de novos materiais e/ou materiais já produzidos. Neste contexto, pode-se abordar nanopartículas em formatos elipsoidais, testes de toxicidade *in vivo* dos materiais adsorvidos com ftalocianinas em presença e ausência de luz, novas condições de síntese para controlar a aglomeração das moléculas de ftalocianinas adsorvidas e também testa-los em abordagens como micoCT, terapia fotodinâmica, fluorescência, magnetohipertermia, dentre outras mais.

ANEXO I

Normas de publicação para a revista Journal of Materials Chemistry B.

23/11/2016

How to prepare your article

[Members' area \(http://www.rsc.org/Membership/Memberzone/index.asp\)](http://www.rsc.org/Membership/Memberzone/index.asp) | [Support us \(/support-us/\)](#)[/](#)

Journals, books & databases

Prepare your article

Guidelines for authors on how to write and structure an article

Article templates

[\(/journals-books-databases/journal-authors-reviewers/author-tools-services/\)](/journals-books-databases/journal-authors-reviewers/author-tools-services/)



Find out how to prepare your article and present your research clearly, ensuring that all the relevant information is included.

You'll also find guidance here on the experimental data you should include in your article and material that can be placed in the electronic supplementary information (ESI).

For detailed information on acceptable formats for your figures, see our section on [Figures, graphics, images & cover artwork \(/journals-books-databases/journal-authors-reviewers/submit-your-article/#figures-graphics-images\)](#).

On this page

[How to write your article](#)

</journals-books-databases/journal-authors-reviewers/prepare-your-article/#how-to-write-article> | [Experimental data](#)

</journals-books-databases/journal-authors-reviewers/prepare-your-article/#experimental-data> | [Preparing electronic supplementary information \(ESI\)](#)

</journals-books-databases/journal-authors-reviewers/prepare-your-article/#preparing-esi>

How to write your article

On this page you'll find guidance and tips for first-time and experienced authors on writing style and how to structure an article. We've also included some [article templates \(/journals-books-databases/journal-authors-reviewers/author-tools-services/#article-templates\)](#) to help you structure and format your manuscript.

These guidelines are relevant to all of our journals. Please make sure you check the specific journal page for additional guidelines; you'll find the journals listed under [Our journals \(/journals-books-databases/about-journals/#journals\)](#).

Article types

23/11/2016

How to prepare your article

Articles commonly fall into one of three main categories: Full papers, Communications and Reviews. However, each journal will have further, specific article types, so you should always refer to a [journal's specific author guidelines \(/journals-books-databases/about-journals/#journals\)](#) while preparing your manuscript.

Full papers are original, unpublished primary research. Extensions of work that has been published previously in short form such as a Communication are usually acceptable.

Communications must contain original and highly significant work whose high novelty warrants rapid publication. Some journals have page limits for Communications.

Reviews may be an authoritative overview of a field, a comprehensive literature reviews, or tutorial-style reference materials. Reviews are usually invited by the editor, but a topic may be proposed by an author via the editorial office.

Format & layout of your article

Articles should be written clearly and concisely, avoiding repetition or embellishment. All submissions must be in English. Standard English or American spelling may be used in our journals, but consistency should be maintained within a manuscript. The use of common or standard abbreviations is encouraged; however, if using non-standard abbreviations, please define these when you first use them.

All articles accepted for publication in our journals are edited and typeset to our house style by professional editors: the manuscript will be formatted for you.

This section describes the content to be included in your article. Note that headings and subheadings are not permitted in articles submitted to *ChemComm*, although they are permitted in Communications submitted to other journals.

Section details & bibliography

Title

The title should be short and straightforward to appeal to a general reader, but detailed enough to properly reflect the contents of the article. Think about keywords and using recognisable, searchable terms – around 70% of our readers come directly via search engines. Avoid the use of non-standard abbreviations and symbols; examples follow.

An effective title

'Alkylation of active methylene compounds with alcohols catalysed by an iridium complex'.

An ineffective title

'Active methylene compounds are alkylated with ROH under catalysis of $[\text{IrCl}(\text{cod})]_2$ '.

Authorship

Full names and affiliations for all the authors should be included. Everyone who made a significant contribution to the conception, design or implementation of the work should be listed as co-authors. The corresponding author has the responsibility to include all (and only) co-authors. The corresponding author also signs a copyright licence on behalf of all the authors.

If there are more than 10 co-authors on the manuscript, the corresponding author should provide a statement to specify the contribution of each co-author. It is possible to have two corresponding authors. Please identify co-corresponding authors on your manuscript's first page and also mention this in your comments to the editor and/or cover letter.

Abstract

The abstract should be a single paragraph (50–250 words) that summarises the content of the article. It will help readers to decide whether your article is of interest to them.

It should set out briefly and clearly the main objectives and results of the work; it should give the reader a clear idea of what has been achieved. Like your title, make sure you use recognisable, searchable terms and keywords.

Introduction

Ç

23/11/2016

How to prepare your article

An introduction should 'set the scene' of the work. It should clearly explain both the nature of the problem under investigation and its background. It should start off general and then focus in to the specific research question you are investigating. Ensure you include all relevant references.

Experimental

You should provide descriptions of the experiments in enough detail so that a skilled researcher is able to repeat them. Standard techniques and methods used throughout the work should just be stated at the beginning of the section; descriptions of these are not needed. Any unusual hazards about the chemicals, procedures or equipment should be clearly identified.

Authors are encouraged to make use of [electronic supplementary information \(ESI\)](#) ([/journals-books-databases/journal-authors-reviewers/prepare-your-article/#preparing-esi](#)) for lengthy synthetic sections. In general there is no need to report unsuccessful experiments.

Only non-standard apparatus should be described; commercially available instruments are referred to by their stock numbers (for example, Perkin-Elmer 457 or Varian HA-100 spectrometers). The accuracy of primary measurements should be stated.

Suitable characterisations of compounds must be included - [read our experimental data guidelines](#) ([/journals-books-databases/journal-authors-reviewers/prepare-your-article/experimental-data/](#)).

[For studies that involve the use of live animals or human subjects please refer to our Human & Animal Welfare policy.](#) ([/journals-books-databases/journal-authors-reviewers/author-responsibilities/#authenticity](#))

Results & discussion

This is arguably the most important section of your article.

Your results should be organised into an orderly and logical sequence. Only the most relevant results should be described in the text; to highlight the most important points. Figures, tables, and equations should be used for purposes of clarity and brevity. Data should not be reproduced in more than one form, for example in both figures and tables, without good reason.

The purpose of the discussion is to explain the meaning of your results and why they are important. You should state the impact of your results compared with recent work and relate it back to the problem or question you posed in your introduction. Ensure claims are backed up by evidence and explain any complex arguments.

Conclusions

This is for interpretation of the key results and to highlight the novelty and significance of the work. The conclusions should not summarise information already present in the article or abstract. Plans for relevant future work can also be included.

Acknowledgements

Contributors (that are not included as co-authors) may be acknowledged; they should be as brief as possible. All sources of funding should be declared.

Footnotes

Footnotes relating to the title and/or authors, including affiliations, should appear at the very bottom of the first page of the article. If ESI is available this is also stated here.

Bibliographic references & notes

We will format your content according to our house style before publication; however, it's important you use Vancouver style (not Harvard style) for all journals except *Chemistry Education Research and Practice* ([/journals-books-databases/about-journals/chemistry-education-research-practice/](#)), which requires the use of Harvard referencing.

[You can also automatically format references from your Endnote citation manager using our style files.](#) ([/journals-books-databases/journal-authors-reviewers/author-tools-services/#article-templates](#))

Notes relating to the main text should appear at the end of the article, just above the references. These might include:

- comments relevant to but not central to the matter under discussion
- limited experimental and spectral data
- crystallographic data.

Referencing in the text

Use superscript numbers to show the reference source of statements in the text – for example, *reactive small molecule species*.³ Usually these should appear at the end of the sentence (after the punctuation), but can be after the relevant word or compound.

The reference numbers should be cited in the correct sequence through the text (including those in tables and figure captions, numbered according to where the table or figure is designated to appear).

If a statement has multiple references you should reference all of the citations in the text. If you have two citations, or if you have more than two and the numbers are not consecutive, use commas (with no spaces) between numbers, examples: ^{12,13} or ^{12,14,15}. If there are more than two numbers and they are consecutive, use an en-dash to separate the first and last citation – for example, ^{14–20}.

The author(s) can be mentioned at their first citation in the text, but initials are not necessary. For papers with one or two authors simply state the surname(s), and for papers with three or more authors you should use the first author's surname followed by *et al.*

Listing your references

The references themselves are listed in numerical order at the end of the main article. The names and initials of all authors should be given in the reference.

Journal articles

The journal abbreviations to be used in Royal Society of Chemistry publications are defined in [Chemical Abstracts Service Source Index \(CASSI\) \(<http://cassi.cas.org/search.jsp>\)](#). If you cannot find a recognised abbreviation for a journal and it is not obvious how the title should be abbreviated, please cite the full journal title.

Journal articles should be cited in the form: A. Name, B. Name and C. Name, *Journal Title*, year, volume, page.

Inclusion of article title is optional for most journals, but required for [Food & Function \(\[journals-books-databases/about-journals/food-function/\]\(http://journals-books-databases/about-journals/food-function/\)\)](#), [Metalomics \(\[journals-books-databases/about-journals/metalomics/\]\(http://journals-books-databases/about-journals/metalomics/\)\)](#) and [Toxicology Research \(\[journals-books-databases/about-journals/toxicology-research/\]\(http://journals-books-databases/about-journals/toxicology-research/\)\)](#).

When page numbers are not yet known, articles should be cited by DOI (Digital Object Identifier) – for example, T. J. Hebden, R. R. Schrock, M. K. Takase and P. Müller, *Chem. Commun.*, 2012, DOI: 10.1039/C2CC17634C.

Books

A. Name, B. Name and C. Name, *Book Title*, Publisher, Publisher Location, year. For example, S T Beckett, *Science of Chocolate*, Royal Society of Chemistry, Cambridge, 2000. If you are referencing published conference proceedings, these should be cited like a book.

Book chapters

A. Name, in *Book Title*, ed. Editor Name(s), Publisher, Publisher Location, edition, year, chapter, pages. The 'ed.' in the example above stands for 'edited by', that is, the editor(s) of the book; if the book has no editors this can be left out.

Theses

A. Name, PhD thesis, University Name, year.

Lectures, meetings & conferences

A. Name, presented in part at Conference Title, Place, Month, year.

Reference to unpublished material

If you reference unpublished material in your article you must provide the editor with copies of the manuscripts with your submission. You should not reference unpublished work without the permission of those who completed the work.

For material accepted for publication, but not yet published: A. Name, *Journal Title*, in press. For material submitted for publication, but not yet accepted: A. Name, *Journal Title*, submitted. For material that has yet to be submitted for publication: A. Name, unpublished work.

Online resources (including databases, websites & wikis)

Name of resource, URL, (accessed date). Please note the most important information to include is the URL and the date accessed. For example, The Merck Index Online, <http://www.rsc.org/Merck-Index/monograph/mono1500000841>, (accessed October 2013).

Preprint servers (for example, arXiv)

For example: V. Krstic and M. Glerup, 2006, arXiv:cond-mat/0601513.

Patents

The name of the patentee must be given. For example, *Br. Pat.*, 357 450, 1986. *US Pat.*, 1 171 230, 1990.

Software

T. Bellander, M. Lewne and B. Brunekreef, GAUSSIAN 3 (Revision B.05), Gaussian Inc., Pittsburgh, PA, 2003.

Experimental data

On submission of a manuscript authors should provide all data required to understand and verify the research presented in the article. The Royal Society of Chemistry believes that where possible all data associated with the research in a manuscript should be freely available in an accessible and usable format, enabling other researchers to replicate and build on that research.

[Read about our data policy and the experimental data \(/journals-books-databases/journal-authors-reviewers/prepare-your-article/experimental-data/\)](#) you should include for the characterisation of new compounds, X-ray crystallography and macromolecular structures.

Preparing electronic supplementary information (ESI)

You can include ESI with your article to enhance and increase the impact of your work, for example by including 3D molecular models and movies. Authors can also improve the readability of their articles by placing appropriate material in the ESI, such as repetitive experimental details or bulky data. All information published as ESI is fully archived and permanently linked to the article using CrossMark.

When preparing your ESI data files, you should keep in mind the following points:

- Supplementary data is peer-reviewed and should therefore be included with the original submission.
- ESI files are published 'as is'; editorial staff will not edit the data for style or content.
- Data are useful only if readers can access it; use common, widely known file formats.
- Large files may prove difficult for users to download and access.

We encourage the submission of supporting information for compounds and spectra in electronic format. For compounds, please supply mol files (exported from your chemical drawing package) as unique compounds, without R-groups or variable attachments. Spectral data such as NMR, IR, Raman, ESR should be supplied in the standard JCAMP-DX (<http://www.jcamp-dx.org>) format (.jdx files).

We offer a service that enables the 3D visualisation of complex molecules. You can use the [FirstGlance in Jmol tool](http://firstglance.jmol.org) (<http://firstglance.jmol.org>) to prepare these.

Multimedia files

We welcome the use of multimedia files (including videos and animations) as these can be an excellent medium to present elements of your work. Any videos of general interest may be shared with the wider community via our YouTube channel or through social media - please notify the editorial team if you prefer for your video(s) not to be promoted in this way.

If you submit a multimedia file alongside your paper, please refer to it within your paper to draw it to the reader's attention. Please also provide a short descriptive title for the video.

Acceptable formats for video or animation clips are:

- WMV
- AVI
- MOV
- MPG

Please minimise file sizes where you can; we recommend a maximum file size of 5MB and a maximum frame size of 640 x 480 pixels. If your video is very short (only a few seconds long) then it is recommended that you loop the section a few times to provide a more detailed view.

Video abstracts

23/11/2016

How to prepare your article

We welcome the opportunity to help authors promote their papers by the placement of video abstracts on YouTube, which we can then promote via social media channels. Video abstracts offer an exciting opportunity to highlight the importance of a paper to the reader in a new and engaging way.

Content

- Start by introducing the conclusion of your article and concentrate on the main results.
- Focus the video on why the article is relevant to the reader.
- Introduce relevant co-workers and mix in images/footage of your laboratory, experiment and equipment to make it more engaging.
- Videos should be approximately two-three minutes in length (no longer than four minutes).
- On screen text should be used sparingly and be large enough to read clearly.


Technical

- Minimum frame size: 320 x 240 pixels; maximum 640 x 480.
- Frames per second: 25 to 30.
- Aspect Ratio: 4:3 preferred - please contact us regarding 16:9.
- Formats accepted: MPG, MOV, AVI, WMV.
- The maximum size should be 40MB - please contact us if this presents a problem.

Notes

- Video abstracts will be hosted on Youtube or another third party hosting provider.
- We may edit your video if required, overlay a logo on your video and add a splash screen at the end of the video.
- All abstracts will be accessed for suitability prior to being uploaded to the Royal Society of Chemistry YouTube Channel.
- You should ensure that you have copyright permission for any images, stock footage or background music used.
- Please also submit a transcript of the video abstract that we can upload to make it more accessible.

Advertisement



http://oas.rsc.org/5c/www.rsc.org/chemistryworld/journals-books-databases/journal-authors-reviewers/prepare-your-article/26/2099535740/Top/RSC/JohnsonMatthey_2016/Johnson_Matthey_728x90_November.qif/70436c693431623849653441433

Contact our Publishing customer services team
 Email: [Send us an email](#)

Share

Anexo II

Confirmação do Qualis da revista para a qual o artigo foi submetido.


ACESE A
PLATAFORMA

[Início](#) | [Sobre](#) | [Solicitações](#) | [Informações do Programa](#) | [Consultas](#) | [Manual](#) | [Contato](#)

Periódicos Qualis

Dados para Consulta

Evento de Classificação:
Qualis 2014 ▼

Área de Avaliação
 INTERDISCIPLINAR ▼ 

ISSN:

Título:
 journal of materials chemistry

Classificação:
 -- SELECIONE -- ▼

Periódicos

ISSN	Título	Área de Avaliação	Classificação
2050-7526	JOURNAL OF MATERIALS CHEMISTRY.	INTERDISCIPLINAR	A1

[Ir para o topo](#)

Versão 2.4.2

Anexo III

Comprovante de envio (submissão) do artigo para a revista Journal of Material Chemistry B.

22/11/2016

ScholarOne Manuscripts

 Journal of Materials Chemistry B[Home](#)[Author](#)

Submission Confirmation

[Print](#)

Thank you for your submission

Submitted to

Journal of Materials Chemistry B

Manuscript ID

TB-ART-11-2016-003040

TitleMaghemite-Gold core-shell nanostructures (γ -Fe₂O₃@Au) surface-functionalized with aluminium phthalocyanine for multi-task imaging and therapy**Authors**

Coelho, Breno
Siqueira, Elis
Ombredane, Alicia
Joanitti, Graziella
Chaves, Sacha
Chaker, Juliano
Longo, João
Bentes de Azevedo, Ricardo
Morais, Paulo
Sousa, Marcelo Henrique

Date Submitted

22-Nov-2016

[Author Dashboard](#)

© Thomson Reuters | © ScholarOne, Inc., 2016. All Rights Reserved.
ScholarOne Manuscripts and ScholarOne are registered trademarks of ScholarOne, Inc.
ScholarOne Manuscripts Patents #7,257,767 and #7,263,655.

[@ScholarOneNews](#) | [System Requirements](#) | [Privacy Statement](#) | [Terms of Use](#)

Anexo IV

Artigo enviado no template da revista Journal of Material Chemistry B.



Maghemite-Gold core-shell nanostructures ($\gamma\text{-Fe}_2\text{O}_3\text{@Au}$) surface-functionalized with aluminium phthalocyanine for multi-task imaging and therapy

Received 00th January 20xx,
Accepted 00th January 20xx

DOI: 10.1039/x0xx00000x

www.rsc.org/

B. C. P. Coelho,^a E. R. Siqueira,^b A. S. Ombredane,^b G. A. Joanitti,^b S. B. Chaves,^b J. A. Chaker,^c J. P. F. Longo,^b R. B. Azevedo,^b P. C. Morais,^{d,e} M. H. Sousa^{*c}

In this study we report on elaboration and characterization of core-shell maghemite-Gold nanoparticles with shell modulated for different thicknesses below 2 nm. Gold-shelled maghemite nanoparticles with average core size about 9 nm were elaborated by a single-step protocol involving reduction of Au^{3+} in the presence of citrated-coated maghemite nanoparticles. Additionally, post-functionalization of the core-shell structures with aluminium phthalocyanine was successfully accomplished, aiming the production of a material platform for photodynamic therapy. The as-produced samples were structurally, morphologically, magnetically and optically characterized and presented long-term colloidal stability at physiological pH. Impressively, we found the as-produced samples showing good X-ray attenuation property, rendering them with ability to be used as a nanoprobe for targeted computed tomography. Moreover, *in vitro* nanocytotoxicity tests confirmed superior biocompatibility of the as-produced samples, making them a very promising multi-task platform for *in vivo* applications.

Introduction

Iron oxide nanoparticles, mainly magnetite (Fe_3O_4) and maghemite ($\gamma\text{-Fe}_2\text{O}_3$), found numerous applications in the biomedical field, credited to their size-dependent physical (e.g. magnetic and optical) and chemical (e.g. surface reactivity) properties, which can be used not only to improve biocompatibility and specificity, but also offer the way to achieve the dual goal of theranostics (diagnostics plus therapy)¹. Along this line, co-assembled nanosized magnetic iron oxide and metallic Gold in a core-shell heteromaterial has attracted broad interest, aiming its application as a multifunctional material nanoplatform². Magnetism associate with the core iron oxide renders for noninvasive manipulation (using gradient of magnetic field) and heating (using AC magnetic field), which are key features for site targeting and magnetohyperthermia³, respectively. Additionally, while lowering nanotoxicity the Gold-shell increases long-term colloidal stability and presents a versatile platform for bioconjugation⁴. Furthermore, at the nanoscale surface plasmon in Gold is enhanced, which results in significant and tunable optical absorption and emission in the visible (VIS) and

near-infrared (NIR) regions, covering the biological window of human tissues while allowing partial transparency to light⁵. Therefore, in addition to magnetohyperthermia, Gold-shelled magnetic nanoparticles are useful in photothermal therapy, where localized heating is accomplished via light irradiation⁶. Besides, due to their unique optical properties Gold-based nanostructures can act as fluorescent probes for *in vivo* imaging⁷. Moreover, fluorophores can easily functionalize Gold-terminated surfaces, thus enhancing the optical performance of Gold-shelled magnetic iron oxide nanoparticles. Particularly interesting for surface-functionalization are phthalocyanines, which are photosensitizers capable of converting specific light energy into chemical potential and widely used in photodynamic therapy (PDT)⁸. However, due to the high hydrophobicity and tendency to self-aggregate in aqueous medium the use of phthalocyanines is quite limited in the bioenvironment. To circumvent this drawback phthalocyanines have been incorporated into nanostructured systems, such as nanoemulsions⁹ or linked to magnetic¹⁰ and Gold¹¹ nanoparticle surfaces, resulting in improvement in PDT efficacy. Still in the diagnostics area, while presenting high electron density and strong X-ray attenuation Gold-based nanostructures can be used as contrast agents for computed tomography (CT) imaging¹². Worth mentioning that the conventional Iodine-based contrast agents usually present severe limitations, such as short imaging time and low specificity.

This study reports on the elaboration and investigation (structural, morphological, magnetic, optical, and biological) of nanostructures comprising a magnetic core (maghemite) surface-shelled with Gold, which is further surface-functionalized with aluminium phthalocyanine to act as a nanoplatform for multi-therapy and multi-imaging combined

^a Instituto Federal de Educação Ciências e Tecnologia de Brasília, Gama, DF 72429-005, Brazil.

^b Department of Genetics and Morphology, Institute of Biological Sciences, Brasília University, Brasília, 70919-900, Brazil.

^c Green Nanotechnology Group, Faculdade de Ceilândia, Universidade de Brasília, Ceilândia, DF 72220-900, Brazil. E-mail: mhsousa@unb.br

^d Universidade de Brasília, Instituto de Física, Brasília DF 70910-900, Brazil.

^e Anhui University, School of Chemistry and Chemical Engineering, Hefei 230601, China.

See DOI: 10.1039/x0xx00000x

techniques. Gold-shelled maghemite nanoparticles, with Au-shell modulated for different thicknesses, were elaborated by borohydride-mediated reduction of Au^{3+} in the presence of citrate-capped maghemite nanoparticles, the latter obtained by co-precipitation in aqueous medium. Maghemite-Gold core-shell nanostructures surface-functionalized with aluminium phthalocyanine is a novelty in the literature, yielding sols with long-term colloidal stability and biocompatibility. The promising application of the as-elaborated materials as contrast agents in computed tomography imaging was herein evaluated using a commercial microtomograph (SkyScan1076, Bruker). In order to support the bioimaging application of the as-elaborated nanoplatform *in vitro* assays were performed to assess the nanocytotoxicity.

Experimental

All chemicals listed in the present report were of analytical degree and used as received without any further purification. Water used to perform the experiments was purified by a Milli-Q water system (Millipore, USA).

Samples

Citrate-capped maghemite nanoparticles (MNP)

As schematically shown in Fig. 1 citrate-capped maghemite ($\gamma\text{-Fe}_2\text{O}_3$) nanoparticles were synthesized using a slightly modified procedure already described in the literature¹³. Briefly, 50 mL of aqueous solution containing 50 mmol of Fe^{2+} , 25 mmol of Fe^{3+} and 20 mmol of HCl were quickly poured into 250 mL of NH_4OH aqueous solution (1 mol/L), under vigorous stirring (1000 rpm) at room temperature. The as-formed black precipitate of magnetite (Fe_3O_4) was magnetically separated and washed with water several times until the solution reached neutral pH. Then, the precipitate was acidified with HNO_3 aqueous solution (0.5 mol/L) and magnetically separated from the supernatant. Next, the slurry containing magnetite was oxidized to maghemite by boiling the precipitate with 0.5 mol/L $\text{Fe}(\text{NO}_3)_3$ for 30 min. The as-treated precipitate was removed out from the solution by magnetic decantation. Citrate-capped maghemite nanoparticle was prepared from the as-produced bare maghemite using trisodium citrate solution (1.0 mol/L) at 80 °C for 30 min (molar ratio of citrate to iron = 0.1). The obtained precipitate was magnetically collected, washed twice with acetone (excess of acetone evaporated), re-suspended in water, adjusted pH to 7.0 and labeled as sample MNP.

Gold-coated nanoparticles (MNP@Au1 and MNP@Au2)

Gold-shelled maghemite was formed by reduction of Au^{3+} (from HAuCl_4) onto citrate-capped maghemite nanoparticles using sodium borohydride (NaBH_4) as reducing agent (see scheme Fig. 1). Typical Au-coating protocol is as follows: 80 μL of 400 mg/mL of the as-produced MNP sample was dispersed in 80 mL of water. Next, under sonication, 180 μL of HAuCl_4 (1 ww%) was added. After 10 min, 150 μL of NaBH_4 (0.3 mol/L, in

ethanol) was added to the reaction medium and the system was sonicated for 10 min more. This $\text{HAuCl}_4/\text{NaBH}_4$ cycle was repeated four times and the final sample was labeled MNP@Au1. Similarly, sample MNP@Au2 was produced, but the amount of HAuCl_4 and NaBH_4 was twice of that used to produce sample MNP@Au1.

Aluminium phthalocyanine-functionalized nanoparticles (MNP/PTC and MNP@Au/PTC)

In order to attach aluminium phthalocyanine (PTC) to the as-produced nanoparticles 100 μL of aluminum phthalocyanine chloride (0.4 mmol/L in DMSO) was added to 7.5 mL (100 $\mu\text{g}/\text{mL}$) of sample MNP (or MNP@Au2) to form the phthalocyanine-modified nanoparticles labeled as MNP/PTC (or MNP@Au/PTC). All PTC-functionalized samples were sonicated for 10 min, centrifuged to eliminate supernatant and re-dispersed in water. All the steps performed while preparing the final MNP/PTC, MNP@Au/PTC samples are schematically shown in Fig. 1.

Characterization

X-ray diffraction (XRD) powder analyses of the samples were carried out in a Miniflex 600 diffractometer (Rigaku) over 2θ range of 20° - 70°, using Cu-K α radiation ($\lambda = 1.541 \text{ \AA}$) and operating at 40 kV and 30 mA. Size and morphology of the as-produced materials were examined by high-resolution transmission electron microscopy (HRTEM) using a JEOL 1100 apparatus. Room temperature magnetization curves were obtained using a vibrating sample magnetometer (VSM) ADE model EV7. Hysteresis loops were recorded in the $\pm 18 \text{ kOe}$ range. Chemical analyses of the as-produced samples¹⁴ were determined using an inductively coupled plasma optical emission spectrometer (ICP-OES) Perkin Elmer model Optima 8000, with radiofrequency power of 1400 W, 1.5 mL/min sample flux, 10 L/min argon plasma flux, nebulizer flux 0.7 L/min and flux of auxiliary gas (argon) of 0.2 L/min. Hydrodynamic average diameter (D_H), polydispersity indexes (PDI) and zeta potential (ζ -potential) of the as-produced nanoparticles were assessed from aqueous dispersions using a dynamic light scattering (DLS) Zetasizer nano ZS system (Malvern Instrument). Ultraviolet visible (UV-vis) spectra of aqueous dispersions were recorded on a spectrophotometer Shimadzu UV 2600. The X-ray density of samples was evaluated in plastic microtubes using a microtomograph device (SkyScan1076, Bruker) with the following parameters: 50kV, 180 μA , 0.5nm Al filter, 100 ms of exposition and pixels size of 35 μm . NRecon[®] and CTA[®] softwares were employed respectively for reconstruction and image analysis. Slices were analyzed with Dataviewer[®] software. The Hounsfield scale (HU units) was used to quantify the X-ray density and a 3D image of the samples was prepared for qualitative evaluation.

Cell culture

Murine fibroblast cells (NIH-3T3) and human keratinocyte cells (HaCAT) were acquired from cell bank of Rio de Janeiro (Brazil). *Dulbecco's Modified Eagle's Medium* (DMEM) (Life, EUA) completed with 10 % of fetal bovine serum and 1 % of antibiotic solution (100 IU/mL Penicillin – 100 µg/mL Streptomycin, Life, EUA) was used to grow the cells at 37 °C and 5% CO₂ in humid atmosphere.

Cell treatment

The cells were grown into polystyrene culture flask of 75 cm². The cells were counted using a Neubauer chamber and the number of the cells per mL was determined by the equation: Number of cells/mL = (number of counted cells/4)*dilution factor*104. For each experiment, the cells were seeded into a 96-well culture plates at the density of 3.103 cells per well in

DMEM. The plates were incubated at 37 °C and 5% CO₂ in humid atmosphere overnight.

Cell-viability assay

Cell-viability assay was realized using MTT (3-[4, 5-dimethylthiazol-2-yl]-2,5-diphenyltetrazolium bromide) dry reduction method. After 24 and 72 hours of incubation, 150 µL of the MTT solution (0.5 mg/mL in DMEM) was added in each well and the plates were incubated for 2 hours at 37 °C and 5% CO₂ in humid atmosphere. The medium culture was discarded and 100 µL of dimethyl sulfoxide (DMSO) were added in each well. The absorbance was monitored using a spectrophotometer with a microplate reader at 595 nm (Molecular Devices, EUA).

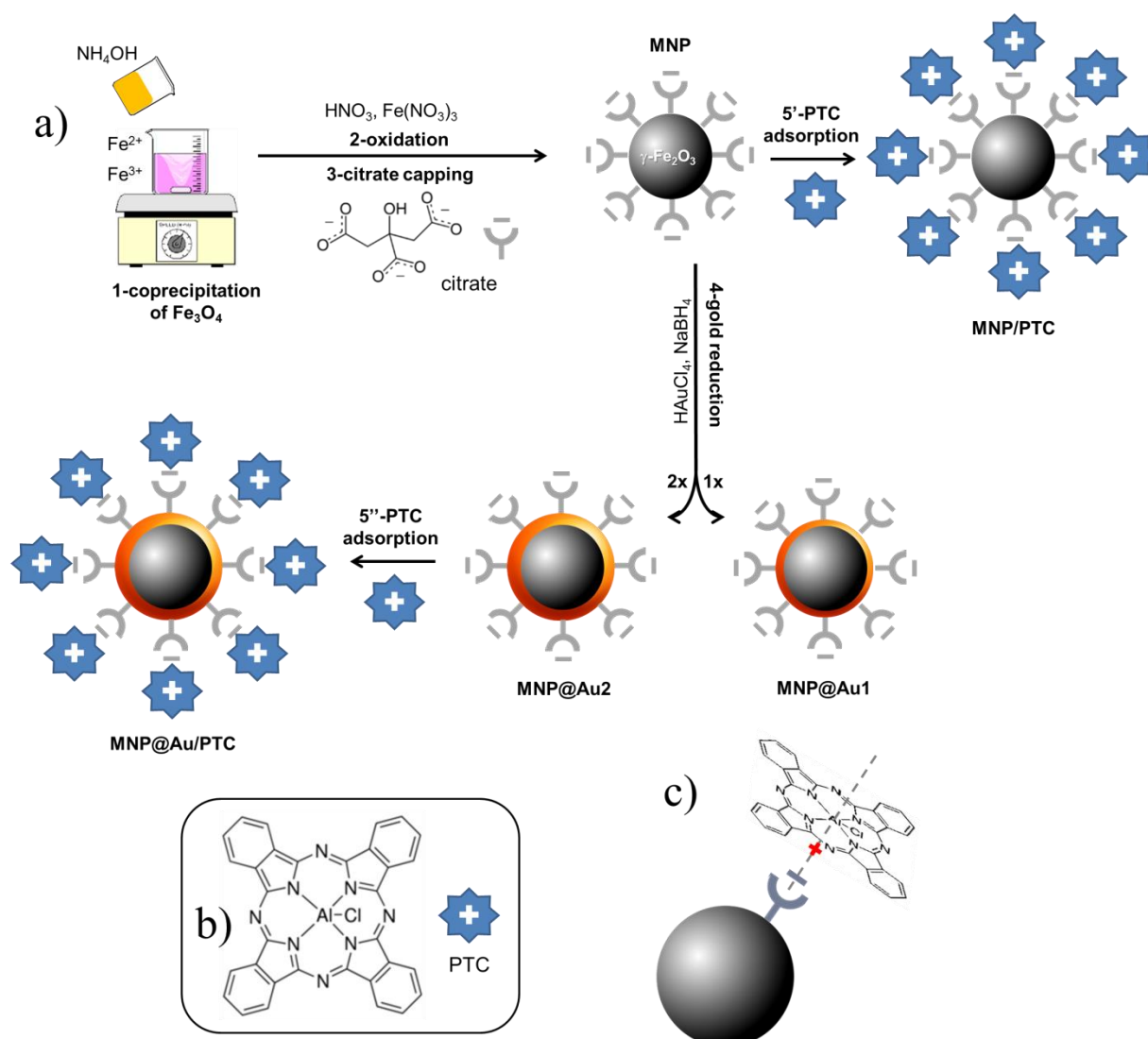


Figure 1. Scheme used in the preparation of samples MNP, MNP/PTC, MNP@Au1, MNP@Au2 and MNP@Au/PTC.

Table 1. Quantitative data of pool content

groups	MNP and MNP@Au ($\mu\text{g/mL}$)	MNP and MNP@Au (μL)	H ₂ O (μL)	culture medium (μL)
Control	-	-	50	150
1	100	50	-	150
2	50	25	25	150
3	25	12.5	37.5	150
4	12.5	6.25	43.75	150
5	6.25	3.12	46.88	150

Statistical analysis

The results were expressed as mean \pm standard error of the mean (SEM). Evaluation of possible significant differences among the groups was determined by analysis of variance (ANOVA) and Bonferroni post-hoc test using the program Prism 5 (EUA). The significance level was set at $P < 0.05$.

Results and discussion

Samples

Fig. 2 shows XRD spectra of samples MNP and MNP@Au2. For the employed synthesis route all diffraction peaks observed sample MNP are consistent with the standard data of maghemite (JCPDS card no. 39-1346). The average crystallite size of the magnetic core, calculated from the 311 XRD line broadening of sample MNP using the Scherrer's formula, is about 9.3 nm. Additionally, for the MNP@Au2 sample, the XRD peaks appearing at 38.4° and 44.6° can be respectively assigned to (111) and (200) crystalline plane diffraction peaks of Gold, in good agreement with standard data of Gold (JCPDS file no. 040784).

Moreover, one can notice a reduction of the maghemite XRD peak intensities after Au-capping, which is more likely due to the heavy atom effect of Gold as a result of the formation of Au-coated $\gamma\text{-Fe}_2\text{O}_3$ nanoparticles¹⁵. Similar results were found in the XRD data of sample MNP@Au1 (XRD data not shown here). Chemical analyses using ICP-OES revealed samples MNP@Au1 and MNP@Au2 with increasing Gold content (Au/Fe₂O₃ ratio) of 7.3% and 12.1% (w/w), in agreement with the preparation protocol. Cross-linking ICP-OES data with XRD analyses strongly supports core-shell ($\gamma\text{-Fe}_2\text{O}_3\text{-Au}$) formation in samples MNP@Au1 and MNP@Au2, which is corroborated by the TEM data. As shown in Fig. 3a, maghemite nanoparticles (MNP) are polydisperse in size, but showing nearly spherical morphology. Moreover, the cubic structure of the maghemite phase is confirmed by fast Fourier transform (FFT) image shown in the inset of Fig. 3b (lower right hand-side), revealing

planes (440), (311), (220) and (111) of the spinel phase. Figure 3c shows a typical TEM image of sample MNP@Au2, with darker $\gamma\text{-Fe}_2\text{O}_3$ nanoparticle spots (darker than in the MNP sample) due to the Au-shell. Sparse-filled (MNP) and dense-filled (MNP@Au2) histogram patterned bars, assessed from the TEM micrographs, are shown in Fig. 3d, where black solid lines are the best fit using the lognormal size distribution. From this analysis, the average diameters (polydispersity index) of maghemite (MNP) and gold-coated nanoparticles (MNP@Au2) are respectively 12.9 nm ($\sigma = 0.34$) and 12.1 nm ($\sigma = 0.30$), suggesting there is no significant difference in average size and polydispersity index of uncoated and Gold-coated nanoparticles. However, HRTEM of Gold-coated nanoparticles shown in Fig. 3e clearly reveal core-shell formation with Au-shell thickness in the range of 1-2 nm, in good agreement with previous works¹⁶. Furthermore, Fig. 3f shows HRTEM of an isolated core-shell (Au- $\gamma\text{-Fe}_2\text{O}_3$) nanoparticle where the interfringe spacings of the face centered cubic (FCC) Gold (111) and (311) reflections are clearly seen in the FFT image (upper left hand-side inset), indicating that the maghemite nanoparticles are coated with a layer of crystalline Gold.

Magnetization measurements were performed for evaluating the Au-coating in the magnetic properties of the as-produced nanoparticles. Figure 4 shows typical room temperature magnetization as a function of applied magnetic field recorded for samples MNP (red data) and MNP@Au2 (black data). We found the saturation magnetization decreasing from 47.9 emu/g (sample MNP) to 44.6 emu/g (sample MNP@Au1) and 42.4 emu/g (sample MNP@Au2), supporting the claim that a magnetic core (maghemite) is coated with a non-magnetic shell (Gold).

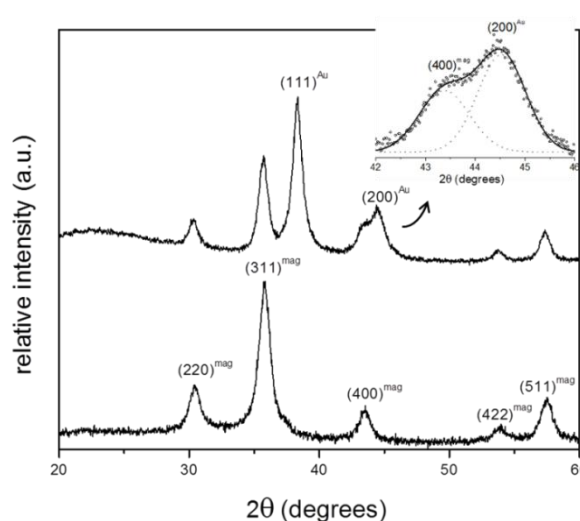


Figure 2 – Diffractograms of samples MNP (lower panel) and MNP@Au2 (upper panel). The inset shows a detail of the XRD spectrum of sample MNP@Au2 in the 2θ range of about 42° to 46° , emphasizing the deconvolution of the 44.6° XRD feature into two components.

Thus, considering there is no phase change of the magnetic core after Au-coating a Au/Fe₂O₃ ratio of 6.6% and 11.3% (w/w) can be estimated from the magnetization data respectively for samples MNP@Au1 and MNP@Au2, in good agreement with the chemical analysis (ICP-OES). Moreover, at room temperature the as-prepared uncoated and Gold-coated nanoparticles shows superparamagnetic behavior, with negligible remanence and coercivity as shown in Fig. 4 (see lower right hand-side inset). Besides, saturation magnetization of the as-prepared core maghemite is lower than typical bulk values (60–80 emu/g), credited to the nanometer size¹⁷ and surface functionalization¹⁸. Likewise, the as-prepared samples

functionalized with phthalocyanine also presented similar magnetic behavior, with no alteration of saturation magnetization. Moreover, as can be observed in the inset of Fig. 4 (upper left hand-side), separation of the magnetic nanoparticles out from the transparent solvent can be observed while adding acetone to the water-based suspension and keeping a permanent magnet attached to the sample holder for several hours. This finding strongly indicates attachment of Gold and phthalocyanine onto maghemite nanoparticles.

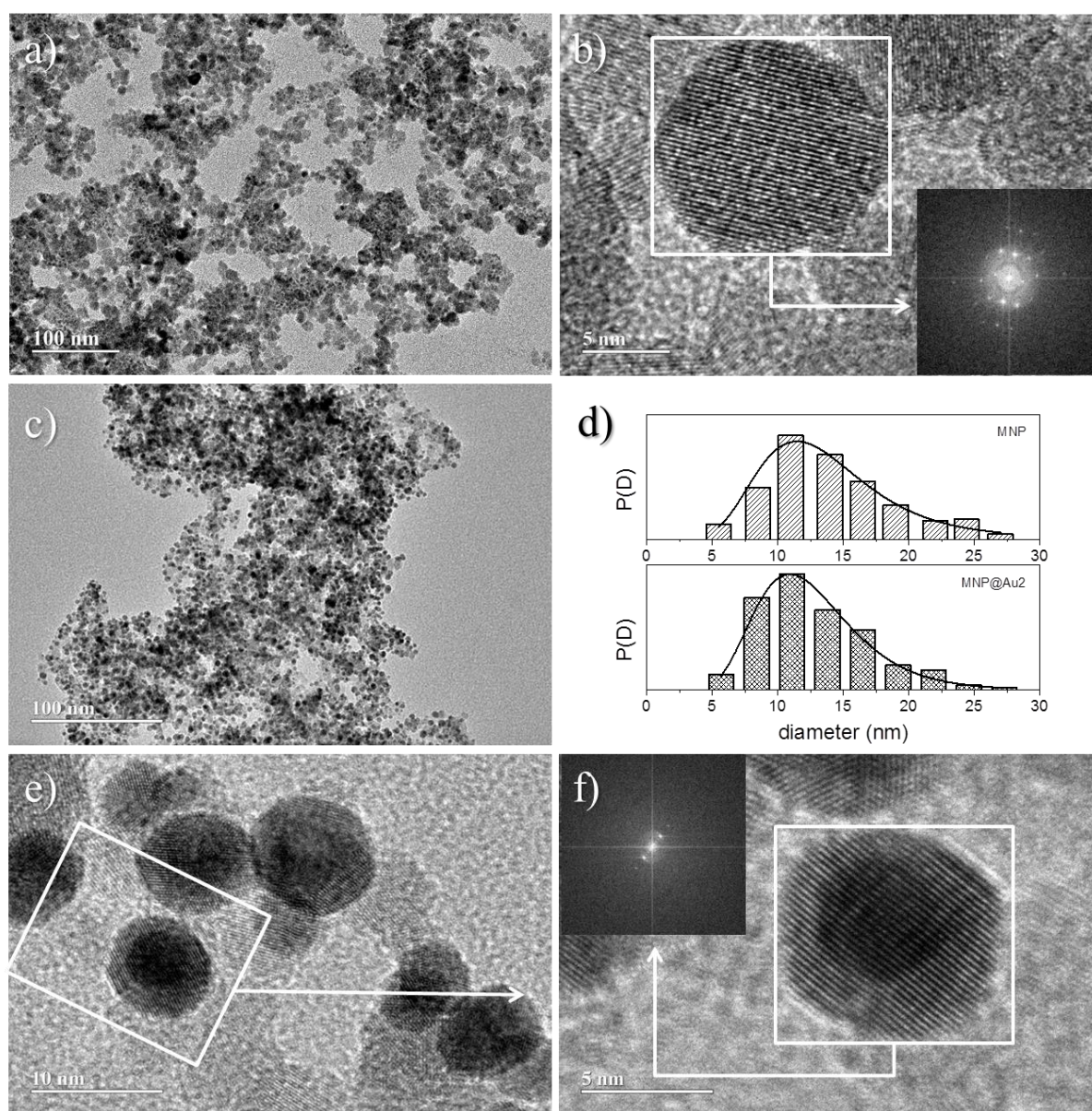


Figure 3 –TEM images of MNP (a) and MNP@Au2 (c) nanoparticles; HRTEM image of selected region in sample MNP (b); histograms of particle diameters for MNP and MNP@Au2 samples (d); HRTEM image of selected region in sample MNP@Au2 (e); magnified TEM image of the boxed region in the left image (f). The insets show the FFT calculated from the areas marked with white squares.

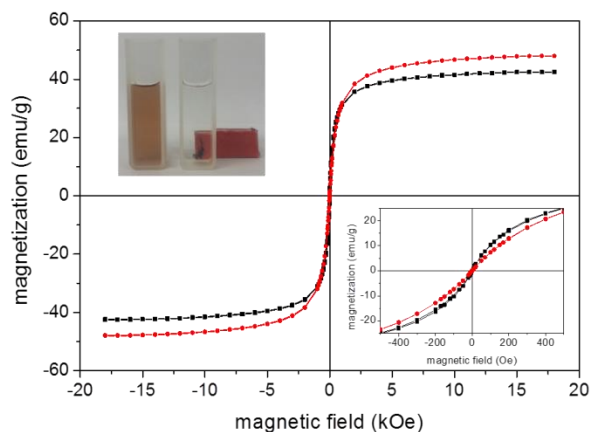


Figure 4. Magnetization hysteresis loops at room temperature for samples MNP (red) and MNP@Au2 (black); picture of the sample MNP@Au2 under action of a permanent magnet (upper left hand-side inset); magnetization at low field range (lower right hand-side inset).

The nature of maghemite surface-coating (Gold, citrate, and/or aluminum phthalocyanine) changes the interface nanoparticle surface/solution and thus colloidal stability, which indeed affects optical properties. Therefore, DLS and UV-vis spectroscopy were used to assess surface modification information of bare maghemite nanoparticles. Table 2 lists DLS data for the as-prepared samples. All measurements were performed at pH~7 and 25 °C. The ζ -potential of citrate-coated maghemite nanoparticles (sample MNP) is highly negative (about -38 mV) and is likely due to the ionization of attached citrate molecules onto the oxide surface^{19,20}. The ζ -potential of Gold-coated nanoparticles (samples MNP@Au1 and MNP@Au2) are also highly negative, not differing significantly from the value found for citrate-coated nanoparticles in sample MNP (see Table 2). Actually, it is well known that reduction of Gold in the presence of sodium citrate yields Gold-coated inorganic core nanoparticles with citrate molecules attached onto the surface, providing a negatively charged surface for the Au-coated nanoparticle²¹. In the case of our samples, at neutral pH the free carboxyl groups of citrate are fully deprotonated, providing extra colloidal stability to the as-suspended nanoparticles via electrostatic repulsion. Magnetic separation of the as-produced sols (see inset of Fig. 4) is only achieved by adding a non-aqueous solvent, such as acetone.

Table 2. Hydrodynamic average diameter, PDI and ζ -potentials of samples

Sample	D_H (nm)	PDI	ζ -potential (mV)
MNP	68.1	0.23	-38.6
MNP@Au1	114.3	0.19	-34.3
MNP@Au2	156.6	0.18	-39.6
MNP/PTC	235.9	0.21	-12.6
MNP@Au/PTC	211.1	0.25	-25.5

Moreover, the hydrodynamic sizes of citrate-coated maghemite nanoparticles (sample MNP) increased from 68.1 nm to 114.3 nm and 156.6 nm for samples MNP@Au1 and MNP@Au2, respectively. This finding is credited to the increasing thickness of the deposited Gold-shell onto the maghemite core. However, possible nanoparticle agglomeration must be considered in this analysis. On the other hand, data listed in Table 2 show that adsorption of aluminium phthalocyanine significantly reduces the ζ -potentials of samples MNP/PTC (-12.6 mV) and MNP@Au/PTC (-25.5 mV). The colloidal stability reduces while the ζ -potential decreases, reflecting on increasing hydrodynamic diameters after PTC coating (see Table 2). These results indicate that electrostatic interaction between negatively charged citrate-coated nanoparticles and positively charged aluminium phthalocyaninate occurs, as schematically shown in Fig. 1c. Previous work⁸ showed similar results where zinc tetrasulfonated phthalocyanine (a tetra-anion) was strongly adsorbed onto positively charged surface of maghemite nanoparticles. Furthermore, once PTC presents small charge-to-area ratio formation of a PTC layer onto the nanoparticle surface is not enough to neutralize all negative nanoparticle surface sites and therefore a net negative surface charge still remains, but smaller than before PTC coating.

Typical UV-vis spectra of surface-coated (citrate, Gold, and PTC) maghemite nanoparticles in suspension are shown in Fig. 5a. Citrated-coated maghemite nanoparticles present a wide silent feature in the visible region. On the other hand, Gold-coated maghemite nanoparticles exhibit an absorption band centered around 555 nm, which is due to the surface plasmon absorption²². In fact, it is reported that the position of this band depends on the core size as well as on the Au-shell thickness²³. In our case, as the ratio Au/Fe₂O₃ increases a blue shift of the surface plasmon peak is observed (see the inset of Fig. 5a), in good agreement with previous works²⁴. A reddish-pink color was observed in the brown tinged γ -Fe₂O₃ sol after Au-coating, indicating the formation of Gold shell onto maghemite nanoparticles (see Fig. 5b). Moreover, after magnetic separation of nanoparticles from suspension of sample MNP@Au2 the supernatant remains colorless (see inset of Fig. 4), supporting this claim.

Figure 5a also shows the UV-vis spectrum of PTC solution, showing a major band at 680 nm, which is characteristic of phthalocyanine monomeric state. Besides, two others bands labeled at 606 nm and 640 nm are present and assigned to vibrational transition²⁵. As shown in Fig. 5b after functionalizing maghemite (sample MNP) and Gold-coated maghemite (sample MNP@Au2) nanoparticles with PTC to prepare samples MNP/PTC and MNP@Au/PTC the color of formed sols drastically changes to green and violet, respectively. Magnetic separation of suspensions of samples MNP/PTC and MNP@Au/PTC led to colorless supernatants, meaning that adsorption of PTC onto magnetic nanoparticles were effective. A surface plasmon absorption at 530 nm was still observed in sample MNP@Au/PTC, due to the Au-shell contribution.

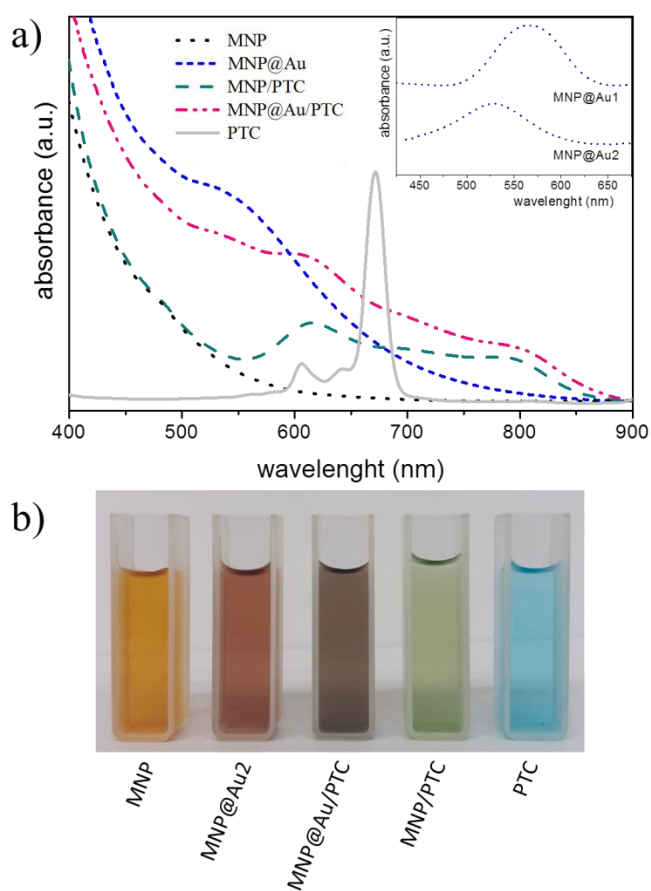


Figure 5. (a) UV-vis spectra of samples MNP (black/dot), MNP@Au2 (blue/short-dash), PTC (gray/solid), MNP/PTC (green/dash) and MNP@Au/PTC (pink/dash-dot). The inset shows a detail of spectra of samples MNP@Au1 and MNP@Au2 in the wavelength range of about 420 to 680 nm; b) Pictures of diluted sol of synthesized samples.

Nevertheless, for PTC-functionalized samples (MNP/PTC and MNP@Au/PTC) the intense absorption band at 684 nm, typical of pure PTC, was practically suppressed. However, in the 606 nm and 640 nm regions, a broad band with a hypsochromic shift appears in PTC-functionalized nanoparticles (samples MNP/PTC and MNP@Au/PTC). This finding indicates interaction of PTC with magnetic nanoparticles²⁶.

Nanocytotoxicity

The cytotoxicity of the nanoparticles on keratinocyte cells after 24 hours of exposure is illustrated in the Fig. 6. The sample MNP and MNP@Au1 presented significant decrease of cell viability in all concentrations (6.25 to 100 $\mu\text{g/mL}$). However, only MNP at higher concentration showed a significant biologically decrease of 30% of cell viability. At others concentrations, the decrease was about 5 to 10%, which is not considered biologically significant.

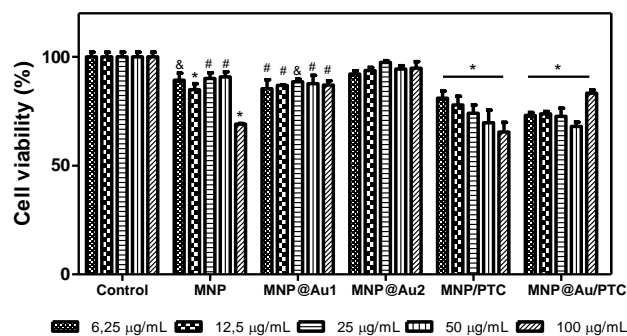


Figure 6. Percent cells viability of keratinocytes - HaCAT in presence of nanostructures: maghemite (MNP), maghemite coated with gold (MNP@Au1) and maghemite coated with 2x gold (MNP@Au2), MNP conjugated with phthalocyanine of aluminium (MNP/PTC) and MNP@Au conjugated with phthalocyanine of aluminium (MNP@Au/PTC) after 24 hours of incubation. Ultrapure water was used as negative control. Viability assay by MTT. Significantly different from the control: * $P < 0,001$ - #: $P < 0,01$ - &: $P < 0,05$.

The nanoparticle MNP@Au2 did not demonstrate cytotoxic activity in any concentration tested, probably due to the presence of gold that turned the nanostructure more biocompatible. In parallel, the nanoparticles associated to phthalocyanine were more cytotoxic. In fact, the MNP/PTC showed a dose-dependent activity and reduced the cell viability of 20 to 35%. The MNP@Au/PTC also demonstrated cytotoxic activity of 17 to 32%, but independent of the concentration.

The effect of the samples on the HaCAT cell viability after 72h of incubation is shown in Fig. 7. The MNP is not represented in the graph because the sample precipitate during the experiment making unfeasible the analysis of the cell viability. It is possible to observe that MNP@Au1 and MNP@Au2 did not show cytotoxic activity. The nanoparticles coated with phthalocyanine showed a dose-dependent activity. The MNP/PTC decreased the cell viability about 30% at higher concentration, similar to the activity observed after 24 hours of exposure. In parallel, the MNP@Au/PTC decreased the cell viability about 45% at 100 $\mu\text{g/mL}$, more than the decrease observed after 24 hours of exposure. Therefore, the MNP@Au/PTC was more efficient after 72 hours of exposure than the MNP/PTC.

The activity of the nanoparticles on the fibroblast cell viability was also investigated after 24 and 72 hours of exposure. Fig. 8 shows the result after 24 hours. In this analysis, it is possible to observe that all samples demonstrated significant decrease of cell viability. The MNP and MNP@Au1 presented a decrease of cell viability about 30 to 40% and 20 to 30%, respectively, with the increase of concentrations.

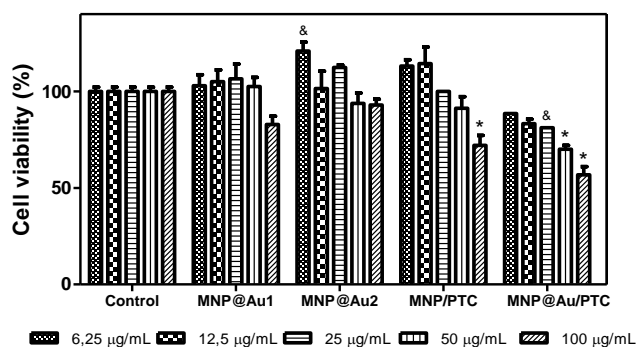


Figure 7. Percent cells viability of keratinocytes - HaCAT in presence of nanostructures: MNP@Au1, MNP@Au2, MNP/PTC and MNP@Au/PTC after 72 hours of incubation. Ultrapure water was used as negative control. Viability assay by MTT. Significantly different from the control: * $P < 0,001$ - &: $P < 0,05$.

The MNP@Au2 demonstrated less activity with reduction of cell viability of only 20%. This reduction of toxicity can be explained by the presence and increment on the gold shell which allowed improving the biocompatibility, in good agreement with previous work²⁷. The sample with phthalocyanine reduced the cell viability in about 30%. Only the higher concentration of the MNP@Au/PTC did not demonstrated cytotoxic activity.

After 72 hours of exposure, MNP in all concentrations and MNP/PTC at 12.5 to 100 $\mu\text{g/mL}$ precipitate during the experiment making unfeasible the analysis of the cell viability. The MNP@Au1 induced reduction of cell viability in about 20%. In parallel, the MNP@Au2 only showed decrease of the cell viability of 10% at 25 $\mu\text{g/mL}$, which is not considered biologically significant. The MNP@Au2 showed biocompatible property in fibroblast cells line NIH3T3. The MNP/PTC did not present cytotoxic activity at 6.25 $\mu\text{g/mL}$ after 72 hours of exposure. However, MNP@Au/PTC demonstrated a decrease of cell viability with the increase of concentration from 20 to 30%, which is more than after 24 hours of exposure (Fig. 9).

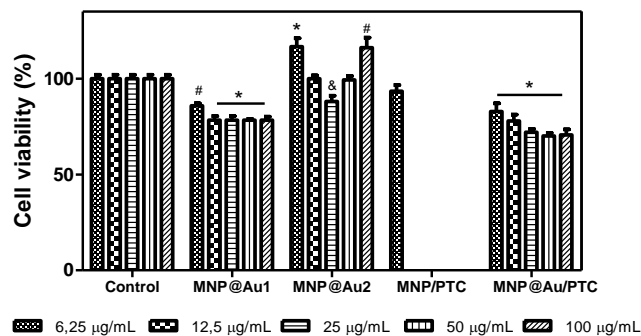


Figure 9. Percent cells viability of fibroblasts – NIH3T3 in presence of nanostructures: MNP@Au1, MNP@Au2, MNP/PTC and MNP@Au/PTC after 72 hours of incubation. Ultrapure water was used as negative control. Viability assay by MTT. Significantly different from the control: * $P < 0,001$ - #: $P < 0,01$ - &: $P < 0,05$.

An important remark is that toxicity studies of PTC-conjugated nanoparticles were carried out under light. As a result, radiation excites the light-sensitive PTC, generating cytotoxic species²⁸, essential tool for PDT application and result that could explain the deflated biocompatibility of these nanostructures.

Computed tomography

Fig. 10a shows the CT signal intensity, in HU, for bare maghemite (MNP) and Gold-shelled MNP@Au1 and MNP@Au2 sols, compared to water (a negative control) and a positive control, an iodine-based contrast agent (ACI). The inset shows a detail of the CT signal for samples MNP, MNP@Au1 and MNP@Au2, compared to water. Moreover, qualitative images that represent the X-ray cell density of these samples are shown in Fig. 10b. These results indicate that X-ray attenuation increases as maghemite is coated with Gold and as the thickness of Au-shell increases, at the same $\gamma\text{-Fe}_2\text{O}_3$ concentration (0.4 mg/mL in maghemite). In spite of the higher X-ray attenuation, when compared to water, the CT signal for ACI is several times more intense.

Nevertheless sols analyzed here were highly diluted, being however more efficient than similar Gold-capped magnetic materials reported elsewhere²⁹. In that work, a signal of ~ 200 HU was observed for samples containing ~ 5 mg/mL of Au. Here, for a ~ 0.06 mg/mL of Au sample MN@Au2, the CT signal is about 430 HU. This enables the Gold-coated samples synthesized here as contrast agents for possible applications in CT imaging. Moreover, despite the high X-ray attenuation, the contrast agents commercially available – which present low molecular weight – are rapidly eliminated by the kidneys, disabling their use in pre-clinical trials. In contrast, the kind of nanoparticles used here present long residence time in the blood stream, overcoming the challenge of pre-clinical tests.

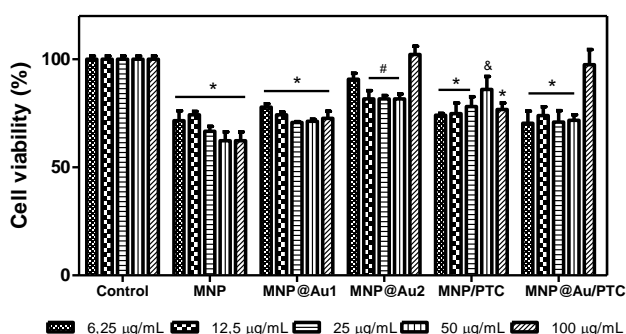


Figure 8. Percent cells viability of fibroblasts – NIH3T3 in presence of nanostructures: MNP, MNP@Au1, MNP@Au2, MNP/PTC and MNP@Au/PTC after 24 hours of incubation. Ultrapure water was used as negative control. Viability assay by MTT. Significantly different from the control: * $P < 0,001$ - #: $P < 0,01$ - &: $P < 0,05$.

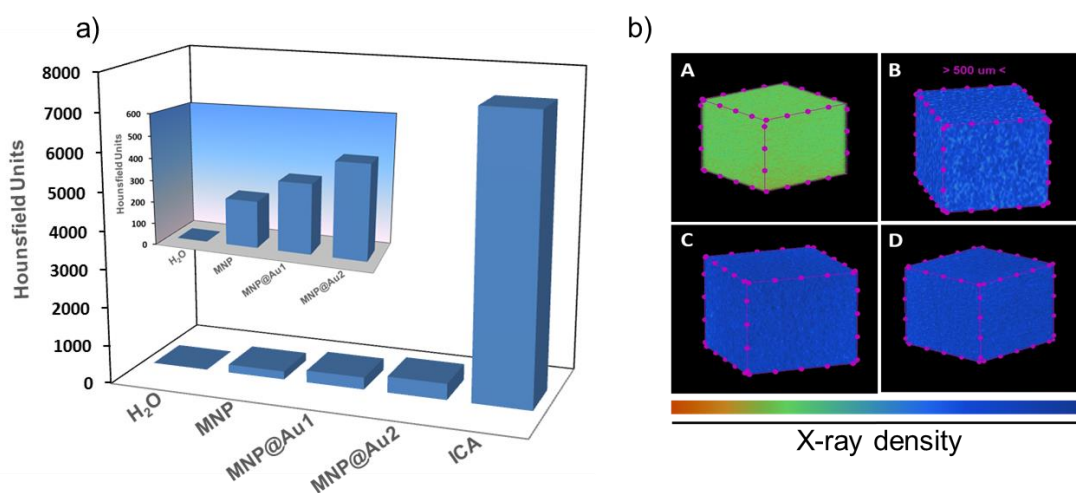


Figure 10. a) X-ray attenuation ability of MNP, MNP@Au1, MNP@Au2, water (negative control) and iodine-based contrast agent (positive control). The inset – highlight for samples MNP, MNP@Au1, MNP@Au2 and water; b) 3D qualitative images obtained for water (A), MNP (B), MNP@Au1 (C) and MNP@Au2 (D) samples, produced in an artificial colored scale presented at the bottom of the figure.

Conclusions

In conclusion, citrate-coated maghemite nanoparticles were elaborated via aqueous co-precipitation, following oxidation and citrate functionalization via an improved chemical route herein described. Gold shells were successfully deposited onto magnetic cores by reducing Au³⁺ ions in the presence of γ -Fe₂O₃ nanoparticles during 2 cycles of borohydride seeding. Moreover, we succeed in modulating the Gold shell thickness while increasing the Au/ γ -Fe₂O₃ ratio during seeding. Successful Gold-shelling was confirmed by different characterization techniques. Particularly interesting were the optical absorption measurements, showing a blueshift depending on the shell thickness. All samples presented a long-term colloidal stability in physiological pH, even after functionalization with aluminium phthalocyanine (PTC), as confirmed by DLS measurements.

Moreover, according to *in vitro* nanocytotoxicity assays the Gold-shelling enhanced the biocompatibility of the γ -Fe₂O₃ nanoparticles. Differently from previous works, in which functionalization with PTC requires several steps to complete, extra-cappings and/or cross-linking molecules to be covalently attached to nanoparticles, our data indicated strong electrostatic coupling between PTC and the nanoparticle surface, yet accomplished by a single-step process. Impressively, the Gold-shelled nanoparticles revealed efficient response as a contrast agent in computed tomography,

dependent upon the Au/ γ -Fe₂O₃ ratio. Possible application of the as-elaborated core-shell nanoparticles will derive from the combination of magnetic properties of the core (maghemite) and the optical properties of the shell (Gold). From the therapeutic point of view, the as-elaborated samples represent a promising multi-task platform to perform magnetic hyperthermia (core) combined or not with photothermal therapy (shell) and/or photodynamic therapy (PTC functionalization). Taking into account the diagnosis approach, the nanomaterials herein reported can also be used as optical probes and contrast agents in *in vivo* medical imaging techniques.

Acknowledgements

The authors gratefully acknowledge financial support from Conselho Nacional de Desenvolvimento Científico e Tecnológico (CNPq), Fundação de Apoio à Pesquisa do Distrito Federal (FAPDF), and Fundação de Empreendimentos Científicos e Tecnológicos (FINATEC).

References

- [1] G. S. Demirel, A. C. Okur, S. Kizilela, *Journal of Materials Chemistry B*, 2015, **3**, 7831-7849.
- [2] L. Wang, H.-Y. Park, S. I. I. Lim, M. J. Schadt, D. Mott, J. Luo, X. Wang and C.-J. Zhong, *Journal of Materials Chemistry*, 2008, **18**, 2629.
- [3] A. Ito, H. Honda and T. Kobayashi, *Cancer immunology, immunotherapy: CII*, 2006, **55**, 320-328.
- [4] K. Saha, S. S. Agasti, C. Kim, X. Li and V. M. Rotello, *Chemical reviews*, 2012, **112**, 2739-2779.
- [5] N. S. Abadeer and C. J. Murphy, *The Journal of Physical Chemistry C*, 2016, **120**, 4691-4716.
- [6] J. Ren, S. Shen, Z. Pang, X. Lu, C. Deng and X. Jiang, *Chemical communications*, 2011, **47**, 11692-11694.
- [7] O. Chen, L. Riedemann, F. Etoc, H. Herrmann, M. Coppey, M. Barch, C. T. Farrar, J. Zhao, O. T. Bruns, H. Wei, P. Guo, J. Cui, R. Jensen, Y. Chen, D. K. Harris, J. M. Cordero, Z. Wang, A. Jasanoff, D. Fukumura, R. Reimer, M. Dahan, R. K. Jain and M. G. Bawendi, *Nature communications*, 2014, **5**, 5093.
- [8] J. C. O. Silva, M. H. Sousa, F. A. Tourinho and J. C. Rubim, *Langmuir*, 2002, **18**, 5511-5515.
- [9] L. A. Muehlmann, M. C. Rodrigues, J. P. Longo, M. P. Garcia, K. R. Py-Daniel, A. B. Veloso, P. E. de Souza, S. W. da Silva and R. B. Azevedo, *Journal of nanobiotechnology*, 2015, **13**, 36.
- [10] O. Penon, M. J. Marin, D. B. Amabilino, D. A. Russell and L. Perez-Garcia, *Journal of colloid and interface science*, 2016, **462**, 154-165.
- [11] Y. Cheng, A. C. Samia, J. D. Meyers, I. Panagopoulos, B. Fei and C. Burda, *Journal of the American Chemical Society*, 2008, **130**, 10643-10647.
- [12] H. Cai, K. Li, M. Shen, S. Wen, Y. Luo, C. Peng, G. Zhang and X. Shi, *Journal of Materials Chemistry*, 2012, **22**, 15110.
- [13] S. Shrestha, P. Jiang, M. H. Sousa, P. C. Morais, Z. Mao and C. Gao, *J. Mater. Chem. B*, 2016, **4**, 245-256.
- [14] M. H. Sousa, G. J. da Silva, J. Depeyrot, F. A. Tourinho and L. F. Zara, *Microchemical Journal*, 2011, **97**, 182-187.
- [15] M. Mandal, S. Kundu, S. K. Ghosh, S. Panigrahi, T. K. Sau, S. M. Yusuf and T. Pal, *Journal of colloid and interface science*, 2005, **286**, 187-194.
- [16] Z. Xu, Y. Hou and S. Sun, *Journal of the American Chemical Society*, 2007, **129**, 8698-8699.
- [17] C. R. Alves, R. Aquino, M. H. Sousa, H. R. Rechenberg, G. F. Goya, F.A. Tourinho and J. Depeyrot, *Journal of Metastable and Nanocrystalline Materials*, 2004, **20**, 694-699.
- [18] M. Mikhaylova, D. K. Kim, N. Bobrysheva, M. Osmolowsky, V. Semenov, T. Tsakalagos, and M. Muhammed, *Langmuir*, 2004, **20**, 2472-2477.
- [19] J.-C. Bacri, R. Perzynski and D. Salin, *Journal of Magnetism and Magnetic Materials*, 1990, **85**, 27-32.
- [20] N. C. Feitoza, T. D. Goncalves, J. J. Mesquita, J. S. Menegucci, M. K. M. S. Santos, J. A. Chaker, R. B. Cunha, A. M. M. Medeiros, J. C. Rubim, M. H. Sousa, *Journal of Hazardous Materials*, 2014, **264**, 153-160.
- [21] Y. C. Yeh, B. Creran and V. M. Rotello, *Nanoscale*, 2012, **4**, 1871-1880.
- [22] K. C.-F. Leung, S. Xuan, X. Zhu, D. Wang, C.-P. Chak, S.-F. Lee, W. K. W. Ho and B. C. T. Chung, *Chemical Society Reviews*, 2012, **41**, 1911-1928.
- [23] L. Wang, J. Luo, Q. Fan, M. Suzuki, I. S. Suzuki, M. H. Engelhard, Y. Lin, N. Kim, J. Q. Wang and C.-J. Zhong, *Journal of Physical Chemistry B*, 2005, **109**, 21593-21601.
- [24] J. L. Lyon, D. A. Fleming, M. B. Stone, P. Schiffer and M. E. Williams, *Nanoletters*, 2004, **4**, 719-723.
- [25] K. Liu, Y. Wang, J. Yao and Y. Luo, *Chemical Physics Letters*, 2007, **438**, 36-40.
- [26] M. Idowu and T. Nyokong, *Journal of Photochemistry and Photobiology A: Chemistry*, 2007, **188**, 200-206.
- [27] Y. Li, J. Liu, Y. Zhong, J. Zhang, Z. Wang, L. Wang, Y. An, M. Lin, Z. Gao and D. Zhang, *International journal of nanomedicine*, 2011, **6**, 2805-2819.
- [28] C. S. de Paula, A. C. Tedesco, F. L. Primo, J. M. Vilela, M. S. Andrade and V. C. Mosqueira, *European journal of pharmaceutical sciences : official journal of the European Federation for Pharmaceutical Sciences*, 2013, **49**, 371-381.
- [29] S. Zhang, Y. Qi, H. Yang, M. Gong, D. Zhang and L. Zou, *Journal of Nanoparticle Research*, 2013, **15**, 1-9.